Modeling and experimental identification of torsional drill string dynamics under uncertainties

Fabio Real

▶ **To cite this version:**

Fabio Real. Modeling and experimental identification of torsional drill string dynamics under uncertainties. Materials. Université Paris-Est; Universidade federal do Rio de Janeiro, 2018. English. NNT : 2018PESC1095 . tel-02134677

HAL Id: tel-02134677

https://theses.hal.science/tel-02134677

Submitted on 20 May 2019

HAL is a multi-disciplinary open access archive for the deposit and dissemination of scientific research documents, whether they are published or not. The documents may come from teaching and research institutions in France or abroad, or from public or private research centers.

L'archive ouverte pluridisciplinaire **HAL**, est destinée au dépôt et à la diffusion de documents scientifiques de niveau recherche, publiés ou non, émanant des établissements d'enseignement et de recherche français ou étrangers, des laboratoires publics ou privés.

Instituto Alberto Luiz Coimbra de
Pós-Graduação e Pesquisa de Engenharia

MODELING AND EXPERIMENTAL IDENTIFICATION OF DRILL STRING TORSIONAL DYNAMICS UNDER UNCERTAINTIES

Fabio Ferreira Real

Tese de Doutorado apresentada ao Programa de Pós-graduação em Engenharia Mecânica, COPPE, da Universidade Federal do Rio de Janeiro, como parte dos requisitos necessários à obtenção do título de Doutor em Engenharia Mecânica.

Orientadores: Thiago Gamboa Ritto
Anas Batou
Christophe Desceliers

Rio de Janeiro
Novembro de 2018

MODELING AND EXPERIMENTAL IDENTIFICATION OF DRILL STRING TORSIONAL DYNAMICS UNDER UNCERTAINTIES

Fabio Ferreira Real

TESE SUBMETIDA AO CORPO DOCENTE DO INSTITUTO ALBERTO LUIZ COIMBRA DE PÓS-GRADUAÇÃO E PESQUISA DE ENGENHARIA (COPPE) DA UNIVERSIDADE FEDERAL DO RIO DE JANEIRO COMO PARTE DOS REQUISITOS NECESSÁRIOS PARA A OBTENÇÃO DO GRAU DE DOUTOR EM CIÊNCIAS EM ENGENHARIA MECÂNICA.

Examinada por:

Prof. Thiago Gamboa Ritto, D.Sc.

Prof. Anas Batou, D.Sc.

Prof. Christophe Desceliers, D.Sc.

Prof. Jean-François Deu, D.Sc.

Prof. Marcelo Areias Trindade, D.Sc.

Prof. Daniel Alves Castello, D.Sc.

Prof. Edson Luiz Cataldo Ferreira, D.Sc.

RIO DE JANEIRO, RJ – BRASIL
NOVEMBRO DE 2018

Real, Fabio Ferreira

Modeling and experimental identification of drill string torsional dynamics under uncertainties/Fabio Ferreira Real. – Rio de Janeiro: UFRJ/COPPE, 2018.

XIII, 95 p.: il.; 29, 7cm.

Orientadores: Thiago Gamboa Ritto
Anas Batou
Christophe Desceliers

Tese (doutorado) – UFRJ/COPPE/Programa de Engenharia Mecânica, 2018.

Referências Bibliográficas: p. 75 – 88.

1. Drill string dynamics. 2. Bit-rock interaction. 3. Hysteresis model. 4. Uncertainty modeling. I. Ritto, Thiago Gamboa *et al.* II. Universidade Federal do Rio de Janeiro, COPPE, Programa de Engenharia Mecânica. III. Título.

This thesis is dedicated to my
parents. True love.

Acknowledgments

Firstly, I would like to thank God for giving me a good life. To my parents, Zilda and Antonio, who has been a source of encouragement and support to me throughout my life. To my brothers Giancarlo and Rodrigo, and my sister-in-law, Vanessa, for the laugh moments during my journey. To all my friends and family, in special Fabricio, Hugo, Danilia, Luiz, Marcelo, Diogo, Elaine, Jackson, and goddaughter Elis, for giving me their kindness and strength.

I would like sincerely to thank my supervisors, Thiago, Anas and Christophe, for their guidance and support during this work, in special to Thiago, for his confidence in me since my masters, and Anas, who had patience to teach me a part of his knowledge.

Loving thanks to my friends and learning partners from LAVI (UFRJ), Tiago, Pedro, Daniel, Diego, Davi, Ádamo and Matheus, from UFSC, Filipe Fontanella, people from MSME, and people from Risk and Uncertainty Institute (University of Liverpool), Marco, Raphael, ”Chinaman”, ”Utche, Bright”, Fabrizzio, Carol, Maria, Peter, Dominic and Roberto for giving me good technical learnings, lunch times, coffee times (I learnt that I cannot drink a ”cappuccino” during the afternoon... just an ”expresso” or a ”flat white”...), and happy hour times. I cannot forget to thank Inmetro, for granting me time to end this work, and where I can apply all the learnt knowledge.

Finally, I would like to acknowledgment the finantial support of the Brazilian agency CAPES, and to thank Brazil people for financing my career in the Brazilian public sector and this thesis. Thank you all!

Resumo da Tese apresentada à COPPE/UFRJ como parte dos requisitos necessários para a obtenção do grau de Doutor em Ciências (D.Sc.)

MODELAGEM E IDENTIFICAÇÃO EXPERIMENTAL DA DINÂMICA TORSIONAL DE UMA COLUNA DE PERFURAÇÃO DE PETRÓLEO CONSIDERANDO INCERTEZAS

Fabio Ferreira Real

Novembro/2018

Orientadores: Thiago Gamboa Ritto
Anas Batou
Christophe Desceliers

Programa: Engenharia Mecânica

Esta tese de doutorado propõe novas formas de modelar a dinâmica torcional de uma coluna de perfuração de petróleo considerando incertezas. Este trabalho propõe um novo modelo estocástico de interação broca-rocha histerético (não-reversível). Primeiramente, um novo modelo nominal de interação o qual depende não somente da velocidade angular da broca, mas também de sua aceleração é proposto. Então, um novo modelo estocástico para a interação broca-rocha levando em consideração as flutuações inerentes é também proposto. Além disso, uma nova bancada experimental é proposta para analisar a dinâmica da coluna de perfuração de petróleo e interação broca-rocha, a qual é apta para reproduzir o fenômeno do *stick-slip* enquanto perfura uma amostra de rocha utilizando broca de concreto comercial, assim como validar modelos de interação broca-rocha. Uma estratégia original para modelar incertezas em nível global baseada em termos da abordagem probabilística não-paramétrica considerando um modelo torcional simples para uma coluna de perfuração de petróleo é também proposta. Esta estratégia permite controlar o nível de dispersão para cada grau de liberdade interno e na interface de cada subestrutura de forma independente, a qual pode prover mais informações para melhorar a segurança operacional.

Abstract of Thesis presented to COPPE/UFRJ as a partial fulfillment of the requirements for the degree of Doctor of Science (D.Sc.)

MODELING AND EXPERIMENTAL IDENTIFICATION OF DRILL STRING TORSIONAL DYNAMICS UNDER UNCERTAINTIES

Fabio Ferreira Real

November/2018

Advisors: Thiago Gamboa Ritto
Anas Batou
Christophe Desceliers

Department: Mechanical Engineering

This D.Sc. thesis proposes new perspectives for modeling drill string torsional dynamics under uncertainties. This work develops a novel stochastic hysteretic (non-reversible) bit-rock interaction model. Firstly, a new nominal interaction model, which depends not only on the bit speed, but also on the bit acceleration is developed. Then, a new stochastic model for the bit-rock interaction, taking into account the inherent fluctuations during the drilling, is also proposed. Furthermore, a new test-rig is proposed to analyze drill string dynamics and bit-rock interaction, which is able to reproduce stick-slip phenomena while drilling a rock sample using standard masonry bits, as well as to validate bit-rock interaction models. An original strategy for modeling uncertainties globally, based on terms of the nonparametric probabilistic approach, considering a simple torsional model for a drill string, is also proposed. This strategy allows to control the dispersion level of each interior and interface DOFs of each drill string substructure independently, which can provide more information to improve the operational safety.

Contents

List of Figures **x**

List of Tables **xiii**

1 Introduction **1**
1.1 General context 1
1.2 Literature review 3
1.3 Purpose and objectives 9
1.4 Organization of the manuscript 10

2 Drill string torsional model **11**
2.1 Torsional model 11
2.2 Reduced-order model 14

3 Bit-rock interaction **15**
3.1 Deterministic average model for bit-rock interaction 15
3.2 Hysteretic model for bit-rock interaction 18
3.3 Stability analysis of the hysteretic model 26

4 Stochastic modeling for bit-rock interaction **30**
4.1 Construction of the stochastic model 31
4.2 Simulation of the stochastic drill string dynamics 34
4.2.1 Analysis of one realization of the stochastic drill string dynamical response 34
4.2.2 Stochastic stability analysis 36

5 Test-rig for experimental results **39**
5.1 Test-rig setup 39
5.2 Experimental planning 43
5.3 Experimental results 43
5.3.1 Test-rig set-up and proceedings 43
5.3.2 Experimental data analysis 44

5.3.3 Comparison between experimental data and mathematical models - validation of test-rig results 49
5.4 Validation of hysteretic models using numerical simulations 52

6 Stochastic computational model of the drill string 54
6.1 Classical nonparametric probabilistic approach - a brief overview 54
6.2 Nonparametric probabilistic approach together with Craig-Bampton substructuring method 56
6.2.1 Craig-Bampton substructuring method 56
6.3 The methodology 59
6.4 New stochastic model: one extension of nonparametric probabilistic approach together with Craig-Bampton substructuring method, which separates of the statistical fluctuations related to the inner and interface DOFs 60
6.5 Comments concerning the nonparametric probabilistic approach - presence of floating substructures 61
6.6 New stochastic model (SM_{CB2}): application and verification 62
6.6.1 Validation of the new stochastic model SM_{CB2}: one comparison . 63
6.6.2 Random response of stochastic model SM_{CB2} 65

7 Conclusions, contributions and future works 72

Bibliography 75

A Modified Euler Scheme 89

B Algorithm 91

C Convergence analysis 92

List of Figures

1.1 General view of a drill string (*source*: University of Aberdeen web page, in https://www.abdn.ac.uk/engineering/research/modeling-and-analysis-of-bha-and-drillstring-vibrations-149.php). 2

2.1 General scheme for modeling a drill string. 12

3.1 Terms of the bit-rock interaction reversible model, Eq. (3.1): *tanh* term in blue, fraction term in green, and complete reversible model in magenta. 16
3.2 Experimental bit speed, according to Ritto et al. [112]. 17
3.3 Experimental bit-rock interaction (Ritto et al. [112]) and identified average model. 18
3.4 Downhole field data, torque [N.m] versus angular speed [RPM] at the bit: six stick-slip cycles available. The path from the top occurs when the bit accelerates, and the path from the bottom occurs when the bit speed decreases. The direction of the cycle is the same for all six cycles. 20
3.5 Downhole field data: six stick-slip cycles and their mean. The mean of all cycles (upper and lower) is in blue, and the mean cycle is showed in green. 21
3.6 Hysteretic term H as a function of the bit acceleration (top graph) and a zoom image (bottom graph). 23
3.7 Hysteretic bit-rock interaction model. Blue line when the bit acceleration is positive and green line when the bit accelaration is negative. 24
3.8 Field data vs. bit-rock interaction reversible model, (Eq. (3.1)): Fitted model in magenta and mean field data in blue. 24
3.9 Field data vs. hysteretic bit-rock interaction model (Eq. (3.3)): fitted model in black, and mean cycle of field data in green. 25
3.10 Bit-Rock interaction models (Eqs. 3.1 and 3.3): (1) reversible (magenta), (2) hysteretic $\beta_1 = 14\%$ (black), and (3) hysteretic $\beta_1 = 56\%$ (black). . . 26
3.11 Stability map for models 1 (reversible) and 2 (hysteretic $\beta_1 = 14\%$). . . . 28
3.12 Stability map for the model 3 (hysteretic $\beta_1 = 56\%$). 29

4.1 Stochastic process $\eta^{\exp}(t)$ obtained experimentaly with field data. 32
4.2 Field data PSD. 33

4.3 Zoom image of the comparison between the calibrated PSD (in red) and the field data PSD (in black). 33
4.4 Two independent realizations of the stochastic process $\eta(t)$. 34
4.5 One realization of the simulated bit-rock interaction. 35
4.6 Bit speed: deterministic bit-rock interaction model (left, 3-cycles periodicity observed) and stochastic bit-rock interaction model (right, no periodicity observed). 36
4.7 Random stick and slip phases duration: probability density functions (black line) and corresponding 3-cycles periodic values calculated with a deterministic bit-rock interaction model (red vertical lines) 36
4.8 Stick-slip severity factor for a deterministic bit-rock interaction. Red dashed line indicates the stability threshold of SS($\dot{\theta}_{top\ drive}$). 37
4.9 Random stick-slip severity factor for a stochastic bit-rock interaction. Solid lines: mean response and 90% confidence region. Dashed line: deterministic case (black), stability threshold (red). 38

5.1 General view of test-rig. 41
5.2 Bit, test-body and platform set view. 42
5.3 Platform design - general and load cell views. 42
5.4 Box-plot of 210 test-rig experiments. 45
5.5 Full data of bit speed, torque on bit and WOB for sample 175. The red box is the time interval used in the detailed stick-slip mechanism analysis. 46
5.6 Data from sample 175 with a time interval from 34 to 37 seconds. 47
5.7 Stick-slip cycle from sample 175 for time interval from 35.3 to 35.67 seconds. (a) bit speed versus time; (b) torque on bit versus bit speed and; (c) WOB versus bit speed. 48
5.8 Stick-slip cycles for 4 different samples (93, 115, 165, and 175). The cycles corresponds to a time interval of 5 seconds in each sample. 49
5.9 Full data of torque on bit, bit speed and WOB data using ϕ 8 mm bit and drive speed setted at 120 RPM (sample 3), where the red box is the selected range for analysis (range between 44s and 59s). 50

6.1 Comparison of three stochastic models - frequency response in acceleration for point $P_{obs,1}$. 64
6.2 Comparison of three stochastic models - frequency response in acceleration for point $P_{obs,2}$. 64
6.3 Comparison of three stochastic models - frequency response in acceleration for point $P_{obs,3}$. 65
6.4 Case study 1, 2 and 3 - frequency response in acceleration for point $P_{obs,1}$. 66
6.5 Case study 1, 2 and 3 - frequency response in acceleration for point $P_{obs,2}$. 67

6.6 Case study 1, 2 and 3 - frequency response in acceleration for point $P_{obs,3}$. 67
6.7 Case study 4 and 5 - frequency response in acceleration for point $P_{obs,1}$. . 68
6.8 Case study 4 and 5 - frequency response in acceleration for point $P_{obs,2}$. . 68
6.9 Case study 4 and 5 - frequency response in acceleration for point $P_{obs,3}$. . 69
6.10 Case study 6 and 7 - frequency response in acceleration for point $P_{obs,1}$. . 70
6.11 Case study 6 and 7 - frequency response in acceleration for point $P_{obs,2}$. . 70
6.12 Case study 6 and 7 - frequency response in acceleration for point $P_{obs,3}$. . 71

C.1 Convergence function $n_s \mapsto Conv(n_s$. 93
C.2 Convergence analysis for number of iterations. 93
C.3 Convergence analysis for DP normal modes. 94
C.4 Convergence analysis for BHA normal modes. 94

List of Tables

3.1 Drill string characteristics, according to Ritto et al. [112]. 17

5.1 Test-rig characteristics. 43
5.2 Statistics related to T_{bit}^{exp} of samples 11, 12, 13,14, 15, 16, 17, 18, 19 and 20. 52

6.1 Case study 1 - values of the dispersion parameters. 65
6.2 Case study 2 - values of the dispersion parameters. 66
6.3 Case study 3 - values of the dispersion parameters. 66
6.4 Case study 4 - values of the dispersion parameters. 67
6.5 Case study 5 - values of the dispersion parameters. 68
6.6 Case study 6 - values of the dispersion parameters. 69
6.7 Case study 7 - values of the dispersion parameters. 70

Chapter 1

Introduction

1.1 General context

The Chinese people are recognized to be the first civilization to drill for oil: already in 300 BC, they pounded holes in the ground with heavy, bronze bits suspended from spring poles, which eliminated some of the manual labor to raise and to drop a heavy bronze bit [31]. In the early 1800's, drillers in the 'modern' oil industry used a variation of this technique called cable-tool drilling, which utilized a steam or internal combustion engine to raise and lower a wooden or metal beam from which the bit was suspended. In cable-tool drilling [86], the cable (manila rope or wire line) pulled the string of tools up and down as brought about by a spring pole or a walking beam at the surface, and the bit has a blunt chisel end which cracks, chips and smashes the rock by the repeated blows delivered in a measured or regular cadence. This kind of drilling is also called percussion drilling.

In the 1860's, some artesian wells were drilled with wooden rods supporting the tools of the drill string, where the rods may have been to the order of 1 3/4" thick, 20 to 30 ft in length and were fastened together by a screw and box [86]. To be pulled out of the hole, each rod had to be unscrewed when it arrived at the surface and fastened again when going back into the hole. The use of wooden rods was soon replaced by thick rope such as manila, sisal hemp or sea grass, thus eliminating the hookup time that wooden rods required.

Nowadays, the drilling operation is done by drill string, which consists of a series of pipe sections (joints) that are screwed together as they are lowered into the borehole [4]. In general, drill strings are composed by two substructures: drill pipe (slender pipes that can reach kilometers, herein called "DP") and bottomhole-assembly pipe (thicker pipes together with a drill bit on its bottom, and its length can reach hundreds of meters

long, herein called BHA), as showed in Fig. 1.1. For vertical drilling operations, the drill string rotates around its longitudinal axis for drilling rocks, and a drilling fluid is injected inside of it in order to transport drilled solids (cuttings) upward in annulus area (space between the drill string and the borehole), avoiding borehole clogging and cooling the bit [102], among other functions. Once the target depth is reached, the drill string is pulled out of the hole, and another length of pipe (the production casing) is cemented in place to prevent hole collapse and to isolate productive formations (from one another) [4]. Its operation is not trivial and involves high costs, especially in deep water oil reserves, which increases the interest of industries to reduce the operational costs to sustain the competitiveness[102].

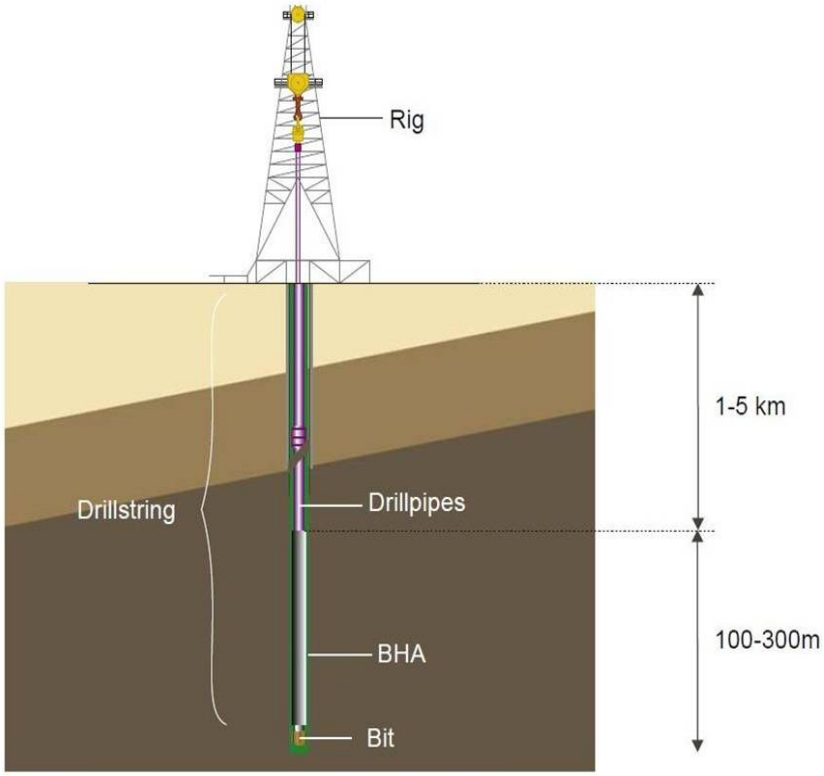

Figure 1.1: General view of a drill string (*source*: University of Aberdeen web page, in https://www.abdn.ac.uk/engineering/research/modeling-and-analysis-of-bha-and-drillstring-vibrations-149.php).

Due to drill string design concept (slender structure), torsional and lateral vibrations can occur when it rotates. Besides, its dynamical behavior combines a complex set of actions under operation, such as friction in bit-rock interaction, axial compression forces, fluid structure interaction, and possible borehole contact. These effects can generate axial, lateral and torsional damped vibrations [134]. Especially for torsional vibrations, the friction during the bit-rock interaction, coupled with the axial efforts (torque applied

at the bottom-end of the BHA - torque on bit), might lead to stick-slip, which is an oscillatory twisting evidenced as a variation of bit speed [37, 51, 57, 61, 84, 98, 139]. Stick-slip oscillations might cause, for instance, measurement equipment failure, low rate of penetration, bit damage, and fatigue [155]. Besides, oscillations can increase the pre-existing number of uncertainty sources, as material properties (column and drilling fluid) and dimensions of whole system (especially borehole). In this context, drill string dynamics might be complex [42, 50, 102, 114, 134, 135], and knowledge thereof is strategic for the industry, in order to reduce the operational costs and sustain the competitiveness.

This work is interested in the modeling of torsional vibrations of a drill string under uncertainties, in order to minimize the operational risks, which means improving its efficiency and safety, avoiding premature material fatigue, saving operational costs concerning the drilling efficiency, driving energy, and drilling reliability.

1.2 Literature review

Over last two centuries, structural dynamic analysis has been discussed by several experts around the world, encouraged by theoretical investigations and by computational methods in different fields like mechanical engineering, for designing and constructing of machineries, and also for controlling of vibration, naval, aeronautics and also civil engineering, for constructions in earthquake zones and under wind effects.

New methods for the calculation of eigenvalues and eigenvectors, with application to structural dynamics, were developed in the first years of the twentieth century. The contributions from 1896 to 1929 by Adolf Kneser (1862-1930), Aleksandr Mikhailovich Lyapunov (1857-1918), Jacques Salomon Hadamard (1865-1963) and Tullio Levi-Civita (1873-1941), plus Liapounov's essay of 1907 on the "*Problème général de la stabilité du mouvement*", opened a new field for mathematical studies applied to structural mechanics and dynamics. Moreover, Giulio Benedetto Isacco Vivanti (1859-1949) published in 1916 "*Elementi della teoria delle equazioni integrali lineari*", where the problem related to the numerous DOFs was resolved introducing integral equations [23]. Particularly regarding random vibrations, in 1905, Albert Einstein (1879-1955) initiated his analysis related to the Brownian motion [28], however, after more than fifty years, Stephen Harry Crandall (1920-2013) made the random vibration analysis accessible for non-researcher engineers through his seminar of 1958. In the literature, there are some books about random vibration analysis with random excitation of linear and non-linear dynamical

systems [22, 56, 64, 70, 151].

Studies concerning structural dynamic analysis for drill strings are more recent. In 1992, Paslay et al. [83] referred to uncoupled models for axial and torsional vibrations, beyond lateral displacements, including the effect of the fluid-added mass, but neglected impacts between the column and the borehole [105]. In Jansen's Ph.D. thesis [42], a detailed discussion about drill string dynamics is made, where he presented simple computational models and also the non-linear formulation of an Euler-Bernoulli beam, even though he did not consider stabilizers and bit-rock interaction (only a simple model for the fluid-structure interaction). Abbassian and Dunayevsky [1] addressed the string-torsional vibration, bit-lateral dynamics, and coupled torsional-lateral vibration of the polycrystalline diamond compact (PDC) bits under induced torsional and lateral vibrations. The papers by Tucker and Wang [140] used the Cosserat theory for modeling the drill string dynamics, while the papers by Khulief et al.[50] and of Sampaio et al. [114] used the Euler-Bernoulli beam stochastic model with the Finite Element Method. These works did not consider a fluid-structure interaction, either inside or outside flows of the column, only in the work of Tucker and Wang [140], the influence of the fluid is considered in a simplistic way. Spanos et al. [134, 135] cited a vibration overview in drilling processes.

In the last ten years, studies related to drill string structural dynamic analysis were object of studies of various authors in different ways. Piovan and Sampaio [90] discretized by finite elements a continuous model for analyzing the coupled extensional flexural and torsional vibrations of a drill string; on the other hand, Germay et al. [33] studied the drill string axial and torsional vibrations using a lumped parameter model characterized by a fast axial dynamics compared to the slow torsional dynamics. Navarro-López and Licéaga-Castro [80] considered a discontinuous lumped-parameter torsional model of four DOFs with four discontinuity surfaces, where one of them is introduced in order to accomplish the control goal despite variations of the weight on the bit, the top-rotary velocity and friction characteristics. Pang et al. [81] focused in the BHA vertical-horizontal-torsional vibrations and their mechanical properties, which are established by the non-linear dynamics considering random impacts and rubs between the well wall and drill string, drill bit and the rock. Tikhonov and Safronov [137] presented a 3D non-linear dynamic model of drill string in a 3D borehole, taking into account the interaction of lateral, torsional, and axial vibrations. Divenyi et al. [25] have shown critical stick-slip and bit-bounce behaviors related to parameter changes, allowing to develop a deep understanding of the drill string dynamics. Liao et al. [63] conducted experimental and numerical investigations series in order to understand the drill string motions, checking the influence of different system parameters such as the

mass imbalance and contact friction on the system dynamics. Liu et al. [65] introduced a discretized non-linear model with eight DOFs, including axial, torsional and lateral dynamics of both the DP and BHA, which showed that the motions can be self-excited through stick-slip friction and time-delay effects, the whirling state of the DP periodically alternates between the sticking and slipping phases, and also that the system response stability is seen to be largely dependent upon the driving speed.

Recently in structural dynamic analysis for drill strings, Depouhon and Detournay [24] analyzed the self-excited axial and torsional vibrations of deep drilling systems by a discrete model that relies on a rate-independent bit-rock interaction law, and reduces to a coupled system of state-dependent delay differential equations governing the axial and angular perturbations to the stationary motion of the bit. This analysis indicated that, although the steady-state motion of the bit is always unstable, the nature of the instability depends on the nominal angular velocity imposed upon the rig of the drill string and, when it is larger than a critical velocity, the angular dynamics are responsible for the instability. Butlin and Langley [12] proposed an efficient drill string dynamics model using digital filters and finite element model to describe the linear dynamics of drill strings and reduced the DOFs of the equations of motion coupled to the non-linear contact effects. Ren et al. [97] developed the mathematical models based on a flexible shell under axial rotation, taking into account the coupling of axial and torsional vibrations, which showed that when the drill string is in a low speed rotation zone, the torsional excitation is overlapping the axial excitation for the coupling vibration, and the opposite occurs in a high speed rotating zone. Field data of a drill string of five kilometers in length is analyzed in Ritto et al. (2017) [112], where once again a pure torsional model presented satisfactory results reproducing field data, where torsional vibration was the dominant phenomenon observed.

To represent the bit-rock interaction, some authors consider it as a non-linear function between torque on bit and bit speed [51, 85, 94, 111, 112], while others apply a switching mechanism [62]. One can find coupled axial-torsional bit-rock interaction models, such as [99, 141]. Richard et al. [99] proposed a novel model to investigate the self-excited stick-slip vibrations of a drilling system with a drag bit, using a discrete model that takes into consideration the axial and torsional vibration modes. Ritto et al. [102] proposed a new strategy of a stochastic computational model to describe the bit-rock interaction, considering the fluid-structure interaction and the impact forces, which uses the nonparametric probabilistic approach for modeling uncertainties in a non-linear constitutive equation. The non-linear dynamical responses obtained were very sensitive to uncertainties in the bit-rock interaction model, showing that uncertainties play an important role in the coupling between axial and torsional responses, and consequently,

in lateral responses. Ritto et al. [104] dealt with a procedure to perform the identification of the probabilistic model of uncertainties related to the non-linear constitutive equation, using the nonparametric probabilistic approach in a bit-rock interaction for the non-linear dynamics of a drill string. Ritto and Sampaio [108] analyzed the stochastic dynamics of a drill string with uncertain top speed by a linearized system with axial and torsional motions to compute how the input power is effectively used to cut the rock and to move the column forward. Nandakumar and Wiercigrochn [79] considered a fully coupled two-DOF drilling model with stick-slip and bit-bounce phenomena, which is composed by a state-dependent time delay and a viscous damping for both the axial and torsional motions. It showed the dependency of cutting forces on the past history of the bit motion, deducing the stable region and concluding that large speeds are eventually stable for all weight on bit values. Recently, Terrand-Jeanne and Martins [136] considered a stick-slip phenomenon in drill string in order to compare different kinds of modeling for some deformable mechanical devices, analyzing the consequences of simplifying model.

Although some publications are not directly concerned with bit-rock interaction, they are very closely related to hysteresis representation. The earliest paper presenting direct measurements showing hysteretic response in friction-induced vibration is noticed by Ko and Brockley [55], where a pin-on-disk tribometer, transducers and other electronic devices permitted the accurate measurement of kinetic friction forces in the presence of friction-induced vibration. Wojewoda et al. [152] described the phenomena of hysteretic behaviour of dry friction occurrences as a representation of the system dynamics, where several dry friction models are presented. They noticed that hysteretic effects can appear by tangential stiffness between the bodies in contact during stick phase and stick-slip transition phase, and they can appear during the slip phase, because the existence of frictional memory caused by a lag in the friction force. The size of this macroscopic sliding loop increases according to the velocity rate. A recent review of models and measurements for dynamic friction is reported by Woodhouse, Putelat and McKay [153], where they described frictional interactions and discussed a great number of friction models, illustrating that friction response can be extremely sensitive according to the choice of frictional constitutive model.

Hysteretic cycles have been observed experimentally for the bit-rock interaction in [62, 85, 94]. As far as the author is aware, the only hysteretic bit-rock interaction model found in the literature was proposed in [37]. The authors in [37] used the experimental results presented in [62], and applied their hysteretic model, which employs a switching mechanism, to the analysis of Proportional-Integral (PI) control strategy, aiming at mitigating stick-slip oscillations. Especially in Real et al. [94], the authors have highlighted large fluctuations of the nonlinear bit-rock interaction law during the

drilling. These fluctuations, which are mainly due to the soil's mechanical properties during the drilling, propagate to the drill string dynamical behavior and have to be taken into account in order to study the drill string stability with a good robustness. This work is described in detail in this thesis.

In addition to the bit-rock interaction models, some fluctuations can be observed in this interaction, which must be characterized as uncertainties [94]. In [133], a stationary random process is considered to model lateral forces at the bit. In [102], an adaptation of the nonparametric probabilistic approach [124] is proposed to model uncertainties in the bit-rock interaction model. For the latter two papers, the probabilistic models are not time-dependent, i.e., the bit-rock interaction model is random but does not vary during the drilling. Constructing such a stochastic computational models including the stochastic fluctuations of the bit-rock interaction forces would be helpful for robust optimization of the drill string [103]. In Ritto et al. [103], the nonparametric probabilistic approach is employed to model uncertainties in the coupled axial-torsional drill string dynamics. Other aspects of uncertainty of the drill string problem were tackled in [104, 106, 107, 108], as in Ritto and Sampaio [106] uncertainties are considered in the bit-rock interaction parameters.

To validate the models, a test-rig is required to reproduce drill string vibrations. Some researches have developed laboratory test-rigs to better understand the drill string dynamics and the bit-rock interaction. Patil and Teodoriu [84] highlighted some contributions in the field of modeling and controlling torsional drill strings vibration. They also summarized some experimental studies carried out in laboratories. Usually, experimental setups consist of a slender bar driven by an electric motor at one end and, at the other end, a heavy disc is attached. Actually, few test-rigs found in the literature drill the rock. To emulate the bit-rock interaction, some authors consider brakes or shakers close to the disc [52, 73, 74, 146]. Torsional models were applied successfully to represent test rigs that were constructed in [74] to analyze the friction-induced limit cycling. Elsayed [30] introduced an approach to represent a drill string test-rig, which offers flexibility to modify, remove or augment the modes representing the system. This approach is based on the multi-degree-of-freedom in-series spring-mass system with Rayleigh damping and, applying the force to the end node (bit), the modes can then be decoupled and their contributions to bit displacement can be added algebraically. His work showed that the lowest frequency modes are not necessarily the most critical.

Raymond et al. [92] developed an advanced BHA simulator able to model the response of more complex representations of a drill string with multiple modes of vibration and to measure the dynamic properties. In this rig, an actual drill bit is used to drill

rock samples. Likewise, Kapitaniak et al. [47] and Wiercigroch et al. [150] investigated the drill string dynamics on an experimental rig, which uses commercial drill bits and rock-samples. This experimental rig uses commercial drill bits and rock-samples, capable of reproducing various phenomena, such as stick-slip oscillations, whirling, drill bit bounce and helical buckling. In Westermann et al. [149], a new laboratory rig is presented, constituted of a rotating shaft representing a BHA section between two stabilizers, which is capable of reproducing lateral drill string vibrations with and without contact and of measuring the contact forces. Wang et al. [147] designed a test-rig to analyze axial oscillation drag reduction mechanism. The authors also performed the identification of the friction parameters for coupled torsional/axial model based on the experimental data. Liu et al. [67] analyzed the multistability in drill strings under stick-slip oscillations in a small-scale test-rig able to drill real rock samples. Cayres et al. [13] proposed a simplified test-rig, which is constructed by a slender shaft and two discs: one simulates the drill bit, and the other one, an intermediary contact region (borehole contact). Finally, the test-rig proposed in this work [95] drills a rock sample using a masonry bit and reproduces stick-slip cycles with a low cost design basis, where the hysteric effects in the bit-rock interaction are noticed.

In addition to the bit-rock interaction uncertainty, there are other sources of uncertainties related to the computational model of the drill string, such as the material properties, geometry variation along the axial axis, mud density, etc. Therefore, a probabilistic model of uncertainties is required to check how robust this computational model is, according some inferred fluctuations. Some works take into account uncertainties in different ways [102, 106, 124, 133], considering parametric and nonparametric probabilistic approaches. For contextualization purposes, a parametric probabilistic approach consists of replacing uncertain parameters with random variables [35, 118, 119], which is very efficient if the computational model is a good representation of the dynamical systems; nonparametric probabilistic approach [124] considers the uncertainties at the operator level globally, by modeling the reduced-order matrices of a dynamical system as random matrices. Therefore, the experimental identification is required to be applied, in order to identify the parameters according to the field data or experimental data, validating the representation of uncertainties behavior without losing its accuracy.

For completeness of the nonparametric probabilistic approach studies, it is important to cite Soize's works [124, 125, 126, 127, 128, 131] and Batou's work [7], which proposed a new methodology for the construction of a probabilistic reduced-order model of uncertainties adapted to the low- and mid-frequency structural dynamics, using a nonparametric approach for the global matrix blocks and the local matrix blocks separately, allowing to control the global fluctuations and the local fluctuations.

In order to model the uncertainties globally, a work by this thesis's author concerning this issue is Real et al. [93], which further develops Soize and Chebli's work [126]. This new strategy considers the separation of uncertainties related to the inner and interface degrees of freedom (DOFs) from nonparametric probabilistic approach applied for each substructure using the Craig-Bampton substructuring method, which means that there is a specific parameter to control the uncertainties for each inner and interface DOFs.

1.3 Purpose and objectives

The purpose of this thesis is to improve the robustness of drilling torsional vibration analysis methods, by taking into account uncertainties in the drill string computational model and the non-linear bit-rock interaction model.

The four objectives are:

1. to establish a novel hysteretic (non-reversible) bit-rock interaction model, which depends not only on the bit speed, but also on the bit acceleration, providing a new representation of stick-slip oscillations due to a torque applied to the bottom-end of the BHA of a drill string, according to experimental and field data observations;

2. to propose a new stochastic model for the bit-rock interaction, considering the stick-slip effects described by the torque on the bit, in terms of parametric probabilistic approach and experimental identification, in order to reproduce the uncertainties related to the cutting process;

3. to construct a new test-rig to analyze drill string dynamics and bit-rock interaction, which is able to reproduce stick-slip phenomena while drilling a rock sample using standard masonry bits, as well as to validate bit-rock interaction models; and

4. to determine an original strategy for modeling uncertainties globally, based on terms of the nonparametric probabilistic approach, considering a simple torsional model for a drill string, which allows to control the dispersion level of each inner and interface DOF of each drill string substructure independently.

An expected result is to provide a new way of modeling the torsional vibrations of a drill string, in order to improve the operational safety and to avoid premature material fatigue, saving operational costs concerning the drilling efficiency, driving energy, and drilling

reliability.

1.4 Organization of the manuscript

In chapter 2, drill string torsional modeling and reduced-order model are described. A new bit-rock interaction model contemplating hysteresis effect is detailed in section 3, and a new stochastic modeling for this new bit-rock interaction model is depicted in chapter 4. In chapter 5, a new test-rig to analyze drill string dynamics and bit-rock interaction is proposed, as well as a comparison of a drilling simulation applying these new models and experimental results is presented. An original strategy for modeling uncertainties globally, based on terms of the nonparametric probabilistic approach, considering a simple torsional model for a drill string, is described in chapter 6, and in chapter 7, conclusions and future works are reported.

Chapter 2

Drill string torsional model

2.1 Torsional model

As mentioned in the introduction (section 1.1), drill strings are composed mainly by two substructures (DP and BHA), as showed in Fig. 2.1. Under operation, drill string rotates around its longitudinal axis due to the angular velocity at the DP top end to drill rocks by the drill bit on the bottom of the BHA. Thereby, a reaction force is applied to the drill bit by the rock in contact with. Although DP and BHA are connected together by shaft couplings, stiffness values of these couplings are considered here as negligible, because they are low enough to bring natural frequencies in torsion down into the range of excitation frequencies [142].

A full description model, including all dynamics, although possible, presents many difficulties due to lack of downhole data. During the drilling process there are many phenomena which are hard to measure, or simply not fully measured. Therefore, simple models can be convenient enough to represent this kind of system. Here, the nominal model of the drill string is constructed as two torsional beams which are discretized by means of the finite element method [42, 50, 106], and a reduced-order model is constructed using the elastic modes. The non-linear bit-rock interaction forces are modeled as a point torque applied at the end of the BHA. This simple model can enable an efficient representation of a drill string.

In this work, a simple torsional model is proposed which considers a drill string as continuous beam with two different parts, characterizing the DP and the BHA with their own stiffness and damping. This proposal is really simple compared to what is found in the literature (see section 1.2), as showed in Fig. 2.1. To do so, it is assumed that there is no warp in cross section under applied torque, there is no lateral contact between the drill string and the borehole, as well the inertial effects due to the global rotation of the drill

string and the gyroscopic effects induced by the transverse displacements are negligible (see [16]). Besides, the transverse and axial deformations are not modeled here.

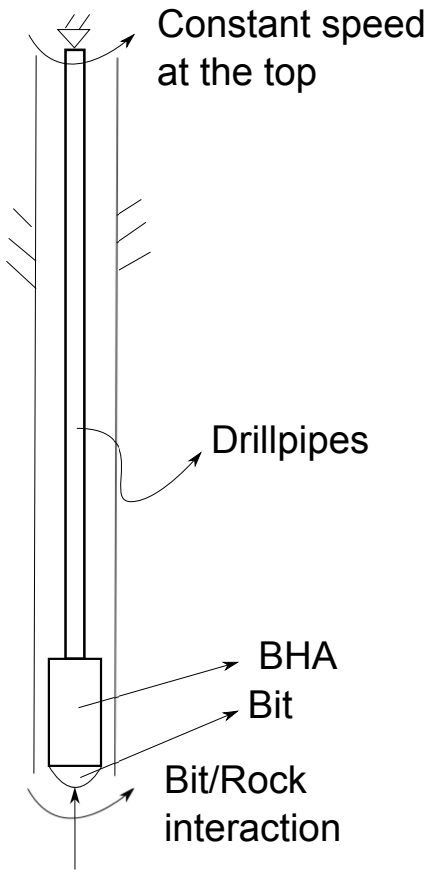

Figure 2.1: General scheme for modeling a drill string.

A simple mathematical model for describing the torsional dynamics of a drill string can be too simple compared to a real system, but it has to be representative enough to describe the phenomena involved [7, 132]. A good mathematical model must be efficient to carry out parametric studies, simple enough to provide insight into the underlying physics, and which retain sufficient details to correlate to real dynamics behaviour. In this case, the torsional dynamics of a drill string can be analyzed by solving the motion equation of a torsional beam [40, 142]

$$\rho J \frac{\partial^2 \theta(x,t)}{\partial t^2} - G \frac{\partial}{\partial x}\left(J \frac{\partial \theta(x,t)}{\partial x} \right) = \mathscr{T}(x,t)\,, \tag{2.1}$$

where $\theta(x,t)$ is the angular rotation about the x-axis (longitudinal axis), J is the cross sectional polar moment of inertia, G is the shear modulus, $\mathscr{T}(x,t)$ is the torque per unit

length. The boundary conditions at the top under constant speed Ω are given by:

$$\begin{cases} \theta(0,t) = \Omega t \\ \dot{\theta}(0,t) = \Omega \end{cases}, \tag{2.2}$$

and the initial conditions are

$$\theta(x,0) = 0, \quad \dot{\theta}(x,0) = \Omega \ , \tag{2.3}$$

Unlike [102, 106], the present strategy solves the system considering its rotational displacements about a rotating frame. Let $\theta^{\text{rel}}(x,t)$ be the relative angular rotation in the rotating frame associated with the imposed angle at the top, as follows

$$\theta(x,t) = \Omega t + \theta^{\text{rel}}(x,t). \tag{2.4}$$

The system is discretized by means of the finite element model, where linear shape functions are applied. Let $\mathbf{u}(t)$ be the vector of $\theta^{rel}(x,t)$ nodal values related to the drill string mesh. Note that, in the rotating frame, the angular displacement is fixed at the top because there is no relative displacement between the top drive and the first node, at the top of the drill string. Adding a proportional damping to the system, the vector $\mathbf{u}(t)$ is solution of the matrix equation [42, 50, 114]

$$[M]\ddot{\mathbf{u}}(t) + [D]\dot{\mathbf{u}}(t) + [K]\mathbf{u}(t) = \mathbf{T}(\dot{\mathbf{u}}(t), \ddot{\mathbf{u}}(t))), \tag{2.5}$$

where $[M]$ is the mass matrix, $[D]$ is the damping matrix, and $[K]$ is the stiffness matrix, and $\mathbf{T}(\dot{\mathbf{u}}(t), \ddot{\mathbf{u}}(t)))$ is the torque vector, which also depends on the angular velocity ($\dot{\mathbf{u}}(t)$) and the acceleration ($\ddot{\mathbf{u}}(t)$), as explained in chapter 3.

According to Eqs. (2.3) and (2.4), the initial conditions in the rotating frame read

$$\mathbf{u}(0) = \mathbf{0}, \quad \dot{\mathbf{u}}(0) = -\Omega\mathbf{1}. \tag{2.6}$$

where $\mathbf{1}$ is a vector with all entries equal to one. All the components of the torque vector are zero except the one corresponding to the drill bit node. For this node, the nonlinear torque applied to the bit is denoted by $T_{\text{bit}}(\dot{\theta}_{\text{bit}}(t), \ddot{\theta}_{\text{bit}}(t))$, where $\dot{\theta}_{\text{bit}}(t)$ is the bit angle within the absolute frame, and will be described in chapter 3.

2.2 Reduced-order model

In order to optimize the computational cost, the size of matrices of the full finite element model n can be reduced by constructing a reduced-order model using the normal modes of the conservative homogeneous system. The m first eigenvalues $0 < \lambda_1 \leq \lambda_2 \leq \ldots \leq \lambda_m$ associated with the elastic modes $\{\phi_1, \phi_2, \ldots, \phi_m\}$ are solutions of the following generalized eigenvalue problem

$$[K]\,\phi = \lambda\,[M]\,\phi\,. \tag{2.7}$$

The reduced-order model is obtained by projecting the full computational model on the subspace spanned by the m first elastic modes calculated using Eq. (2.7). Let $[\Phi]$ be the $n \times m$ matrix whose columns are the m first elastic modes. Then, the displacement vector $\mathbf{u}$ can be approximated by

$$\mathbf{u} = [\Phi]\,\mathbf{q}\,, \tag{2.8}$$

in which $\mathbf{q}$ is the vector of the m generalized coordinates obtained from the following reduced matrix equation

$$[\widetilde{M}]\ddot{\mathbf{q}} + [\widetilde{D}]\dot{\mathbf{q}} + [\widetilde{K}]\mathbf{q} = \widetilde{\mathbf{T}}(\dot{\mathbf{q}}(t), \ddot{\mathbf{q}}(t))\,, \tag{2.9}$$

in which $[\widetilde{M}] = [\Phi]^T\,[M]\,[\Phi]$, $[\widetilde{D}] = [\Phi]^T\,[D]\,[\Phi]$ and $[\widetilde{K}] = [\Phi]^T\,[K]\,[\Phi]$ are the $m \times m$ mass, damping and stiffness generalized matrices, $\widetilde{\mathbf{T}}(\dot{\mathbf{q}}(t), \ddot{\mathbf{q}}(t)) = [\Phi]^T\,\mathbf{T}(t)$ is the vector of the reduced-order generalized torque, with the initial conditions

$$\mathbf{q}(0) = \mathbf{0}, \quad \dot{\mathbf{q}}(0) = -\Omega\,[\widetilde{M}]^{-1}[\Phi]^T[M]\mathbf{1}. \tag{2.10}$$

The set of equations (2.8), (2.9) and (2.10) can be solved using commonly used integration schemes, such as the Euler scheme or the Runge-Kutta, for instance.

Chapter 3

Bit-rock interaction

Due to the bit-rock friction, the slender structure and the contact with mud, drill string dynamic behaviour is under axial, lateral and torsional damped vibrations. As stated previously, this thesis is interested in the steady-state small torsional vibrations of a drill string due to a non-linear torque applied at the bottom-end of the BHA, named torque on bit and denoted $T_{\text{bit}}(\dot{\theta}_{\text{bit}}(t), \ddot{\theta}_{\text{bit}}(t))$, that might lead to stick-slip oscillations.

Stick-slip is an oscillatory twisting evidenced as an oscillatory variation of bit speed ($\dot{\theta}_{\text{bit}}(t)$) [37, 51, 57, 61, 84, 98, 139], which turns the bit locked for a period. In severe conditions, the drill bit sticks (zero bit speed) then slips (high bit speed), and might cause, for instance, measurement equipment failure, low rate of penetration, bit damage, and fatigue [155].

In next sections will be presented some ways to represent the non-linear torque on bit, including hysteretic effects.

3.1 Deterministic average model for bit-rock interaction

As it mentioned before, there are several papers available in the literature concerned with the drill string torsional dynamics and stick-slip oscillations [51, 57, 74, 80, 111, 112, 144]. A model proposed by Tucker and Wang (1997) [138] and used, for instance, by [51, 114, 139], describes a deterministic torque on bit model ($\bar{T}_{\text{bit}}(\dot{\theta}_{\text{bit}}(t))$) which takes into account a non-linear behaviour of a bit-rock interaction for a vertical borehole:

$$\bar{T}_{\text{bit}}(\dot{\theta}_{\text{bit}}(t)) = \mu W_{\text{bit}} \bar{r} \left[tanh(\alpha_0 \dot{\theta}_{\text{bit}}) + \frac{\alpha_1 \dot{\theta}_{\text{bit}}}{1 + \alpha_2 \dot{\theta}_{\text{bit}}^2} \right], \tag{3.1}$$

where μ is friction coefficient, W_{bit} is weight on bit, the bit radius is $\bar{r}$, and $\alpha_{0,1,2}$ are parameters of this model.

This deterministic model for torque on bit ($\bar{T}_{\text{bit}}(\dot{\theta}_{\text{bit}}(t))$) is a reversible model, because it can provide the same torque value for each $\dot{\theta_{bit}}(t)$ value. This model is based on a superposition of the three distinct effects: Coulomb friction (hyperbolic tangential behaviour), Stribeck friction (negatively sloped behaviour) and viscous friction (directly proportional to angular velocity).
Figure 3.1 shows separately the two terms of Eq. (3.1): the first term (*tanh*, in blue) increases fast, and reaches a limit torque value as the speed increases; the second term (fraction term, in green) is responsible for the peak in the bit-rock interaction model, and it dies out as the bit speed increases. The reversible model (Eq. (3.1)) is the sum of these two terms which is represented by the magenta curve. Near zero speed the applied bit-rock interaction model is regularized. Other models consider explicitly stick and slip phases as it can be found in[62].

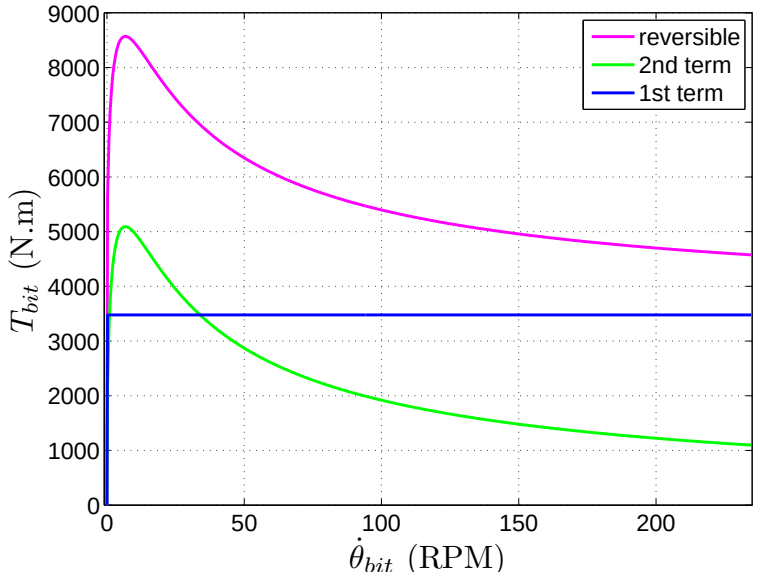

Figure 3.1: Terms of the bit-rock interaction reversible model, Eq. (3.1): *tanh* term in blue, fraction term in green, and complete reversible model in magenta.

Equation (3.1) fits to a common field average behaviour. In order to show that, let consider a real example of drill string described in the table 3.1, according to Ritto et al. [112]. Field data related to this drill string are torque and bit speed, which are observed in a frequency of 50 Hz, during 60 seconds (3,000 records). Thanks to a research collaboration between service company and operator, the BHA was equipped with a high-frequency measurement device. The sub is capable of measuring axial forces,

torque, bending moments, angular speed, and tri-axial accelerations. The data set used in this study corresponds to 3 meters of drilling, where only the on-bottom data (actual drilling) was used. Figure 3.2 shows these measurements during a drilling operation of an ultra-deep-water well.

Table 3.1: Drill string characteristics, according to Ritto et al. [112].

	DP	BHA
Elastic Modulus [GPa]	220	220
Poisson's coefficient	0.29	0.29
Volumetric mass density [kg/m^3]	$7,800$	$7,800$
Length [m]	$4,733.60$	466.45
Inner radius [m]	0.0595	0.0363
Outer radius [m]	0.070	0.0803

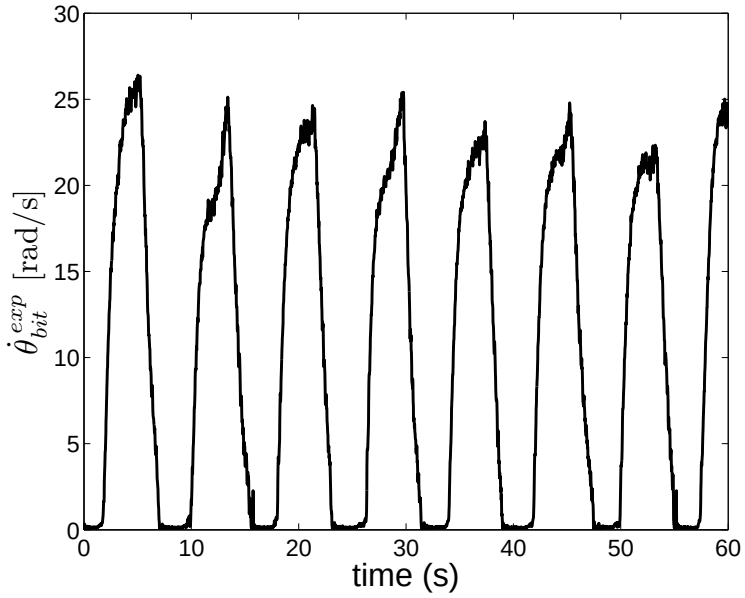

Figure 3.2: Experimental bit speed, according to Ritto et al. [112].

Figure 3.2 shows seven stick-slip entire cycles: when the bit speed is close to zero, the bit is in stick phase; when the bit speed is going up and down, the bit is slipping (slip phase).

For the deterministic curve, the parameters α_0 , α_1, and α_2 were calibrated using the field data disposal in [112]. Classical least square method [3] is applied to identify the parameters of Eq. (3.1): $4,700$ for μ multiplied by weight on bit ($\mathbf{W}_{bit}$), $\alpha_0 = 1.67x10^4$, $\alpha_1 = 5.30$, and $\alpha_2 = 3.45$, all with appropriate units. Figure 3.3 compares the fitted model to the experimental measurements.

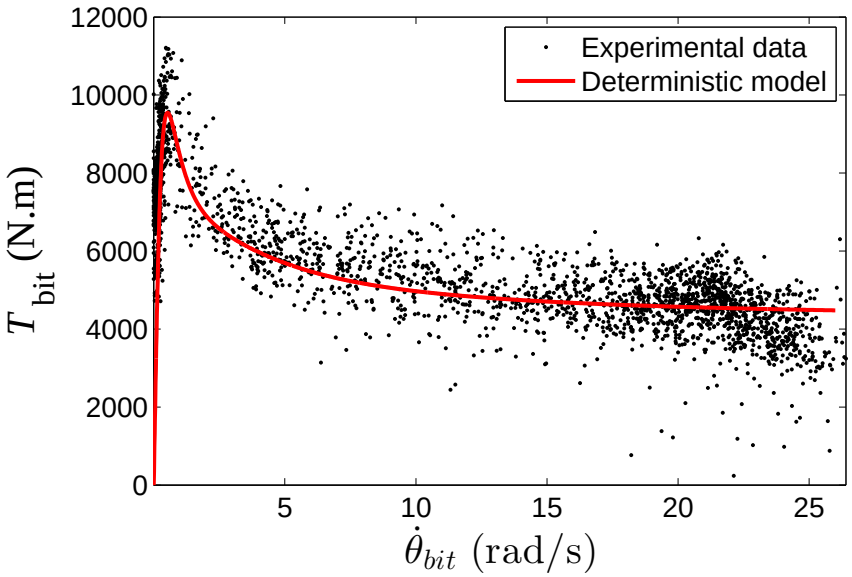

Figure 3.3: Experimental bit-rock interaction (Ritto et al. [112]) and identified average model.

Figure 3.3 shows a good agreement between the deterministic model of bit-rock interaction and the field data. Nevertheless, it can be seen that the experimental data show large fluctuations related to the deterministic model. These fluctuations are explained in the next chapter.

3.2 Hysteretic model for bit-rock interaction

Some authors have highlighted large fluctuations of the nonlinear bit-rock interaction during the drilling, which present a behaviour of hysteretic cycles [62, 85, 94]. Wojewoda et al. [152] noticed that hysteretic effects in dry friction occurrences can appear by tangential stiffness between the bodies in contact during stick phase and stick-slip transition phase, and they can appear during the slip phase, because the existence of frictional memory caused by a lag in the friction force.

Bit-rock interaction is not a real dry friction because the drilling fluid (mud). However, the average behaviour of bit-rock interaction has been represented as a dry friction process, for instance the model proposed by Tucker and Wang (1997) [138]. Therefore, if the average behaviour of bit-rock interaction seems like a dry friction process, hysteresis

can be also valid for bit-rock interaction.

Considering that experimental observations have shown the presence of loops mainly during the slip, and according to [152] the size of this macroscopic sliding loop is related to the velocity rate, we present here a novel hysteretic (non-reversible) bit-rock interaction model [94], which is verified by field data presented in [112] and validated by experimental results. Non-reversible means that the torque on bit is represented not only by the bit speed, but also by the bit acceleration (velocity rate), producing a type of hysteretic cycle, even though when unloaded the torque goes back to zero.

The field data used in section 3.1 was separated in seven entire stick-slip cycles (last one is despised), for which have been smoothed using a time sliding window average (SWA) to remove the measurement noise. Figure 3.4 shows six field data stick-slip cycles. As indicate the arrows of the first graphic of Fig. 3.4, when the bit accelerates, the upper path occurs, and when the bit speed decreases, the lower path occurs. These paths for each entire cycle can be considered as fluctuations of the hysteretic cycles. Based on field experience, the possible cause of the variability of cycles is due to the heterogeneity of rock formation drilled.

These cycles indicate that (1) for each cycle, the torque value for positive and negative accelerations are not the same, that means the hysteretic (non-reversible) phenomenon and (2) each observed cycle is different from one another. This section tackles the first point, i.e., it proposes a bit-rock interaction model including hysteresis, which represents a mean behaviour; the second one will be addressed in chapter 4.

The mean cycle is obtained by applying a SWA methodology, at each bit speed, for the upper phases (positive acceleration) and the lower phases (negative acceleration) separately. Figure 3.5 shows the field stick-slip cycles and their mean. The mean of all cycles (upper and lower) is in blue, and the mean cycle is showed in green. The upper green curve is the mean of upper cycles and the lower green curve is the mean of lower cycles.

If we look at the green line as showed in Fig. 3.5, i.e. the field data mean hysteretic cycle, it is remarked that the thickness of this cycle decreases as the bit speed increases. At some point, the upper and lower curves collapse.

Once fitted, the bit-rock interaction model described by Eq. (3.1) yields an accept-

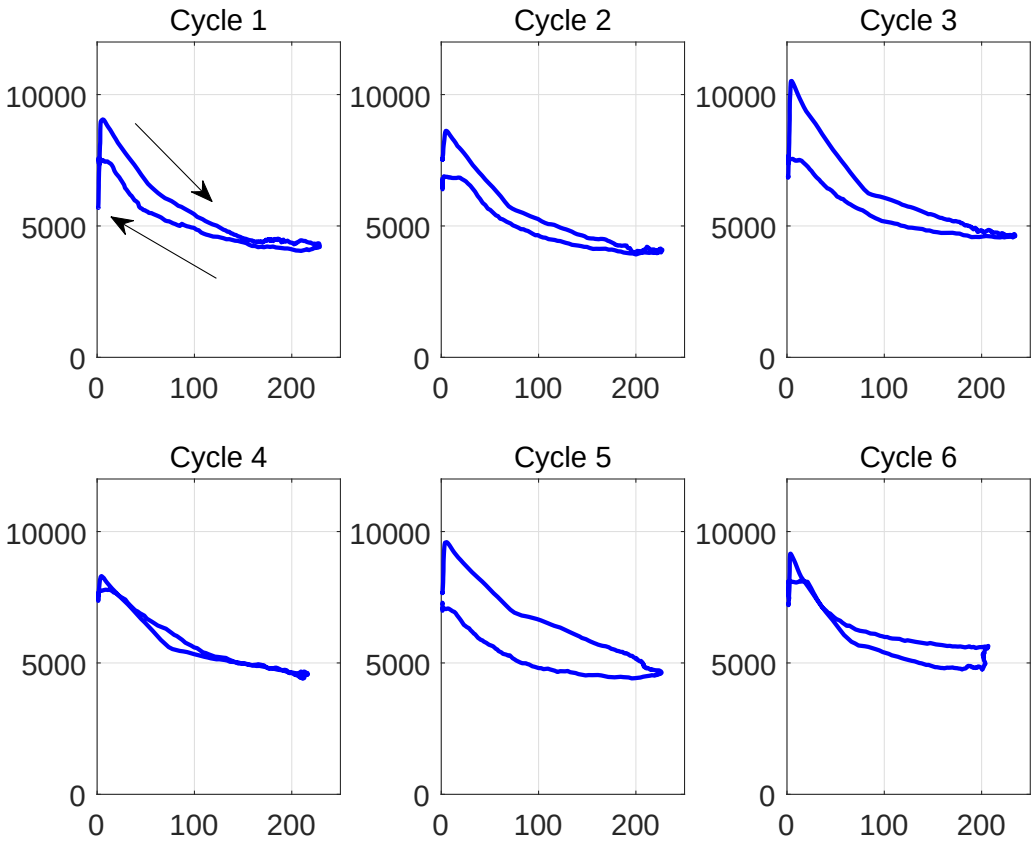

Figure 3.4: Downhole field data, torque [N.m] versus angular speed [RPM] at the bit: six stick-slip cycles available. The path from the top occurs when the bit accelerates, and the path from the bottom occurs when the bit speed decreases. The direction of the cycle is the same for all six cycles.

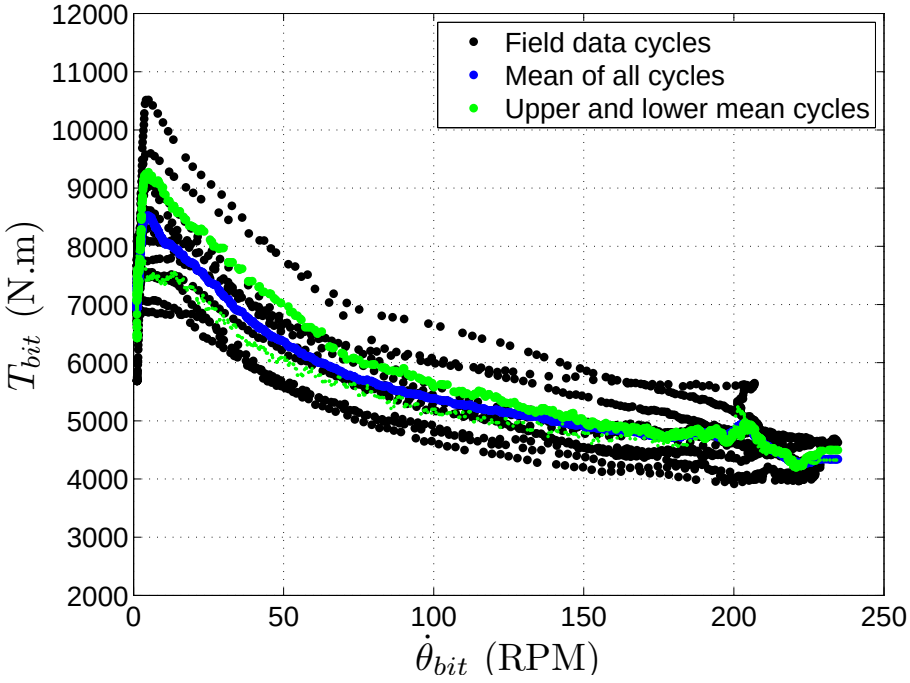

Figure 3.5: Downhole field data: six stick-slip cycles and their mean. The mean of all cycles (upper and lower) is in blue, and the mean cycle is showed in green.

able agreement with the average experimental plots (blue plots in Fig. 3.5). Nevertheless it suffers from two drawbacks: (1) it is not flexible enough to fit correctly the experiments for both low and large velocities; and (2) it cannot generate hysteresis effects in order to separate the forward and backward behaviours (green plots in Fig. 3.5).

In order to improve the model Eq. (3.1), it is proposed two modifications to address these two issues: (1) the power exponents of the bit speed in the fraction term can vary in order to give to the model more flexibility; and (2) the fraction term is modulated by an acceleration (and speed)-dependent factor to obtain different amplitudes for the forward and backward phases.

The new bit-rock interaction model proposed here contains these improvements, and is described by Eq. (3.2).

$$T_{\text{bit}}^{\text{HYS}}(\dot{\theta}_{\text{bit}},\ddot{\theta}_{\text{bit}}) = b_0\left(\tanh(b_1\dot{\theta}_{\text{bit}}) + \frac{b_2|\dot{\theta}_{\text{bit}}|^{b_4}\text{sign}(\dot{\theta}_{\text{bit}})}{1+b_3|\dot{\theta}_{\text{bit}}|^{b_5}}(1+H(\dot{\theta}_{\text{bit}},\ddot{\theta}_{\text{bit}}))\right). \quad (3.2)$$

It is usually observed that the reaction torque is much lower when the bit speed is negative. That is because the bit cutters are not symmetrical. Actually, we do not have enough field data to support any interaction model for $\dot{\theta}_{\text{bit}} < 0$, but, in the cases analyzed in this work, the values of bit speed were always equal or greater than zero.

Note that if $b_4 = 1$, $b_5 = 2$ and $H = 0$ it can be retrieved the bit-rock interaction model found in Eq. (3.1). The parameters b_4 and b_5, with $0 < b_4 < b_5$, depend on the bit and rock properties. The parameter b_0 [N.m] represents the weight on bit, the friction coefficient and the bit radius (for instance, this parameter might be written as $b_0 = \mu W_{\text{bit}} \bar{r}$).

The proposed model, Eq. (3.2), allows a better fit with the field data points. H is the hysteretic function: if it is equal to zero, the model is reversible, with no hysteretic cycles. The hysteretic model is only activated if H is different from zero, where H is presented in Eq. (3.3).

$$H(\dot{\theta}_{\text{bit}}, \ddot{\theta}_{\text{bit}}) = \beta_1 \tanh(\beta_2 \ddot{\theta}_{\text{bit}}) \operatorname{sign}(\dot{\theta}_{\text{bit}}), \tag{3.3}$$

which means that the variation of bit speed (bit angular acceleration) should be taken into account, and the hysteretic cycle is limited $(1 \pm \beta_1)$. Figure 3.6 shows the hysteretic term as a function of the bit acceleration. It increases fast, and reaches a limit value as the acceleration increases/decreases. In the present case, β_1 is identified experimentally as 14%, i.e., the hysteretic cycle is within plus or minus 14% of the reversible model. In addition, note that $(1 + H)$ is multiplying only the second term of the bit-rock interaction model (the fraction term), such that as the bit speed increases the thickness of the hysteretic cycle decreases, as it is observed in most field data cycles showed in Fig. 3.4, and also in the field data mean cycle showed in Fig. 3.5.

Figure 3.7 shows the hysteretic bit-rock interaction model for positive bit speeds. The arrows indicate the path of the cycle. The curve in blue happens when the bit acceleration is positive, and the curve in green happens when the bit accelaration is negative.

First, the Eq. (3.2) with $H = 0$ is considered, in order to check the equivalence to Eq. (3.1). The fitted parameters of the bit-rock interaction model are: $b_0 = 3478$, $b_1 = 938$, $b_2 = 2.56$, $b_3 = 0.38$, $b_4 = 0.78$, and $b_5 = 1.1$, with appropriate units. Figure 3.8 shows the mean of the field data together with the fitted model. The blue line is the same field data blue line as showed in Fig. 3.5. There is a very good agreement between the bit-rock interaction model and the field data.

Now the model including hysteresis is considered, Eq.(3.2) with $H \neq 0$. The fitted

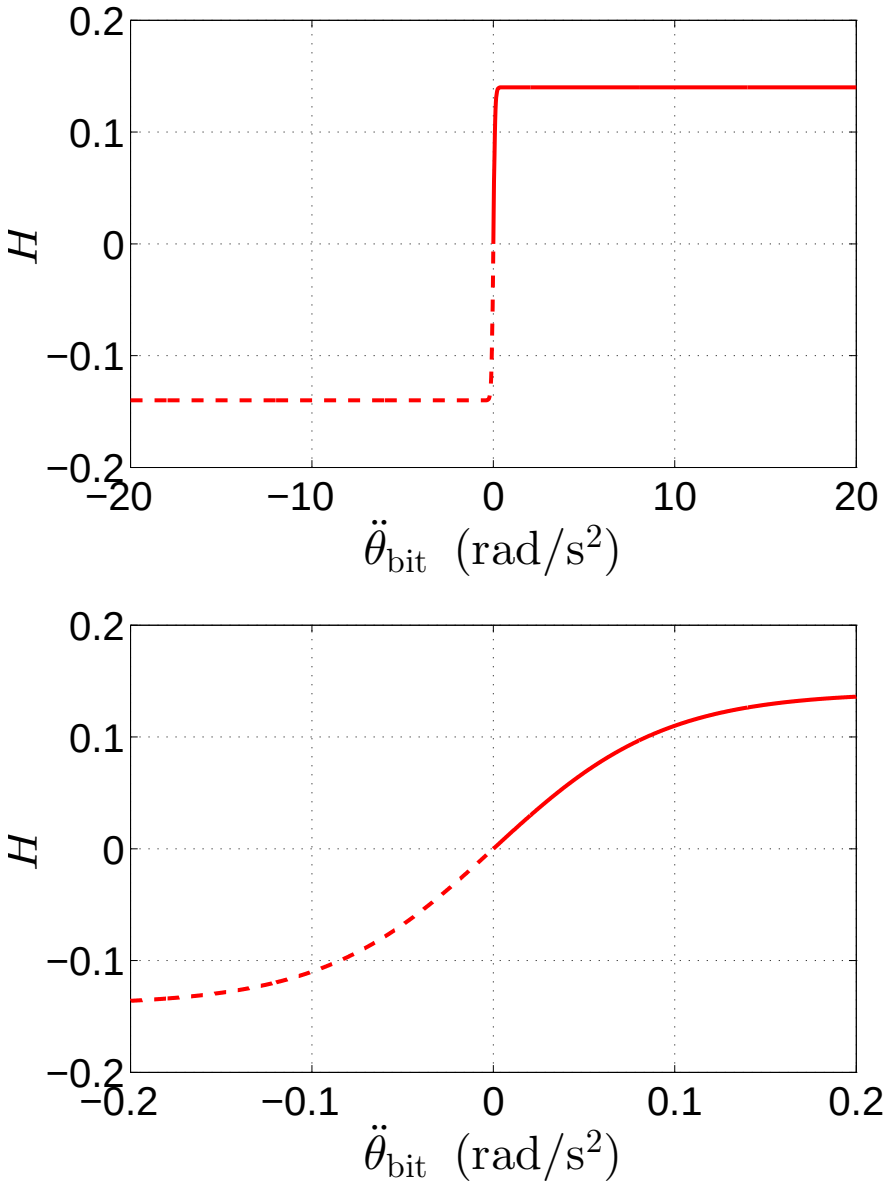

Figure 3.6: Hysteretic term H as a function of the bit acceleration (top graph) and a zoom image (bottom graph).

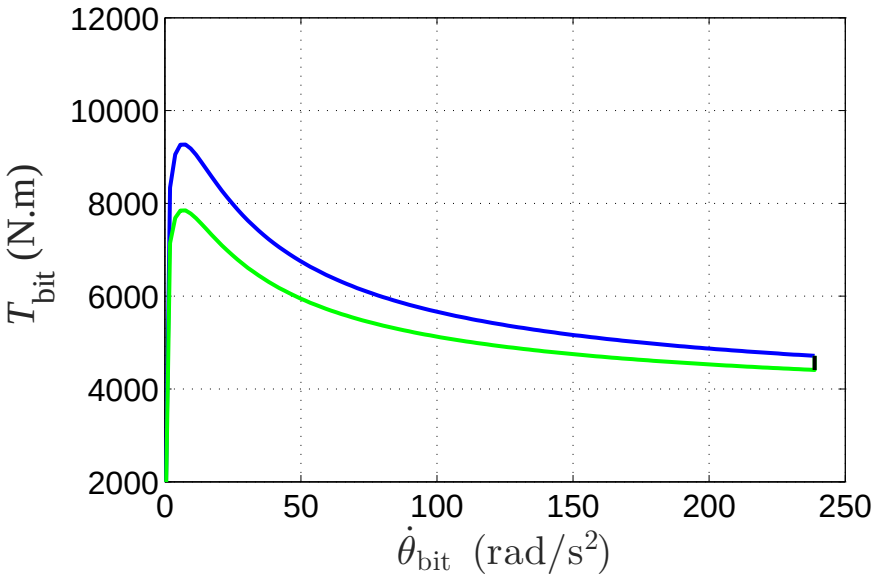

Figure 3.7: Hysteretic bit-rock interaction model. Blue line when the bit acceleration is positive and green line when the bit accelaration is negative.

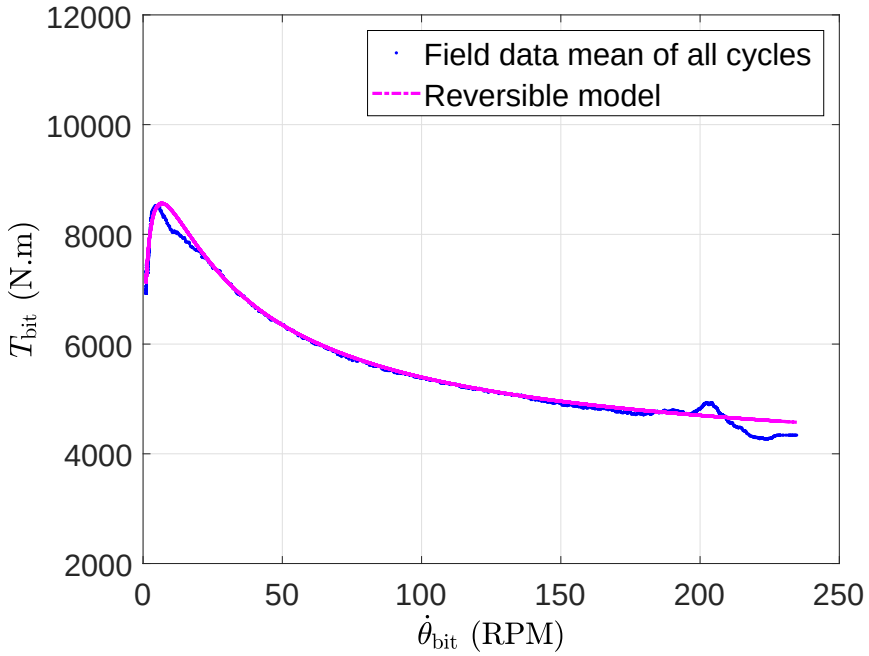

Figure 3.8: Field data vs. bit-rock interaction reversible model, (Eq. (3.1)): Fitted model in magenta and mean field data in blue.

parameters of the hysteretic function are: $\beta_1 = 14\%$, $\beta_2 = 10.6$, with appropriate units. Figure 3.9 shows the field data upper and lower mean cycles together with the fitted hysteretic bit-rock interaction model. The green lines are the same field data green lines as showed in Fig. 3.5. Again, there is a very good agreement between the proposed bit-rock interaction model and the field data.

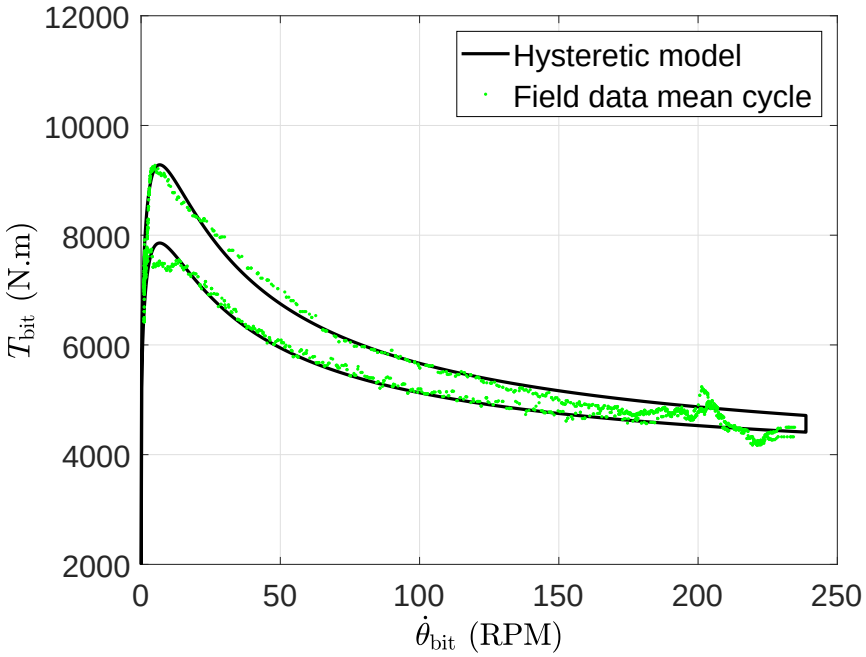

Figure 3.9: Field data vs. hysteretic bit-rock interaction model (Eq. (3.3)): fitted model in black, and mean cycle of field data in green.

A larger hysteretic cycle is also considered, with $\beta_1 = 56\%$. This parameter was chosen such that all field data cycles (black lines in Fig. 3.5) fit in. Finally, Fig. 3.10 shows the three bit-rock interaction models that will be used for computations: (1) fitted reversible model (magenta line), (2) fitted model with hysteresis effects (black line), and (3) model with large hysteresis effects (red line). The parameters used in the computational model are the ones that were fitted with the available field data: $b_0 = 3478$, $b_1 = 938$, $b_2 = 2.56$, $b_3 = 0.38$, $b_4 = 0.78$, $b_5 = 1.1$ and $\beta_2 = 10.6$. For model number (1) $H = 0$, for model number (2) $\beta_1 = 14\%$, and for model number (3) $\beta_1 = 56\%$.

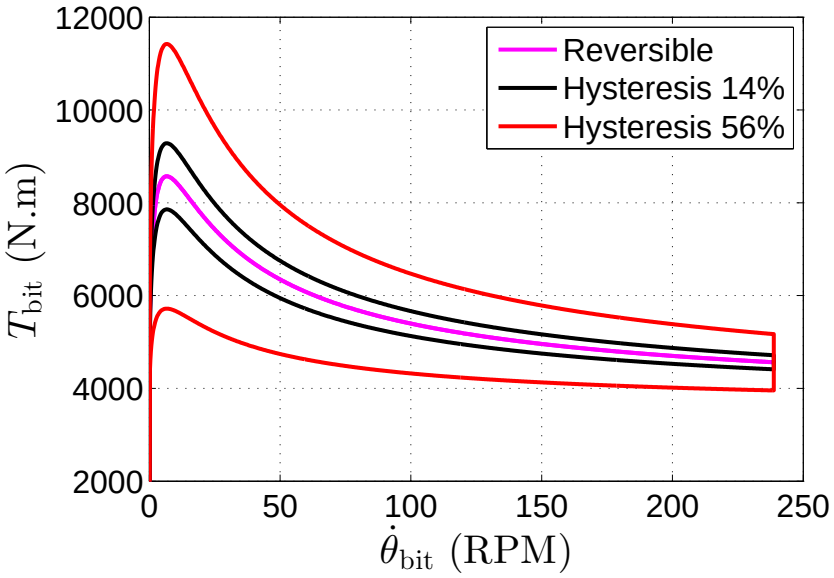

Figure 3.10: Bit-Rock interaction models (Eqs. 3.1 and 3.3): (1) reversible (magenta), (2) hysteretic $\beta_1 = 14\%$ (black), and (3) hysteretic $\beta_1 = 56\%$ (black).

3.3 Stability analysis of the hysteretic model

In order to construct a stability map, Monte Carlo simulations are done considering the variation of top speed from 50 up to 160 RPM, and the WOB from 5 up to 60 klbf (22 to 267 kN). Simulations consider the drill string described on table 3.1, mass and stiffness matrices using 100 finite elements, damping matrix is diagonal with damping ratios (identified experimentally) equal to 0.095 for the first mode, and 0.02 for all the other modes, and the modified Euler scheme (see Appendix A) with a time step 0.512 ms is implemented to approximate the solution of the ordinary differential equation (ODE). The first five natural frequencies computed for the system are: 0.13, 0.42, 0.74, 1.07, 1.41 Hz.

The bit-rock interaction model showed in Eq. (3.2) was calibrated considering 245 kN, and the model assumes that $T_{\mathrm{bit}}^{\mathrm{HYS}}(\dot{\theta}_{\mathrm{bit}}, \ddot{\theta}_{\mathrm{bit}})$ is linear with respect to the WOB, varying the coefficient b_0 linearly. Thus, a coefficient is used to multiply the coefficient b_0 of the Eq. (3.2) such that different values of WOB can be simulated. For example, if the WOB is 200 kN, then the coefficient b_0 of the Eq. (3.2) must be multiplied by $200/245 = 0.816$.

The torsional stability of a drill string can be quantified through the stick-slip severity factor, defined by

$$SS(\dot{\theta}_{top\ drive}) = \frac{\dot{\theta}_{bit}^{MAX} - \dot{\theta}_{bit}^{MIN}}{2\dot{\theta}_{top\ drive}} \tag{3.4}$$

where $\dot{\theta}_{bit}^{MAX}$ and $\dot{\theta}_{bit}^{MIN}$ are maximum and minimum values respectively for bit speed of a chosen range sample, and $\dot{\theta}_{top\ drive}$ is top drive speed.

In case of pure slipping, $SS(\dot{\theta}_{top\ drive}) = 0$. If there are stick-slip oscillations then $SS(\dot{\theta}_{top\ drive}) > 0$. If there is no torsional oscillations, $SS(\dot{\theta}_{top\ drive}) = 0$. If there is stick-slip oscillations ($\dot{\theta}_{bit}^{MIN} = 0$) and the maximum bit speed ($\dot{\theta}_{bit}^{MAX}$) is two times the nominal surface speed ($\dot{\theta}_{top\ drive}$), then $SS(\dot{\theta}_{top\ drive}) = 1$. If $SS(\dot{\theta}_{top\ drive})$ is lower than 0.5 the system will be consider stable, otherwise it is considered unstable [112].

The stability map is constructed as follows. For each pair (WOB,$\dot{\theta}_{top\ drive}$) the bit speed is computed and $SS(\dot{\theta}_{top\ drive})$ is recorded for the steady state response. Figure 3.11 shows the stability map when employing the bit-rock interaction models 1 (reversible) and 2 (small hysteresis effects). It can be noted that the maximum $SS(\dot{\theta}_{top\ drive})$ value is greater for the reversible bit-rock interaction model (model 2), but, at the same time, the stability region (dark blue) is a little bigger when employing this model. Now let us analyze Fig. 3.12, which shows the stability map when employing the bit-rock interaction model 3 (large hysteresis effects). This last chart presents a stability region (dark blue region) bigger than the other two charts.

This means, in one hand, that the hysteresis favours the stability of the system. It seems that when the bit speed decreases, and $T_{\text{bit}}^{\text{HYS}}(\dot{\theta}_{\text{bit}}, \ddot{\theta}_{\text{bit}})$ is in the lower curve of the hysteretic cycle (see Fig. 3.10), it allows the system to escape from instability. On the other hand, it can also be obverved that the instability region (orange-red region) in Fig. 3.12 presents values of $SS(\dot{\theta}_{top\ drive})$ higher than the charts in Fig. 3.11. Hence, at the same time that the hysteresis in the bit-rock interaction model favours the stability of the system for low values of weight on bit and high values of nominal surface speed, it favours the aggravation of the torsional oscillations of the system for high values of weight on bit and low values of nominal surface speeds. Since $T_{\text{bit}}^{\text{HYS}}(\dot{\theta}_{\text{bit}}, \ddot{\theta}_{\text{bit}})$ passes through the upper curve of the hysteretic cycle (see Fig. 3.10) the amplitude of the stick-slip oscillations increases as well.

In summary, hysteretic effect favors the stability of the system for high nominal surface speeds and low WOB and induces also higher stick-slip oscillations for low nominal surface speeds and high WOB.

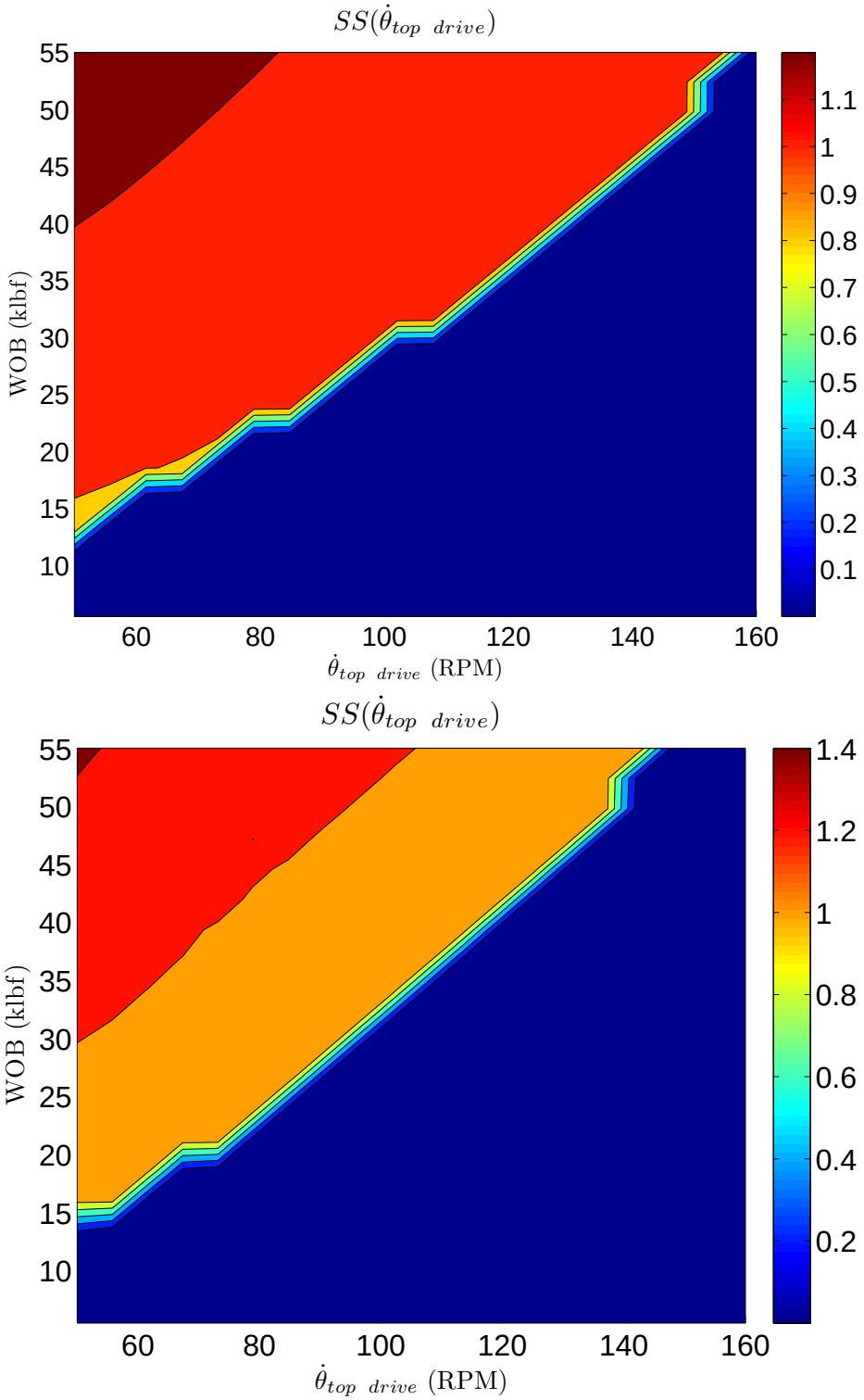

Figure 3.11: Stability map for models 1 (reversible) and 2 (hysteretic $\beta_1 = 14\%$).

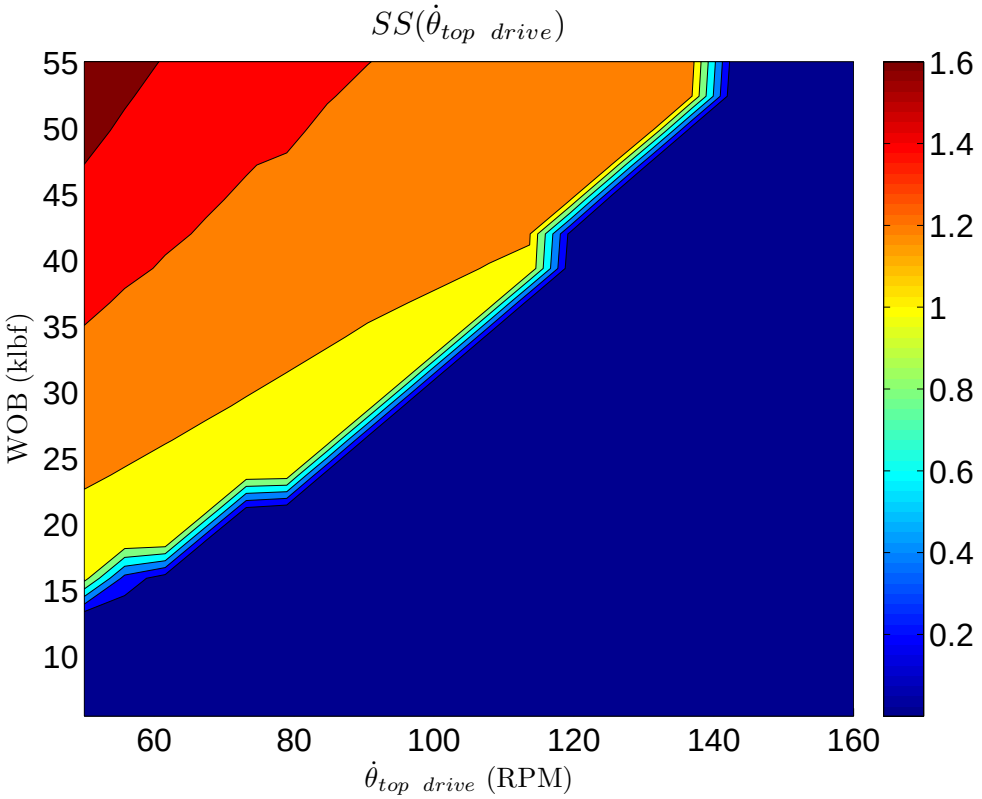

Figure 3.12: Stability map for the model 3 (hysteretic $\beta_1 = 56\%$).

Chapter 4

Stochastic modeling for bit-rock interaction

There are sources of uncertainties related to the drill string dynamics and bit-rock interaction, such as material properties, unknown geometry, rock properties and its resistance for cutting process, etc. Besides, the linear torsional model used here is a simple representation of the torsional vibration of the drill string yielding some model-form uncertainties.

In this chapter, we are interested in uncertainties related to the stochastic fluctuations of the torque on bit. Here we propose a new stochastic model for the bit-rock interaction considering these uncertainties. The proposed stochastic model considers the hysteretic model for torque on bit presented in the previous chapter, including a multiplicative stochastic process.

The idea concerning the stochastic fluctuations of the bit-rock interaction model by including a multiplicative stochastic process to the deterministic models is because the range variation of these fluctuations: if it take a look at the field data in Fig.3.5, it is noticed that the torque on bit varies from about 7 to 10.5 kNm, when the bit speed is close to 10 RPM; for higher speeds (above 200 RPM), the torque on bit varies from about 4 to 5.8 kNm. The distance between the higher and lower values is very different, depending on the bit speed: 3.5 and 1.8 kNm. But, for both speeds the torque on bit is varying plus or minus 20%.

Here we describe this new stochastic non-linear bit-rock interaction model which is constructed by introducing a multiplicative stationary Gaussian stochastic process. Field data are used to calibrate the power-spectral density function of this stochastic process. Once calibrated, independent realizations can be generated and statistics on the drill string dynamical behaviour can be estimated using the Monte Carlo simulation method.

4.1 Construction of the stochastic model

Stochastic fluctuations of the bit-rock interaction model are taken into account introducing a multiplicative stochastic process to the hysteretic model according to the Eq. (3.2), as follows:

$$T_{\text{bit}}^{STO}(\dot{\theta}_{\text{bit}}, \ddot{\theta}_{\text{bit}}) = T_{\text{bit}}^{\text{HYS}}(\dot{\theta}_{\text{bit}}, \ddot{\theta}_{\text{bit}})\,(1 + \eta(t)), \tag{4.1}$$

where $\eta(t)$ is a centred stochastic process $\eta(t)$ which can be rewritten as

$$\eta(t) = \frac{T_{\text{bit}}^{STO}(\dot{\theta}_{\text{bit}}, \ddot{\theta}_{\text{bit}})}{T_{\text{bit}}^{\text{HYS}}(\dot{\theta}_{\text{bit}}, \ddot{\theta}_{\text{bit}})} - 1. \tag{4.2}$$

The experimental stochastic process $\eta^{\text{exp}}(t)$ can be computed using Eq. (4.2) and the field data related to the torque on bit (see Fig.3.5 in section 3.2), which means the upper phases (positive acceleration) and the lower phases (negative acceleration) as $T_{\text{bit}}^{STO}(\dot{\theta}_{\text{bit}}, \ddot{\theta}_{\text{bit}})$ (green lines), and $T_{\text{bit}}^{\text{HYS}}(\dot{\theta}_{\text{bit}}, \ddot{\theta}_{\text{bit}})$ equal to the mean of all cycles obtained by SWA methodology (blue line). This stochastic process is showed in Fig.4.1. Unfortunately, there is not enough field data to completely characterize this stochastic process. Here, it will assume that $\eta(t)$ is a centred stationary Gaussian stochastic process. This assumption will be verified in experimental data (see chapter 5).

A model for the stochastic range $\eta(t)$ must be constructed using the information provided by the experimental stochastic process $\eta^{\text{exp}}(t)$. In that case, if it is assumed a Gaussian distribution, $\eta(t)$ is completely determined by its Power Spectral Density ($S(f)$) [75]. $S(f)$ is estimated using the Periodogram Method [91]. There are variations of Periodogram Method, including filters for smoothing. Here, it is appropriate to use the classical method proposed by Schuster (1898) [120], in order to preserve a raw behaviour from the field data. For this reason, it is necessary to obtain average functions for $S(f)$, represented by the function $\bar{S}(f)$), in order to regularize its behaviour.

Periodogram Method requires interpolated data from the field data over a regular grid. Therefore, interpolated data is measured in peaks from the torque on bit field data related to its average, and normalized by it. The regular grid is obtained by the limits of

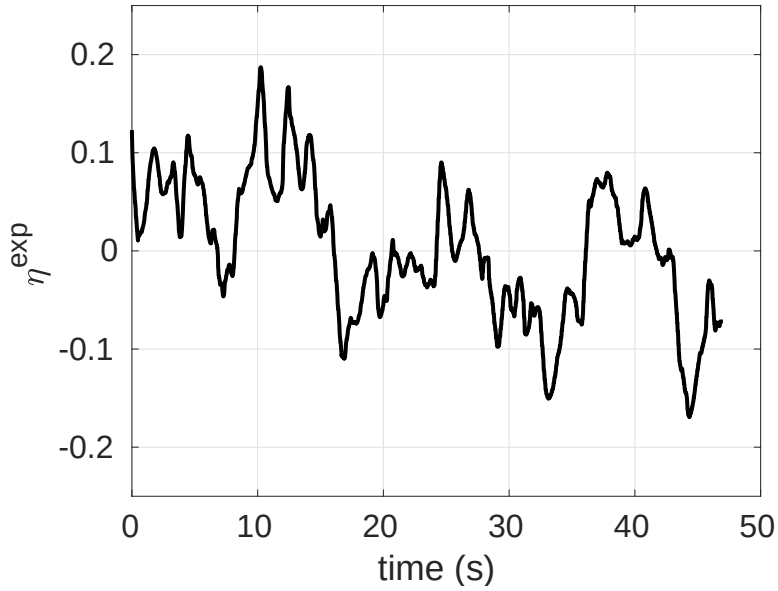

Figure 4.1: Stochastic process $\eta^{\exp}(t)$ obtained experimentaly with field data.

time range, which is divided by a regular step, as follows:

$$\bar{T}_{\mathrm{bit}_{\mathrm{Interp}}}(\dot{\theta}_{\mathrm{bit}}(t),\ddot{\theta}_{\mathrm{bit}}(t)) = \frac{\sum_{i=1}^{nb} \bar{T}^{exp}_{\mathrm{bit}_{\mathrm{inside-window}}}(\dot{\theta}_{\mathrm{bit}}(t),\ddot{\theta}_{\mathrm{bit}}(t))}{nb}, \tag{4.3}$$

where $\bar{T}_{\mathrm{bit}_{\mathrm{Interp}}}(\dot{\theta}_{\mathrm{bit}}(t),\ddot{\theta}_{\mathrm{bit}}(t))$ is the interpolated torque on bit, $\bar{T}^{exp}_{\mathrm{bit}_{\mathrm{inside-window}}}(\dot{\theta}_{\mathrm{bit}}(t),\ddot{\theta}_{\mathrm{bit}}(t))$ is the normalized torque on bit interpolated over a regular grid, and *nb* is related to a given precision parameter proportional to the number of records. The window width is determined by *nb* close to the available data values for $\dot{\theta}_{\mathrm{bit}}(t)$, that means for each interpolated point, it is going to be used the same size of sliding-window (same *nb*). Figure 4.2 shows the estimated field data PSD.

Regarding Fig. 4.2, the PSD is constant until a critical frequency and then decreases linearly (in log-log scale). This type of PSD is often encountered when addressing turbulent forces [5]. Then the proposed PSD model $\bar{S}(f)$ is written as

$$\begin{aligned} \log(\bar{S}(f)) &= A_0 \quad \text{for} \quad \mathrm{f} < \mathrm{f}_0\,, \\ \log(\bar{S}(f)) &= a\log(f) + b \quad \text{for} \quad \mathrm{f} \geq \mathrm{f}_0\,, \end{aligned} \tag{4.4}$$

where f_0, A_0, a and b are the parameters of the model. These parameters are calibrated using the experimental PSD such that $f_0 = 0.27$, $A_0 = -7.6$, $a = -3.13$ and $b = -11.67$ (with appropriate units). Figure 4.3 compares the calibrated PSD model with field data PSD, where a reasonable agreement is observed.

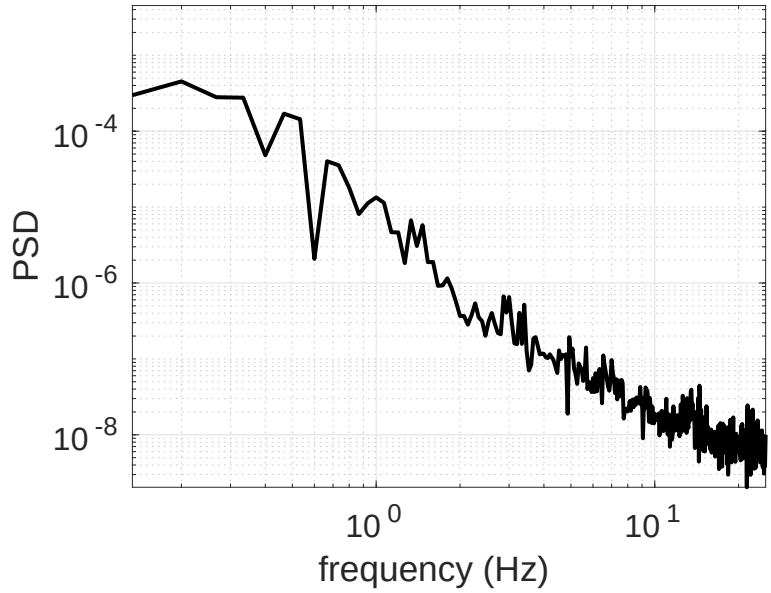

Figure 4.2: Field data PSD.

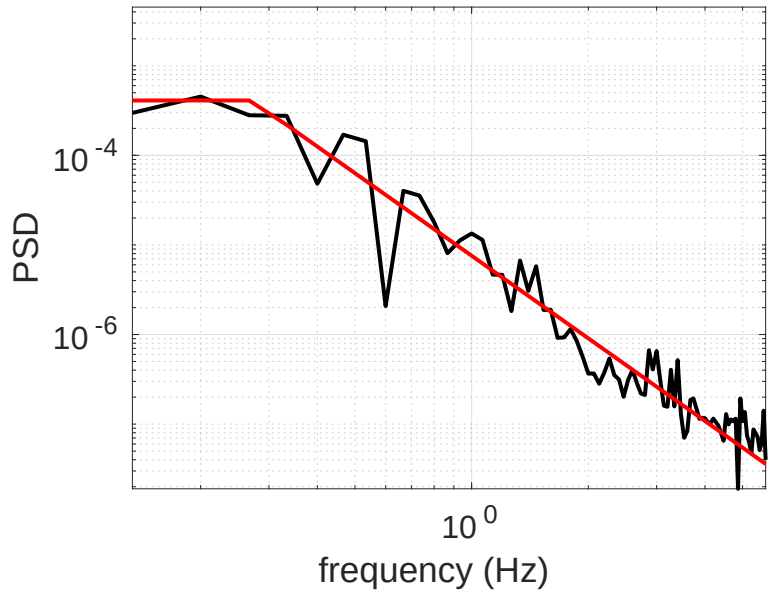

Figure 4.3: Zoom image of the comparison between the calibrated PSD (in red) and the field data PSD (in black).

With the PSD $\bar{S}(f)$ in hands one can generate independent realizations of the stochastic process $\eta(t)$ using a classical generator of Gaussian process [8], i.e., an aleatory Gaussian process is generated using values provided by PSD $\bar{S}(f)$ over a given f range. Figure 4.4 shows two independent trajectories of $\eta(t)$, which again give reasonable agreement with the observed process $\eta^{\text{exp}}(t)$ showed in Figure 4.1.

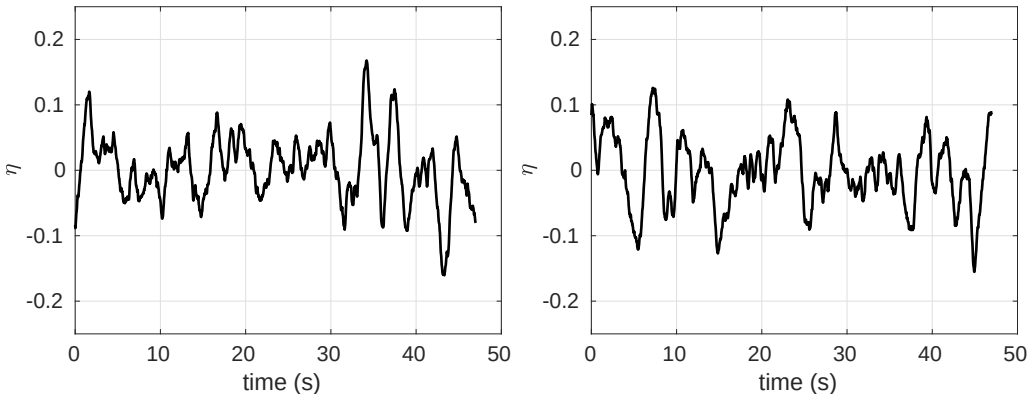

Figure 4.4: Two independent realizations of the stochastic process $\eta(t)$.

4.2 Simulation of the stochastic drill string dynamics

4.2.1 Analysis of one realization of the stochastic drill string dynamical response

The previous section was concerned with the construction of a stochastic bit-rock interaction model including hysteretic cycles fluctuations. A stationary stochastic process was introduced for the computation of the torque on bit, Eq. (4.1). The stochastic bit-rock interaction model is then added to the torsional drill string model, Eq. (2.9), and the stochastic non-linear dynamical response of the drill string is computed and analyzed. Note that Eq. (2.9) becomes random because of the random bit-rock interaction, Eq. (4.1). The general integration scheme for one realization of the stochastic bit-rock interaction model is presented in Algorithm 1 using field data from table 3.1. A step-by-step algorithm for drilling simulation is described in Appendix B.

The mass and stiffness matrices are constructed using 100 finite elements, after convergence check. The generalized damping matrix is diagonal with damping ratios equal to 0.095 for the first mode, and 0.02 for all the other modes, where these values are identified experimentally. The first five natural frequencies computed for the system are: 0.13, 0.42, 0.74, 1.07, 1.41 Hz.

The non-linear equation (2.9) is solved using a modified Euler scheme (see Appendix A) with a time step 0.512 ms. For one realization of the stochastic bit-rock interaction model, Figure 4.5 shows the stochastic response of the drill string in the stationary regime. In comparison with Fig. 3.5, it can be observed the same stochastic behaviour but with a slightly larger value of the maximum bit speed. This difference is due to the finite element model used here which can not reproduce all the complexity of a real drill string dynamics. But the objective here concerns the construction of the stochastic bit rock interaction model which should not depend on the computational model of the drill string.

Algorithm 1: Simulation of the drill string dynamics.

INITIALIZATION:

Generate a realization of stochastic process $\eta(t)$;

$\mathbf{q}_0 = \mathbf{0}$;

$\dot{\mathbf{q}}_0 = -\Omega\,[\widetilde{M}]^{-1}[\Phi]^T[M]\mathbf{1}$;

LOOP: for $k = 1,\ldots,(n_t)$ **do**

Update the angle and angular speed (depending on the integration scheme):

$(\dot{\mathbf{q}}_{i-1}, \dot{\mathbf{q}}_{i-1}) \rightarrow (\dot{\mathbf{q}}_i, \dot{\mathbf{q}}_i)$;

$\dot{\mathbf{u}}_i = [\Phi]\,\dot{\mathbf{q}}_i$;

$\dot{\theta}_{\text{bit,i}} = \dot{u}_{\text{bit,i}} + \Omega$;

$\ddot{\theta}_{\text{bit,i}} = \ddot{u}_{\text{bit,i}}$;

Calculate the torque on bit:

$T^{STO}_{\text{bit,i}}(\dot{\theta}_{\text{bit,i}}, \ddot{\theta}_{\text{bit,i}}) = T^{\text{HYS}}_{\text{bit}}(\dot{\theta}_{\text{bit,i}}, \ddot{\theta}_{\text{bit,i}})(1+\eta_i(t))$;

Calculate the torque vector $\mathbf{T}_i$;

Calculate the reduced-order torque vector $\tilde{\mathbf{T}}_i = [\Phi]^T\mathbf{T}_i$

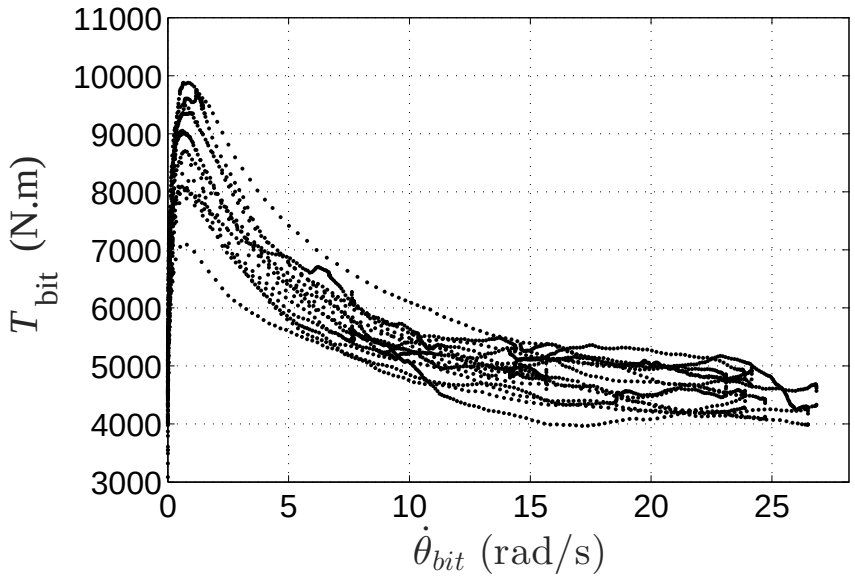

Figure 4.5: One realization of the simulated bit-rock interaction.

Figure 4.6 compares the random bit response using the proposed stochastic bit-rock interaction model with the response obtained using the deterministic model described by Eq. (3.2). While a 3-cycles periodic regime (limited by red dash-dot lines) is reached for the deterministic case, as expected, no periodicity is observed in the stochastic case.

For the deterministic case, the 3-cycles periodic sequence for the duration of the stick and slip phases are respectively $(1.34, 2.53, 2.48)$ s and $(5.4, 6.28, 6.41)$ s . For the stochastic case, these durations are random and their associated probability distribution (obtained

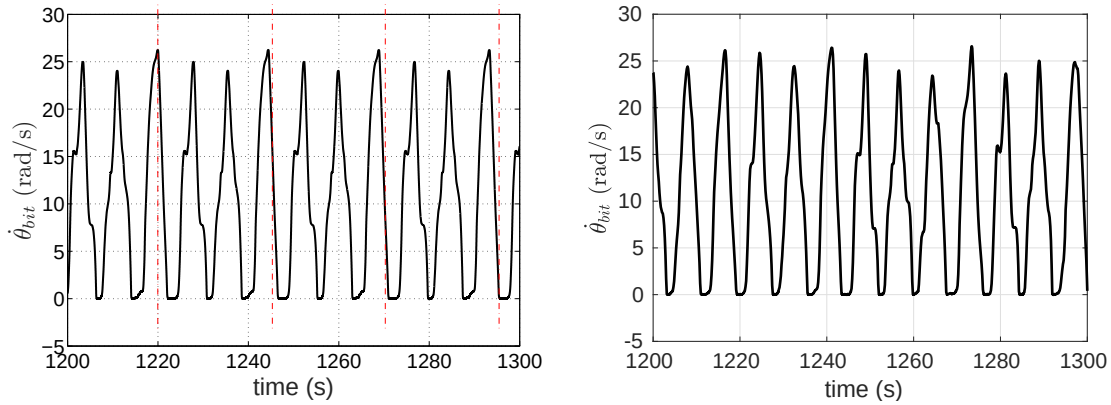

Figure 4.6: Bit speed: deterministic bit-rock interaction model (left, 3-cycles periodicity observed) and stochastic bit-rock interaction model (right, no periodicity observed).

statistically using 750 cycles) are represented on Fig. 4.7.

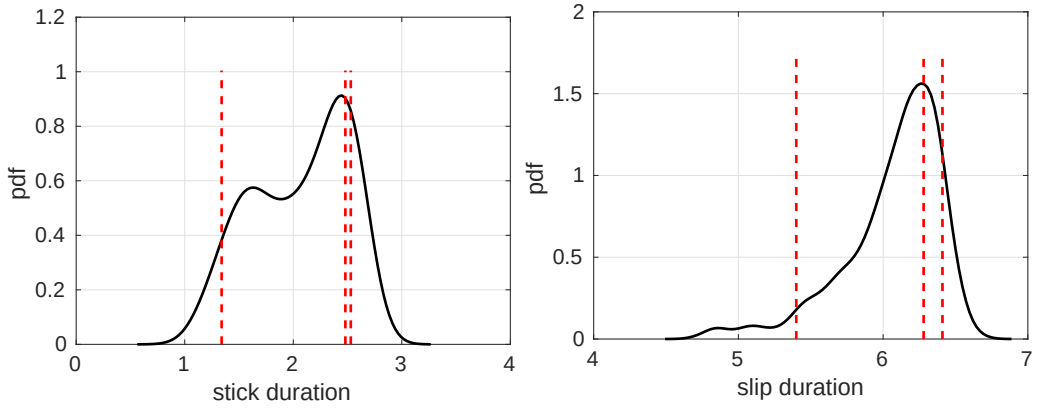

Figure 4.7: Random stick and slip phases duration: probability density functions (black line) and corresponding 3-cycles periodic values calculated with a deterministic bit-rock interaction model (red vertical lines)

It can be seen in these figures, a large variability of the stick and slip durations with modes closed to values corresponding to the values calculated with a deterministic bit-rock interaction model.

4.2.2 Stochastic stability analysis

Now the analysis is extended to quantify statistics on the stability threshold of the system, as the imposed speed at the top varies. The torsional stability of a drill string can be quantified through the stick-slip severity factor as defined in Eq. (3.4).

First, the deterministic system is analyzed. The stick-slip severity factor in the range $B = [6;27]$ rad/s is plotted in Fig. 4.8. As expected, the stick-slip severity factor decreases when the imposed rotation at the top increases. If the speed at the top is lower than 16 rad/s, $SS(\dot{\theta}_{top\ drive})$ is greater than 0.5.

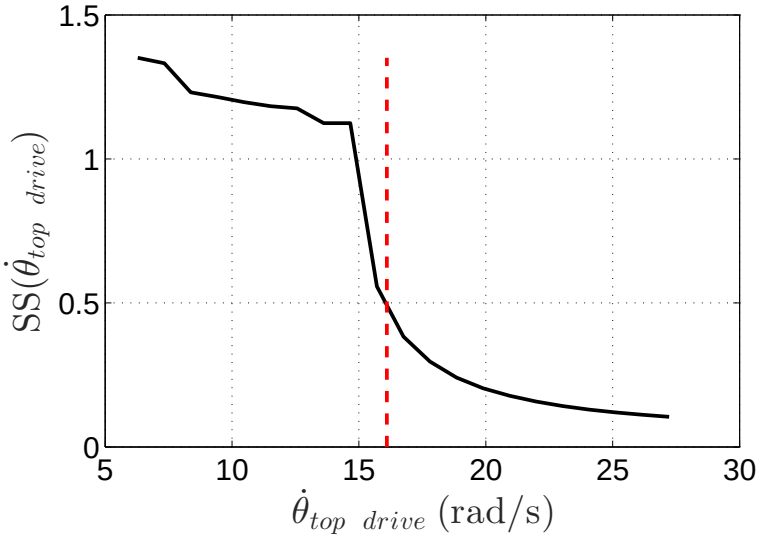

Figure 4.8: Stick-slip severity factor for a deterministic bit-rock interaction. Red dashed line indicates the stability threshold of SS($\dot{\theta}_{top\ drive}$).

For the stochastic bit-rock interaction model, the stick-slip severity factor becomes random and its statistics are estimated using the Monte Carlo simulation method with $n_s = 500$ samplings, according the Eq. (C.1) of convergence analysis in Appendix C.

Figure 4.9 shows statistics on the random stick-slip severity factor. The statistical envelope showed in Fig. 4.9, due to the stochastic bit-rock interaction, yields large fluctuation in the random stick-slip severity factor. This means that bit-rock interaction variability has a direct impact on the drill string stability and should therefore be taken into account for a robust analysis of the drill string dynamics. The results show that when the top speed is about 20.5 rad/s the system has 5% probability of having the value of $SS(\dot{\theta}_{top\ drive})$ greater than 0.5. The probability of instability increases as the speed decreases. This result brings much more information comparing with the deterministic result, where, for the same threshold of $SS(\dot{\theta}_{top\ drive}) < 0.5$, the limit speed of 16 rad/s was obtained.

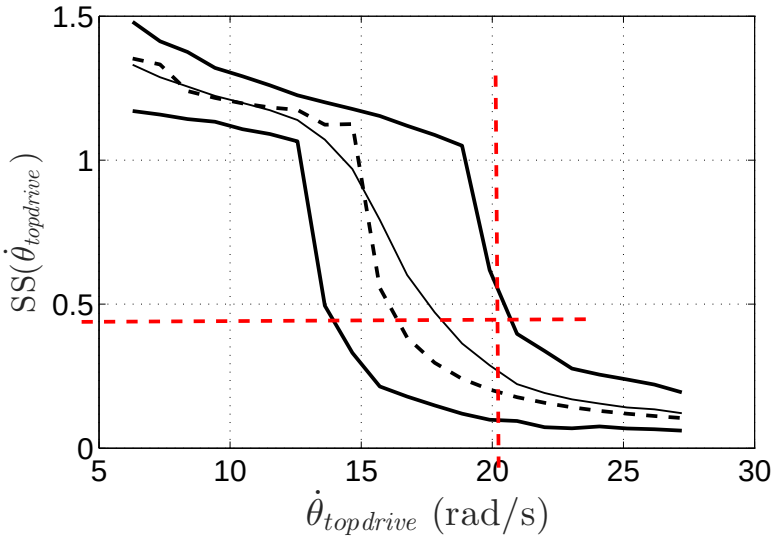

Figure 4.9: Random stick-slip severity factor for a stochastic bit-rock interaction. Solid lines: mean response and 90% confidence region. Dashed line: deterministic case (black), stability threshold (red).

Chapter 5

Test-rig for experimental results

A test-rig has been developed in order to simulate torsional drill string dynamics for validating and calibrating deterministic and stochastic models for the bit-rock interaction [95]. The concept was to design and to construct a test-rig which would be able to reproduce stick-slip phenomena while drilling a rock sample. The proposed test-rig was based on the project developed by [13] with some improvements: (1) test-rig is in vertical position instead of horizontal; (2) a mandrel and a standard masonry bit are used to drill a rock sample (made of concrete), while in [13] friction is induced by pins; (3) a platform holds the test-body and an electrical jack provides the test-body lift. In the design process, low-cost and simple construction were prerequisites.

The designed test-rig is showed in Fig. 5.1. The idea is to isolate torsional and axial vibrations from lateral ones by assembling a slender steel bar, representing the drillpipes, between two bearings that are disposed on two extremes of it (one right after the top drive and another one just before the mandrel). The upper part of the rig consists on an electric drive motor, a slender cylindrical bar, a inertial disk, and a masonry bit. Those elements represent the top drive, the drillpipes (DP), the bottom-hole assembly (BHA), and the drill bit, respectively. The lower part consists of a rock sample, a holder, a platform to support the holder and an electrical jack to lift the sample for drilling.

5.1 Test-rig setup

DP is represented by a slender and cylindrical steel bar with 1,530 mm length and 5 mm diameter. On the cylindrical bar bottom, BHA is made by an inertial disk with 28.4 mm thickness and 138 mm diameter and a mandrel, as showed in Fig. 5.1. A drill bit (standard masonry bit) is attached to them for drilling a concrete cylinder (test-body),

which is placed in a rock holder and can be changed for another kind of rock according to the user's desire. Rock holder is fixed in a platform set (see Fig. 5.2) that can rotate along vertical axis and it is attached to an electrical jack that is responsible for vertical displacement to turn possible its drilling.

Top drive is composed by a DC Brushless motor, which is controlled using an Eletronic Speed Control Module (ESC) model ESC Emax 25A. This drive set is capable of achieving 300 RPM, 8 Nm torque, and it is responsible for applying the torque and for creating an angular speed on the cylindrical bar. A cantilever load-cell (model BSPH4-10kg, Weightech) at the top is connected to the back of DC Brushless Motor in order to measure the torque made by this motor through the measured force. Two encoders (model H40, LS Mecapion) are also used to measure the angular position of the cylindrical bar at the top (close to the drive) and at the bottom (close to the bit).

Rock holder (where the test-body is fixed) is placed on the platform set supported over 3 load-cells (capacity range equal to 0-50 kg of each one) that measure the normal interaction force between the drill bit and the test-body, which corresponds to weight on bit (WOB) (see Fig. 5.3). WOB, as expressed in the oil industry, is the amount of downward force exerted on the drill bit. Although this set is free to rotate, a perpendicular rod was installed under it, which is fixed on a cantilever load-cell (capacity range equal to 0-10 kg) for measuring the torque on bit. This load-cell is fixed at the electrical jack that is not free to rotate. This system allows the measurement of the torque on bit just in one direction. Supporting the rock holder and the platform, there is an electrical jack to lift it to turn viable the drilling. This system is able to simulate an usual condition of penetration for Polycrystalline Diamond Compact (PDC) bits, that means 2.8-4.2 mm/s. Lift distance and rate of penetration (ROP) are measured by two optical sensors (Balluf BOD26K LA01 C 06) disposed side by side to get the distance average. This system is able to measure a distance between 0 and 30 mm according to the principle of triangulation. Drive torque, torque on bit, drive and bit speeds, drive and bit rotation, and WOB are recorded by a data acquisition device controlled by Labview graphical interface that allows the real-time response monitoring.

Figure 5.1: General view of test-rig.

Figure 5.2: Bit, test-body and platform set view.

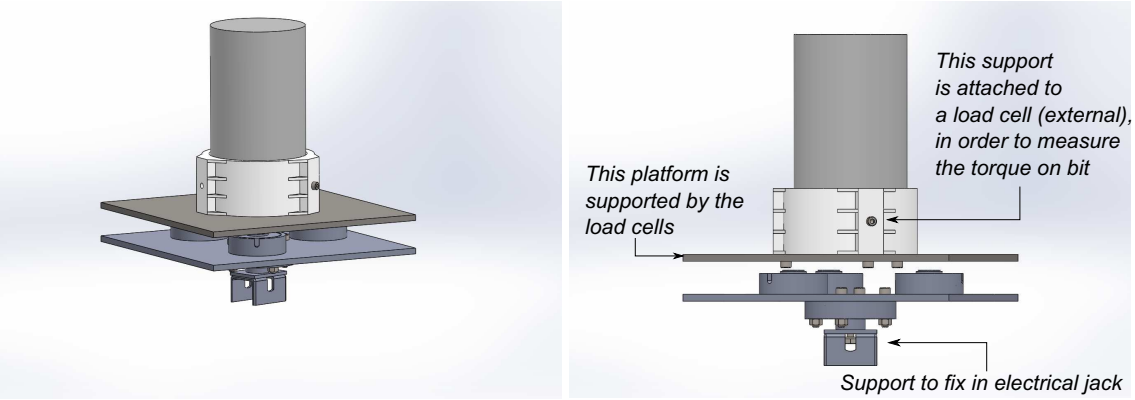

Figure 5.3: Platform design - general and load cell views.

5.2 Experimental planning

Matlab is used to design the experiments considering just one kind of material (test-body of ordinary concrete - 30 fck, 100 mm diameter, 200 mm length), one target value of rate of penetration (ROP), close to 2 mm/s, and 10 samples, and drive speed varying from 100 to 220 RPM, in increasing steps of 20 RPM. For these conditions, the experimental planning has resulted at 210 tests during 70 hours, considering 20 minutes per test. The planning has considered the top drive speed and bit diameter as input variables, and the WOB, torque on bit and bit speed as output variables.

5.3 Experimental results

5.3.1 Test-rig set-up and proceedings

Experiments are demanded to check the consistency of data results to improve the reliability of test-rig results. Test-rig constitutive characteristics are showed in table 5.1.

	DP	BHA
Elastic Modulus [GPa]	220	220
Poisson's coefficient	0.29	0.29
Volumetric mass density [kg/m^3]	7,800	7,800
Length [m]	1.700	0.028
Radius [m]	0.0025	0.069
Mass [kg]	0.260	3.921

Table 5.1: Test-rig characteristics.

Masonry bits (average mass of bits are considered in BHA mass) are assembled in mandrel of diameters equal to 8 mm, 10 mm, and 12 mm. Test-body of ordinary concrete (30 fck, 100 mm diameter, 200 mm length) is applied as rock (for bit-rock interaction), and 10 samples for each target drive speed (100, 120, 140, 160, 180, 200, and 220 RPM). All these combinations mean 210 tests, as previewed by 5.2.

Experimental natural frequencies are measured: 20 Hz is the first natural frequency for platform set plus electrical jack set, and 3 Hz is the value for the torsional natural frequency of the column. To mitigate the influence of platform set vibrations, a second order filter of Infinite Impulse Response (IIR) is applied with lowpass band set to 10

Hz for the hole sensors in Labview code (software for acquiring experimental data), including the encoders.

The test procedure relates the test-rig operation in order to get experimental results of torsional drill string dynamics, as drive torque, torque on bit, drive speed, bit speed, and WOB, being able to simulate torsional vibrations (stick-slip oscillations). Tests are done according to steps as follow:
(1) run the bridge calibration for all active modules for acquiring data, where is applicable;
(2) lift the platform set close to the drill bit of 12 mm;
(3) adjust the power supplier of the electrical jack for desired platform set lifting;
(4) adjust the desired drive motor rotation;
(5) lift the platform set in order to drill the body-proof adding water;
(6) observe the WOB values until stick-slip begins (WOB value will vary according to rotation, bit and test-body hardness);
(7) drill at least 10 mm depth into the test-body, checking the time range equal to 60 seconds as a minimum, a total of 10 holes;
(8) Change to the 10 mm diameter drill bit and repeat from item (4) to (7) in the existing holes, in order to optimize the use of test-body, and, after that, change to the 8 mm diameter drill bit and repeat from item (4) to (7) again.

5.3.2 Experimental data analysis

Matlab is used to obtain graphics from experimental data. Figure 5.4 summaries all 210 tests through stick-slip severity factor (Eq. (3.4)). All experimental data are available on blog [100]. All results refer to some of the phenomena that occur in real drilling operations. Stick-slip oscillations are present in all the situations with different severities depending on the drilling conditions (top drive speed, rock strength, bit diameter, etc), being more evident between 120 and 160 RPM in 10 and 12 diameter bits.

Top drive speed decreases between 40% and 60% during drilling, oscillating around a mean value. It happens because the top drive control is based on open-loop system. Some measurements presented long time of stick phase due to the lateral friction between drilled material and the bit, enforcing how is important to establish a maximum value for borehole depth in test procedure. *SS* sustains its average until 160 RPM and decreases after that.

A bit wear control was done to verify if there is some influence on the results: after all tests, the bit wear is 2% for each masonry bit, lower than the uncertainty of test measurements which is 3%. Uncertainty of test measurements is calculated by sum between the biggest value of intrinsic uncertainty of all instruments in parallel (1%) and the acquisition data set (2%).

Besides, fluctuations of these 210 samples were analyzed to check if a previous assumption is correct concerning the centered stationary Gaussian random process. For the whole samples, the fluctuations $\eta^{\exp}(t)$ are analyzed and the its average is equal to 7.8296×10^{-5}, and its standard deviation is approximately constant, and equal to 0.4674, that means these fluctuations can be considered as a centered stationary Gaussian random process.

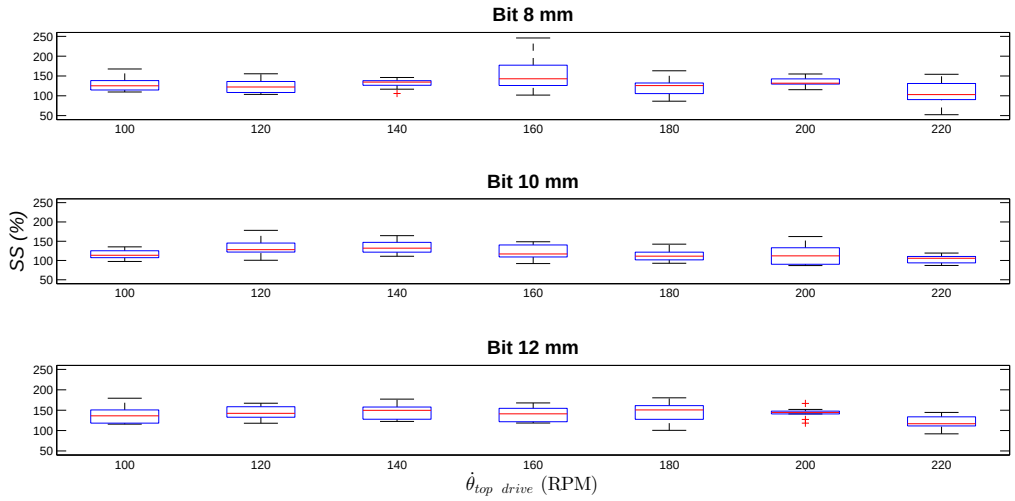

Figure 5.4: Box-plot of 210 test-rig experiments.

One sample is extracted from the total ones and it is explored below. The chosen sample number is 175 in which the bit diameter is 12 mm and the nominal top drive speed is 160 RPM. The total sample time is 60 seconds and 3 seconds are separated in order to allow an analysis in detail of the stick-slip mechanism.

Figure 5.5 shows the experimental results for sample 175 in test time. The stick-slip phenomenon is clearly present during almost all the time of test. Stick-slip is identified by high fluctuations of bit speed that achieves values between 0 and almost 200 RPM while the average top drive speed is 78 RPM. These variations are also noticed in torque on bit and WOB. It is possible to identify 3 time intervals (28s-30s, 50s-52s and 56s-58s, approximately) in which bit sticks for a longer time. This happens when

the top drive is not able to overcome the reactive torque. Sometime, the bit sticks and achieves a reactive torque that electrical motor is not able to overcome. In these cases, it is necessary to relief WOB in order to decrease the torque on bit. Besides the variations due to stick-slip in WOB, there is also a lower frequency variation. This lower frequency variation is due to the control mechanism of electrical jack (that is performed setting input voltage constant and using a switch).

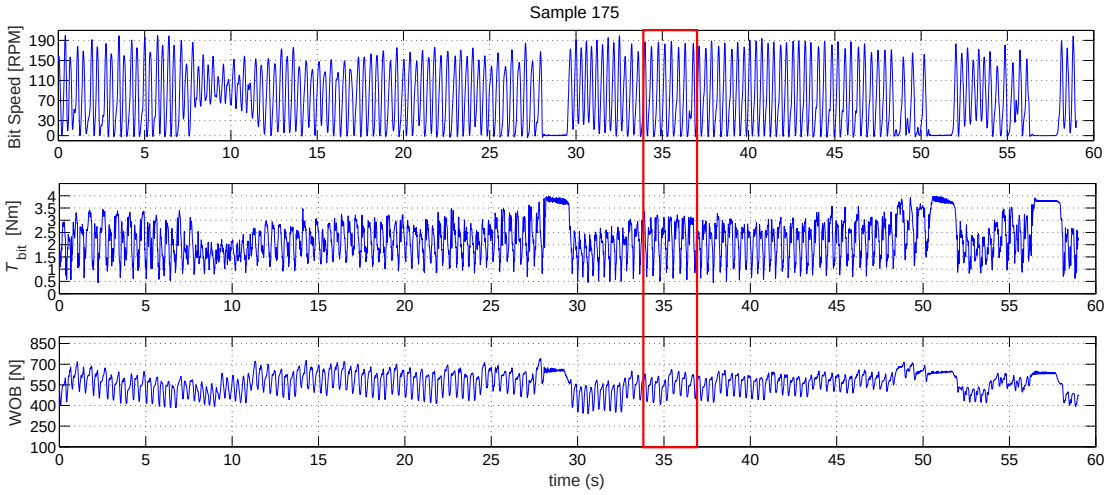

Figure 5.5: Full data of bit speed, torque on bit and WOB for sample 175. The red box is the time interval used in the detailed stick-slip mechanism analysis.

In Fig. 5.6, seven stick-slip cycles are separated from sample 175 to be analyzed. Six vertical lines are drawn for one cycle in order to explain the mechanism in detail. This cycle was chosen because bit sticks at a sufficient time to provide an influence in the other variable. The explanations presented here are in agreement with the ones presented by Shen et. al [122], which used field data to explain stick-slip mechanism. The description of the mechanism for each point highlighted in fig. 5.6 is as follows:

1. Bit is stuck, the torque on bit starts to increase due to the accumulation of strain energy in the drill string and WOB is high.

2. Bit is released and speed starts to increase. Torque on bit achieves its maximum value that represents the maximum cutting resistance imposed by the rock. WOB is approximately at the same level.

3. Bit speed is increasing and achieves the value of average top drive speed indicating that drill string start to lose strain energy. Torque on bit starts to decrease and WOB achieves its local maximum value and starts to decrease as well.

4. Bit speed is at local maximum and torque on bit is at local minimum, as WOB. At this point, torque on bit starts to increase again and bit speed reduces.

5. Bit speed is decreasing and torque on bit is increasing. WOB starts to increase. The behavior of WOB can be explained because just before bit sticks, it induces a reduction of ROP and this is done by an increase in WOB.

6. Bit sticks again and stick-slip cycle restarts. Torque on bit achieves maximum value again just before decreasing to a value just enough to overcome applied torque and maintain the bit stuck. WOB increases and achieves a new value.

This analysis reinforces the fact that torsional vibrations are coupled with axial vibrations, and the bit-rock interaction is an important source of this coupling.

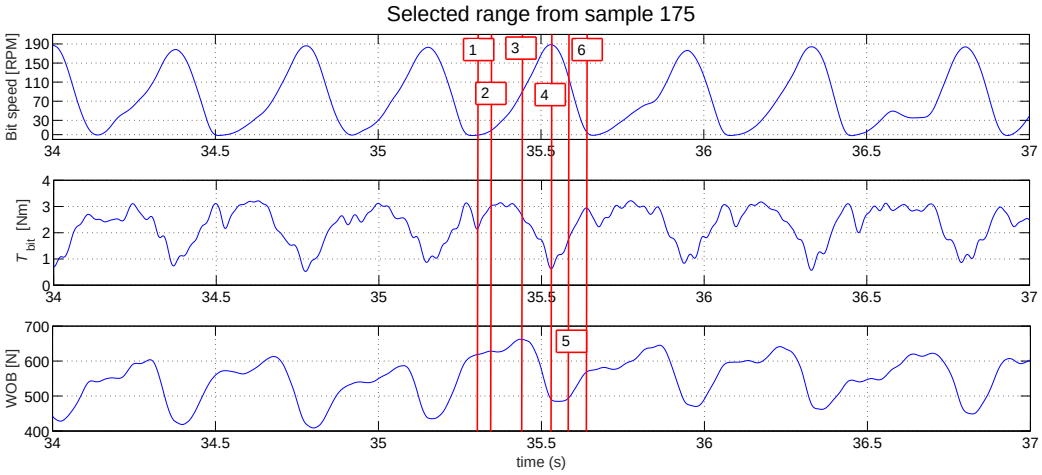

Figure 5.6: Data from sample 175 with a time interval from 34 to 37 seconds.

Figure 5.7 is generated considering the stick-slip cycle explained before. The red dots represent the start point of the cycle and the red arrows indicate the progressive direction of stick-slip cycle. Figure 5.7(a) shows the bit speed variation which begins at zero, achieves its local maximum value and then returns to zero, as noticed before. Figure 5.7(b) plots the torque on bit versus bit speed. This graph is generally used to describe bit-rock interaction in torsional vibration of drill strings. The so called velocity weakening effect [85, 112] is present in which torque on bit decreases with bit speed. Another identified phenomenon is the hysteresis effect, i.e., the fact that torque on bit decreases when bit speed increases in a different path then torque on bit increases while bit speed decreases. In all the analyzed situations, torque on bit decreasing path is almost always above the increasing path. This phenomenon was first mentioned in literature in [85] and modeled in [37, 94]. Shen et. al [122] also observed this behavior through field

data. In fig. 5.7(c), the WOB is plotted versus bit speed and another cycle is noticed. This cycle can be one of the factors that contributes for stick-slip being a self sustained phenomenon. As in torque on bit, there is a hysteric effect in this system in which the path during bit speed increasing is different from the path during bit speed decreasing.

Rock resistance variation of test-body material can cause the WOB variation. That is related to the cutting process and the severity of stick-slip: during the cutting process, WOB increases when the bit is starting the cutting process and it is relieved according to the rock resistance decreases, when it appears an upward force acting on the drill bit due to helical deformation of the steel cylindrical bar [48]. Depending on the magnitude of rock resistance, WOB can decrease in different rates and, depending on the cumulative energy during the stick and rock resistance, WOB can ”return” below or above its initial trajectory. If the bit deceleration in slip phase is more severe, the trend is to ”return” above its initial trajectory (higher magnitude); otherwise, the trend is to ”return” below its initial trajectory.

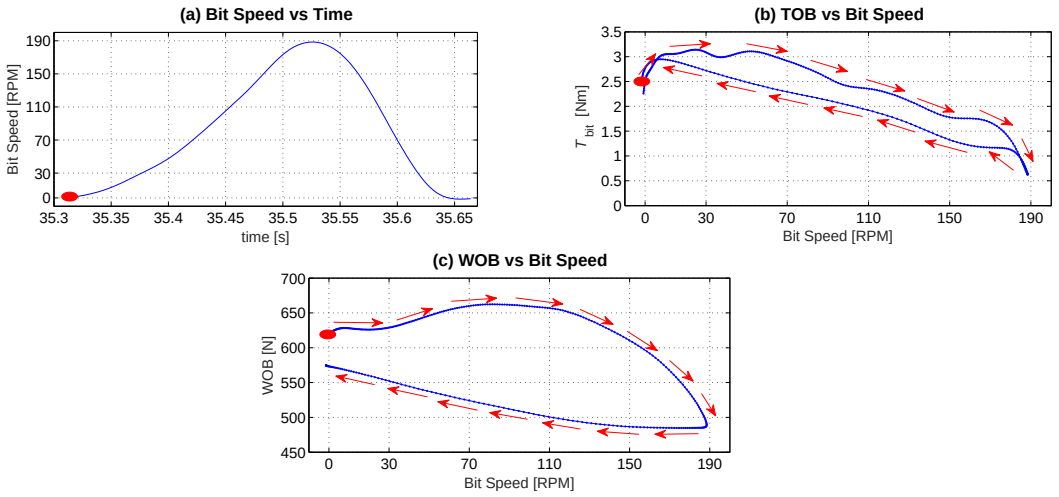

Figure 5.7: Stick-slip cycle from sample 175 for time interval from 35.3 to 35.67 seconds. (a) bit speed versus time; (b) torque on bit versus bit speed and; (c) WOB versus bit speed.

Three more samples were selected to show other stick-slip cycles. Figure 5.8 shows time intervals of 5 seconds of stick-slip cycles for 4 samples. The orange line represents the sliding-window average. In samples 93 and 115, the bit diameter is 10 mm and average top drive speed is approximately 65 and 82 RPM, respectively. Otherwise, samples 165 and 175 are related to a bit diameter of 12 mm and average top drive speed of 81 and 78 RPM, respectively. There are two types of variation in this figure: the first is related to the cycles of the same sample with theoretically the same drilling conditions; the second is related to the variation between the samples. The first kind of variation elucidates the

presence of uncertainties in bit-rock interaction. The second kind shows that bit-rock interaction depends on the drilling conditions.

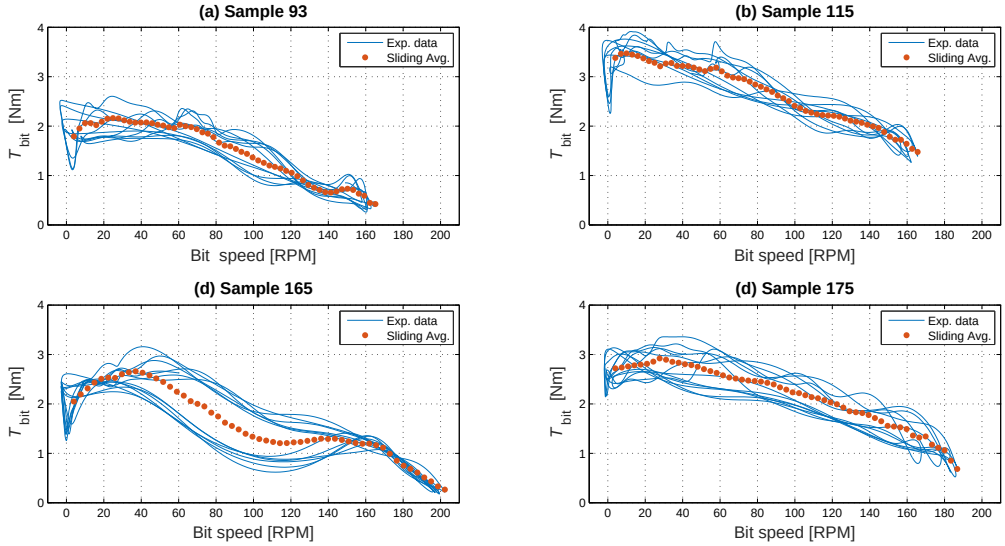

Figure 5.8: Stick-slip cycles for 4 different samples (93, 115, 165, and 175). The cycles corresponds to a time interval of 5 seconds in each sample.

5.3.3 Comparison between experimental data and mathematical models - validation of test-rig results

To validate the test-rig results, experimental data are compared to mathematical models. Experimental results are compared to two known models: (1) a commonly used nonlinear reversible (regularized model) bit-rock interaction model which is given by Eq. (3.1); (2) a simple non-regularized and reversible bit-rock interaction model, which is introduced by [112] using polynomial functions:

$$T_{\mathrm{bit}_{\mathrm{non-reg}}}(\dot{\theta}_{\mathrm{bit}}) = \begin{cases} r_{WOB}(a_0 + a_1\dot{\theta}_{\mathrm{bit}})1.36, for \dot{\theta}_{\mathrm{bit}} \leq 0.01(\bar{\dot{\theta}}_{\mathrm{bit}}); \\ r_{WOB}(a_2 + a_3\dot{\theta}_{\mathrm{bit}})1.36, for 0.01(\bar{\dot{\theta}}_{\mathrm{bit}}) < \dot{\theta}_{\mathrm{bit}} \leq 0.05(\bar{\dot{\theta}}_{\mathrm{bit}}) \\ r_{WOB}(a_4 + a_5\dot{\theta}_{\mathrm{bit}} + a_6\dot{\theta}^2_{\mathrm{bit}} + a_7\dot{\theta}^3_{\mathrm{bit}})1.36, for \dot{\theta}_{\mathrm{bit}} \geq 0.05(\bar{\dot{\theta}}_{\mathrm{bit}}) \end{cases}, \quad (5.1)$$

where $T_{\mathrm{bit}_{non-reg}}$ is the "non-regularized" torque on bit in N.m, r_{WOB} = 0.8058 is the ratio WOB/WOB_{ref}, where WOB_{ref} is the reference WOB, and the parameters a_0, a_1, a_2, a_3, a_4, a_5, a_6, and a_7 are coefficients with the appropriate units.

SWA methodology has been applied to selected time range of experimental data to

get the average behaviour for parameter identification. The deterministic models of bit-rock interaction given by Eq. (3.1) as regularized model and Eq. (5.1) as non-regularized model were taken to evidence the experimental data compliance. Least-Square method and graphical identification was applied to identify the parameters for calibration of these models.

Compliance using the sample number 13 is done as follows, which corresponds to bit speed set to 120 RPM and bit diameter equal to 8 mm, as showed in Fig. 5.9. Time range between 44 and 59 seconds is taken to analyze the bit-rock interaction.

In total, there are 19 stick-slip cycles for selected range, with different kind of

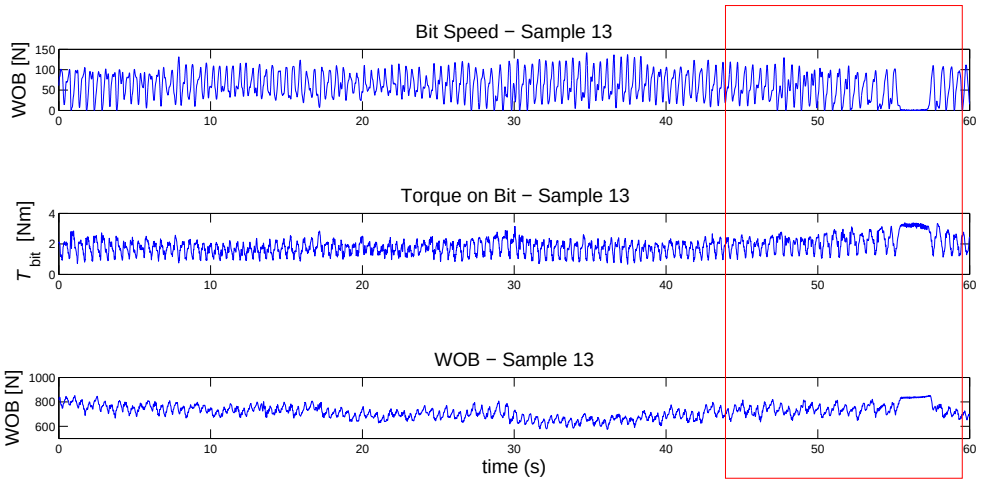

Figure 5.9: Full data of torque on bit, bit speed and WOB data using ϕ 8 mm bit and drive speed setted at 120 RPM (sample 3), where the red box is the selected range for analysis (range between 44s and 59s).

behaviour and levels of severity. All of them present a hysteresis behaviour, because the lost of energy during the stick-slip occurrence.

For better fitting model evaluation, a comparison between the regularized model and non-regularized model is done by variance of mean squared error ($Var[MSE]$) [11], where the better fitting model presents lower $Var[MSE]$ lower values, which is given by

$$Var[MSE] = var[(\bar{T}^{exp}_{\text{bit}_{\text{inside-window}}}(\dot{\theta}_{\text{bit}}(t), \ddot{\theta}_{\text{bit}}(t)) - \bar{T}^{Model_i}_{\text{bit}}(\dot{\theta}_{\text{bit}}(t)))^2], \tag{5.2}$$

where $\bar{T}^{exp}_{\text{bit}_{\text{inside-window}}}(\dot{\theta}_{\text{bit}}(t), \ddot{\theta}_{\text{bit}}(t))$ is given by Eq. (4.3), and $\bar{T}^{Model_i}_{\text{bit}}(\dot{\theta}_{\text{bit}}(t))$ can be given by Eq. (3.1) or Eq. (5.1).

Therefore, $Var[MSE]$ using Eq. (3.1) model is 20.8601, while $Var[MSE]$ using Eq. (5.1) model is 0.0017. These $Var[MSE]$ values show that the Eq. (5.1) model fits better the data than Eq. (3.1) model.

Three points are important in tests: accuracy, repeatability and reproducibility. According to [46], accuracy is related to the precision of measurements; repeatability is the agreement between the results of successive measurements carried out under the same conditions of measurement; and reproducibility is the agreement between the results of measurements carried out under changed conditions of measurement.

Accuracy is insured by calibration of sensors and system filters. All sensors were verified previously comparing to known standard-mass or to calibrated instruments, where any necessary adjustments are done. This issue are overcomed.

Reproducibility is noticed changing the input variables, that means bit diameter and top drive speed. Figure 5.4 in section 5.3.2 is a summary of all 210 tests, where all results fit the expected field behaviour, showing that the proposed test-rig reflects the bit-rock interaction of a drill string.

Repeatability can be insured by test-procedure (see section 5.3.1), but some limitations of test-rig, uncertainties or uncontrolled variables can affect this issue. To have a good analysis about that, table 5.2 shows some statistics of samples 11, 12, 13, 14, 15, 16, 17, 18, 19 and 20, as the variance of mean squared error for each sample and each model(according to Eq. (5.2)), coefficient of variation (CV), standard-deviation (std(T_{bit}^{exp})) and mean (mean (T_{bit}^{exp})) of each sample.

According to table 5.2, the repeatability is not ensured because of the stochasticity of bit-rock interaction process. However, the non-regularized model fits the sample data better than the regularized model (lower $Var[MSE]$ values). Some samples presented a huge off-set, that may be caused by another factor. In case of Sample 12, it is clear that there is a problem: some torque measurements are negative, that means the platform set was not stable enough during the drilling because the borehole was drilled close to the test-body border.

Coefficient of variation (CV) concept is the ratio between standard-deviation (std(T_{bit}^{exp})) and mean (mean (T_{bit}^{exp})), which is related to the hysteresis fluctuations; stochastic fluctuations are more related to the variation of rock properties and rock resistance.

Sample	$Var[MSE]$ Regularized Model	$Var[MSE]$ Non-Regularized Model	mean (T_{bit}^{exp})	std (T_{bit}^{exp})	CV
11	52.9938	0.2725	1.3812	0.6430	0.4656
12	58.0845	1.8469	0.7390	0.5208	0.7048
13	20.8601	0.0017	1.8502	0.5266	0.2846
14	9.1219	0.0072	2.2292	0.5144	0.2307
15	17.7767	0.0109	1.4754	0.9759	0.6615
16	0.0302	0.0075	1.9774	0.5903	0.2985
17	8.2123	0.0302	1.6453	0.5441	0.3307
18	43.1178	0.2388	0.9307	0.5450	0.5856
19	37.7625	0.2410	1.5059	0.2140	0.3222
20	27.8216	0.0264	1.9485	0.4453	0.2285

Table 5.2: Statistics related to T_{bit}^{exp} of samples 11, 12, 13,14, 15, 16, 17, 18, 19 and 20.

An acceptance criteria to evaluate the samples, it can be spanned by the blend of CV average and the variation of concrete properties. According to the field knowledge, an acceptance criteria of quality related to variation of concrete resistance is 10%. CV average of samples according to table 5.2 is 0.329 can be used, that means an acceptance criteria equal to 43% of variation. Considering 39% of variation over the torque on bit values, an acceptable value for $Var[MSE]$ of regularized model is 47.93 and 0.26 for non-regularized model. That means, the samples 14, 15, 16, 17, 18, 19 and 20 are acceptable for regularized and non-regularized models.

Therefore, 8 among 10 samples are acceptable according to the established criteria, which is enough to validate the test-rig results (bigger than 70%) and can prove the test-rig is able to reproduce torsional oscillations of a drill string. However, results can be improved including a safety region to drill the test-bodies (excluding the borders region - see Sample 12 results).

5.4 Validation of hysteretic models using numerical simulations

As mentioned before, observed stick-slip cycles in field and experimental results indicate that for each cycle the torque value for positive acceleration and for negative acceleration are not the same ([62, 85]), that means non-reversible phenomenon. According to [94], non-reversible means that the torque on bit depends not only on the bit speed, but also on the bit acceleration, producing a type of hysteretic cycle. Besides, each observed

cycle is different from one another, because the independence of cycles: each stick-slip cycle depends on the saving energy during the stick phase and how this energy is applied to motion in slip phase. It happens because the effect of the WOB combined to acceleration and deceleration behaviour, simulating an axial-torsional coupled model into non-coupled model, that is a great advantage.

As hysteretic function (Eq. (3.3)) was applied to regularized model, as showed in Eq. (3.2), it can be applied to non-regularized model according to Eq. (5.1), as follows

$$T^{HYS}_{\text{bit}_{non-reg}}(\dot{\theta}_{\text{bit}}, \ddot{\theta}_{\text{bit}}) = T_{\text{bit}_{non-reg}}(\dot{\theta}_{\text{bit}})(1 + H(\dot{\theta}_{\text{bit}}, \ddot{\theta}_{\text{bit}})) \tag{5.3}$$

Validation of the proposed models using numerical simulations will be done in the future works.

Chapter 6

Stochastic computational model of the drill string

Chapter 4 describes a new stochastic model of the bit-rock interaction. However, there are sources of uncertainties related to the computational model of the drill string presented in the Eq. (2.5), such as material properties and variability of geometry along the axial axis. Besides, the modeling of interfaces for the present model is very simple compared to complex mechanical real link between the DP and BHA. Then, the linear torsional model is a simple representation of the torsional vibration of the drill string yielding some model-form uncertainties in the model.

For these reasons, a new probabilistic model of uncertainties is constructed in order to quantify the sensitivity of outputs with respect to these uncertainties efficiently. This new strategy is an extension of the nonparametric probabilistic approach [124], which considers the uncertainties at the operator level globally, allowing to control the dispersion level of each inner and interface DOFs of each drill string substructure, independently. This strategy allows to control the level of the uncertainties related to the inner and interface DOFs from the nonparametric probabilistic approach together with Craig-Bampton substructuring method, extending the work developed by Soize and Chebli [126].

6.1 Classical nonparametric probabilistic approach - a brief overview

Nonparametric probabilistic approach is based on the random matrix theory [72, 124], which consists in replacing the deterministic reduced-order matrices of the deterministic

computational model by random matrices, and acts directly at the reduced operator level. In its basic version, this approach assumes that there are no rigid body modes, that means the deterministic reduced matrices are symmetric positive-definite. Systems may not be attached to a fixed frame, that means they present rigid body modes - in such case, see section 6.5. Some substructures

For contextualizing, nonparametric probabilistic approach [124] considers the uncertainties at the operator level globally: the constructed stochastic model is controlled by a few number of dispersion parameters which make their experimental identification feasible [14, 15, 26, 27, 32, 129]. Furthermore, by randomizing the reduced-order operators, this approach allows to extend the range of prediction of the computational model without modifying the reduced displacement subspace [93].

Let $[A]$ denote the mass, damping or stiffness reduced order matrix of substructure S_k, that means $A = M, D$ or K. The nonparametric probabilistic approach consists in replacing $[A]$ by a random matrix $[\mathbf{A}]$, such as

$$[\mathbf{A}] = [L_A][\mathbf{G}_A][L_A]^T, \tag{6.1}$$

where $[\mathbf{G}_A]$ is a normalized random matrix and $[L_A]$ is a lower triangular matrix related to the Cholesky factorization of matrix $[A]$, i.e.,

$$[A] = [L_A][L_A]^T. \tag{6.2}$$

Probability density function of random matrix $[\mathbf{G}_A]$ is constructed using the maximum entropy principle [45], and depends on a dispersion parameter δ_A, which controls the level of the statistical fluctuations of the random matrix $[\mathbf{G}_A]$ around its mean value (the unit matrix $[I_m]$. Then,

$$\delta_A = \left(\frac{E\{||[\mathbf{G}_A] - [I_m]||_F^2\}}{||[I_m]||_F^2} \right)^{1/2}, \tag{6.3}$$

where $||\cdot||_F$ is the Frobenius norm and $E\{\cdot\}$ is the mathematical expectation. A generator of independent realizations of random matrix $[\mathbf{G}_A]$ has been proposed in [124].

Stochastic model in terms of nonparametric probabilistic approach ($\mathrm{SM}_{\mathrm{full}}$) for the reduced order computational model without substructuring method is constructed in replacing each deterministic matrices $[M]$, $[D]$ and $[K]$ in Eq. (2.5) by random matrices $[\mathbf{M}]$, $[\mathbf{D}]$ and $[\mathbf{K}]$, according to Eq. (6.1). In this way,

$$[\mathbf{M}]\ddot{\mathbf{q}} + [\mathbf{D}]\dot{\mathbf{q}} + [\mathbf{K}]\mathbf{q} = \widetilde{\mathbf{T}}(\dot{\mathbf{q}}(t), \ddot{\mathbf{q}}(t)), \tag{6.4}$$

which yields in the frequency domain

$$(-\omega^2[\mathbf{M}] + j\omega[\mathbf{D}] + [\mathbf{K}])\mathbf{q}(\omega) = \widetilde{\mathbf{T}}_{\omega}(\omega). \tag{6.5}$$

For $\mathbf{A} = \mathbf{M}, \mathbf{D}$ or $\mathbf{K}$, the probabilistic model of the random reduced-order matrix $[\mathbf{A}]$ is constructed by using the nonparametric probabilistic approach which is briefly presented above. Hence, the stochastic model $\mathrm{SM}_{\mathrm{full}}$ is completely defined by only three dispersion coefficients δ_M, δ_D, δ_K, one for each the random reduced-order matrix, that means $\mathbf{M}, \mathbf{D}$ or $\mathbf{K}$ respectively.

6.2 Nonparametric probabilistic approach together with Craig-Bampton substructuring method

6.2.1 Craig-Bampton substructuring method

Reduced-order model reduces the order of the matrices according to the elastic modes of the whole structure, as showed in section 2.2. In some cases can be more interesting to divide this one in substructures, for instance complex structures or to get access in specific parts of the structure, saving computational cost. Since 60's, aerospace and automotive industries have used substructuring techniques called Component Modal Synthesis (CMS), in order to model the dynamical responses of complex structures [20]. CMS involved basically two steps[82]:
(1) definition of modal sets of each system component; and
(2) coupling of these sets to form a reduced-order model.

In 1968, Craig and Bampton [21, 77] created a simple strategy of substructuring method based on over-positioning of normal and static modes of each substructure (CMS step (1)) through coupled matrix composition (CMS step (2)), which is able to reduce drastically the computational cost[20].

The structure is decomposed into n_s substructures $S_1, S_2, \ldots, S_{n_s}$. For $k = 1, \ldots, n_s$, the displacement $\mathbf{u}_k$ of S_k consists in $n_{\mathrm{I},k}$ inner DOFs $\mathbf{u}_k^{\mathrm{I}}$ and in $n_{\Gamma,k}$ interface DOFs $\mathbf{u}_k^{\Gamma}$,

i.e.,

$$\mathbf{u}_k = \begin{pmatrix} \mathbf{u}_k^{\mathrm{I}} \\ \\ \mathbf{u}_k^{\Gamma} \end{pmatrix}. \tag{6.6}$$

Let $[A_k]$ be the mass, damping or stiffness matrix of substructure S_k, that means $A = M, D$ or K, and let $\mathbf{f}_k$ be the force vector of substructure S_k. Then,

$$[A_k] = \begin{pmatrix} [A_k^{\mathrm{II}}] & [A_k^{\mathrm{I}\Gamma}] \\ \\ [A_k^{\Gamma\mathrm{I}}] & [A_k^{\Gamma\Gamma}] \end{pmatrix} \quad \text{and} \quad \mathbf{f}_k = \begin{pmatrix} \mathbf{f}_k^{\mathrm{I}} \\ \\ \mathbf{f}_k^{\mathrm{c}} \end{pmatrix}, \tag{6.7}$$

in which $\mathbf{f}_k^{\mathrm{I}}$ is the inner force and $\mathbf{f}_k^{\mathrm{c}}$ is the coupling force at the interface. In Eq. (2.5), it is assumed that there is no external force applied on the interfaces.

Craig-Bampton substructuring method [21] consists in reducing the number of inner DOFs by using fixed-interface elastic modes and static modes, such that

$$\begin{pmatrix} \mathbf{u}_k^{\mathrm{I}} \\ \\ \mathbf{u}_k^{\Gamma} \end{pmatrix} = \begin{pmatrix} [\Phi_k^{\mathrm{I}}] & [R_k^{\mathrm{I}}] \\ \\ [0] & [\mathrm{I}_{n_{\Gamma,k}}] \end{pmatrix} \begin{pmatrix} \mathbf{q}_k^{\mathrm{I}} \\ \\ \mathbf{u}_k^{\Gamma} \end{pmatrix}, \tag{6.8}$$

where $[\Phi_k^{\mathrm{I}}]$ is the matrix of the m_k fixed-interface elastic modes, R_k^{I} are the matrix of the static modes described such that

$$R_k^{\mathrm{I}} = -[K_k^{\mathrm{II}}]^{-1}[K_k^{\mathrm{I}\Gamma}], \tag{6.9}$$

and $[I_{n_{\Gamma,k}}]$ is the $(n_{\Gamma,k} \times n_{\Gamma,k})$ identity matrix. In Eq.(6.8), $\mathbf{q}_k^{\mathrm{I}}$ is the vector of the m_k generalized coordinates related to the fixed-interface elastic modes. The Eq. (6.8) can be rewritten as

$$\mathbf{u}_k = [\Psi_k]\,\mathbf{q}_k \tag{6.10}$$

with

$$[\Psi_k] = \begin{pmatrix} [\Phi_k^{\mathrm{I}}] & [R_k^{\mathrm{I}}] \\ \\ [0] & [I_{n_{\Gamma,k}}] \end{pmatrix} \quad \text{and} \quad \mathbf{q}_k = \begin{pmatrix} \mathbf{q}_k^{\mathrm{I}} \\ \\ \mathbf{u}_k^{\Gamma} \end{pmatrix}. \tag{6.11}$$

Let $n_k = m_k + n_{\Gamma,k}$. Let $[\tilde{A}_k]$ be $(n_k \times n_k)$ such that

$$[\tilde{A}_k] = [\Psi_k]^T [A_k][\Psi_k] = \begin{pmatrix} [\tilde{A}_k^{\mathrm{II}}] & [\tilde{A}_k^{\mathrm{I}\Gamma}] \\ [\tilde{A}_k^{\Gamma\mathrm{I}}] & [\tilde{A}_k^{\Gamma\Gamma}] \end{pmatrix}. \tag{6.12}$$

Let $[P_k^{\mathrm{I}}] = ([I_{m_k}]\,[0])$ and $[P_k^{\Gamma}] = ([0]\,[I_{n_{\Gamma,k}}])$ be the projection matrices on the inner and interface coordinates, respectively. Then,

$$[\tilde{A}_k^{\mathrm{II}}] = [P_k^{\mathrm{I}}]^T [\tilde{A}_k][P_k^{\mathrm{I}}], \quad [\tilde{A}^{\mathrm{I}\Gamma}] = [P_k^{\mathrm{I}}]^T [\tilde{A}_k][P_k^{\Gamma}], \quad [\tilde{A}_k^{\Gamma\Gamma}] = [P_k^{\Gamma}]^T [\tilde{A}_k][P_k^{\Gamma}]. \tag{6.13}$$

For the stiffness matrices, the coupling blocks are algebraically equal to zero. For instance, there are two substructures (DP + BHA) for the drill string showed in the figure 2.1, that means $n_s = 2$ substructures. Taking into account the continuity of the displacement at the interface, the force equilibrium at the interface and the relation Eq. ((6.10)) for each substructure, the dynamical matrix equation of the assembled structure for the substructuring Craig-Bampton method are written with lower subscript CB as follow

$$[M_{\mathrm{CB}}]\ddot{\mathbf{q}}_{\mathrm{CB}}(t) + [D_{\mathrm{CB}}]\dot{\mathbf{q}}_{\mathrm{CB}}(t) + [K_{\mathrm{CB}}]\mathbf{q}_{\mathrm{CB}}(t) = \mathbf{T}_{t_{\mathrm{CB}}}(t), \tag{6.14}$$

for time domain, and

$$(-\omega^2[M_{\mathrm{CB}}] + j\omega\,[D_{\mathrm{CB}}] + [K_{\mathrm{CB}}])\mathbf{q}_{\mathrm{CB}}(\omega) = \mathbf{T}_{\omega_{\mathrm{CB}}}(\omega), \tag{6.15}$$

for frequency domain, in which

$$\mathbf{q}_{\mathrm{CB}} = \begin{pmatrix} \mathbf{q}_1^{\mathrm{I}} \\ \mathbf{q}_2^{\mathrm{I}} \\ \mathbf{u}^{\Gamma} \end{pmatrix}, \quad \mathbf{T}_{k_{\mathrm{CB}}} = \begin{pmatrix} [\Psi_1]^T \mathbf{T}_{k1}^{\mathrm{I}} \\ [\Psi_2]^T \mathbf{T}_{k2}^{\mathrm{I}} \\ [R_1^{\mathrm{I}}]^T \mathbf{T}_{k1}^{\mathrm{I}} + [R_2^{\mathrm{I}}]^T \mathbf{T}_{k2}^{\mathrm{I}} \end{pmatrix}, \tag{6.16}$$

and

$$[A_{\mathrm{CB}}] = \begin{pmatrix} [\tilde{A}_1^{\mathrm{II}}] & [0] & [\tilde{A}_1^{\mathrm{I}\Gamma}] \\ [0] & [\tilde{A}_2^{\mathrm{II}}] & [\tilde{A}_2^{\mathrm{I}\Gamma}] \\ [\tilde{A}_1^{\Gamma\mathrm{I}}] & [\tilde{A}_2^{\Gamma\mathrm{I}}] & [\tilde{A}_1^{\Gamma\Gamma}] + [\tilde{A}_2^{\Gamma\Gamma}], \end{pmatrix}. \tag{6.17}$$

The displacement vector $\mathbf{u}$ is finally calculated as

$$\mathbf{u} = [\Psi]\,\mathbf{q}_{\mathrm{CB}}\,, \tag{6.18}$$

where $[\Psi]$ is constructed by assembling matrices, that means $[\Psi_1]$ and $[\Psi_2]$ for $n_s = 2$ substructures (for n_s substructures, $[\Psi_1], \ldots, [\Psi_{n_s}]$).

6.3 The methodology

Soize and Chebli [126] proposed a probabilistic model (called here as stochastic model $\mathrm{SM}_{\mathrm{CB1}}$) for taking into account different levels of uncertainties in each substructure: for each substructure S_k , the reduced matrices were replaced by random matrices whose probabilistic models were constructed by using the nonparametric probabilistic approach that has been briefly presented in section 6.1. Hence, for $A = M, D$ or K and for each substructure S_k, deterministic matrices $[\tilde{A}_k^{\mathrm{II}}]$, $[\tilde{A}_k^{\Gamma\mathrm{I}}]$, $[\tilde{A}_k^{\Gamma\Gamma}]$ introduced in section 6.2.1 and involved in the assembling of the deterministic matrix $[A_{\mathrm{CB}}]$ are replaced by the random matrices $[\tilde{\mathbf{A}}_k^{\mathrm{II}}]$, $[\tilde{\mathbf{A}}_k^{\Gamma\mathrm{I}}]$ and $[\tilde{\mathbf{A}}_k^{\Gamma\Gamma}]$, defined as [93]

$$[\tilde{\mathbf{A}}_k^{\mathrm{II}}] = [P_k^{\mathrm{I}}]^T [\tilde{\mathbf{A}}_k][P_k^{\mathrm{I}}], \quad [\tilde{\mathbf{A}}^{\mathrm{I}\Gamma}] = [P_k^{\mathrm{I}}]^T [\tilde{\mathbf{A}}_k][P_k^{\Gamma}], \quad [\tilde{\mathbf{A}}_k^{\Gamma\Gamma}] = [P_k^{\Gamma}]^T [\tilde{\mathbf{A}}_k][P_k^{\Gamma}], \tag{6.19}$$

where $[\tilde{\mathbf{A}}_k]$ is a random matrix for which its statistical fluctuation due to the uncertainties is related to $[\tilde{A}_k]$ (see section 6.2.1), P_k^{I} and P_k^{Γ} are described in Real et al. (2017) [93], and whose probabilistic model is constructed by using the nonparametric approach that is briefly presented in section 6.1. The assembling of those random matrices yield a random matrix $[\mathbf{A}_{\mathrm{CB1}}]$ that models the statistical fluctuation related to uncertainties on $[A_{\mathrm{CB}}]$. For instance, for $n_s = 2$, and for $\mathbf{A} = \mathbf{M}, \mathbf{D}$ or $\mathbf{K}$, $[\mathbf{A}_{\mathrm{CB1}}]$ is given by

$$[\mathbf{A}_{\mathrm{CB1}}] = \begin{pmatrix} [\tilde{\mathbf{A}}_1^{\mathrm{II}}] & [0] & [\tilde{\mathbf{A}}_1^{\mathrm{I}\Gamma}] \\ [0] & [\tilde{\mathbf{A}}_2^{\mathrm{II}}] & [\tilde{\mathbf{A}}_2^{\mathrm{I}\Gamma}] \\ [\tilde{\mathbf{A}}_1^{\Gamma\mathrm{I}}] & [\tilde{\mathbf{A}}_2^{\Gamma\mathrm{I}}] & [\tilde{\mathbf{A}}_1^{\Gamma\Gamma}]+[\tilde{\mathbf{A}}_2^{\Gamma\Gamma}] \end{pmatrix}. \tag{6.20}$$

Stochastic model $\mathrm{SM}_{\mathrm{CB1}}$ allows different levels of uncertainties to be modeled in each substructure and here are 6 dispersion parameters because $n_s = 2$ substructures. In a general way, the total number of parameters is equal to $3 \times n_s$ parameters, which control

the uncertainties of the system: $\delta_{M,1}, \delta_{D,1}, \delta_{K,1}, \ldots, \delta_{M,n_s}$, δ_{D,n_s}, δ_{K,n_s}.

6.4 New stochastic model: one extension of nonparametric probabilistic approach together with Craig-Bampton substructuring method, which separates of the statistical fluctuations related to the inner and interface DOFs

In nonparametric probabilistic approach together with Craig-Bampton substructuring method proposed by Soize and Chebli [126] ($\mathrm{SM_{CB1}}$), every components of a given random matrix $[\tilde{\mathbf{A}}_k]$ are related to the same dispersion coefficient for each substructure. Nevertheless, each component of random matrix $[\tilde{\mathbf{A}}_k]$ is related to a linear system of stochastic second order ordinary differential equations, in terms of random generalized coordinates and random displacements on the interfaces between two substructures. Stochastic model $\mathrm{SM_{CB1}}$ does not allow to take into account different levels of statistical fluctuation on those coefficients. In order to circumvent such a limitation, a new stochastic model (called here stochastic model $\mathrm{SM_{CB2}}$) is proposed here, extending the work developed by Soize and Chebli [126]. For each substructure S_k and for $\mathbf{A} = \mathbf{M}, \mathbf{D}$ or $\mathbf{K}$, two statistically independent random matrices $[\tilde{\mathbf{A}}^{\mathrm{I}}_k]$ and $[\tilde{\mathbf{A}}^{\Gamma}_k]$ are introduced to model the statistical fluctuations that are related to each matrix $[\tilde{A}_k]$ (see section 6.2.1). Their probabilistic model are constructed using the nonparametric probabilistic approach as briefly presented in section 6.1, and for two different dispersion cofficients $\delta_{A,\mathrm{I},k}$ and $\delta_{A,\Gamma,k}$. Cholesky factorisation of these random matrices yields two random lower triangular matrices $[\mathbf{L}^{\mathrm{I}}_{A,k}]$ and $[\mathbf{L}^{\Gamma}_{A,k}]$, such that

$$[\tilde{\mathbf{A}}^{\mathrm{I}}_k] = [\mathbf{L}^{\mathrm{I}}_{A,k}][\mathbf{L}^{\mathrm{I}}_{A,k}]^T, \quad [\tilde{\mathbf{A}}^{\Gamma}_k] = [\mathbf{L}^{\Gamma}_{A,k}][\mathbf{L}^{\Gamma}_{A,k}]^T . \tag{6.21}$$

Hence, for each substructure S_k, the deterministic matrices $[\tilde{A}^{\mathrm{II}}_k]$, $[\tilde{A}^{\Gamma\mathrm{I}}_k]$, $[\tilde{A}^{\Gamma\Gamma}_k]$ related to assembly of the deterministic matrix $[A_{\mathrm{CB}}]$ introduced in section 6.2.1 are replaced by the random matrices $[\tilde{\mathbb{A}}^{\mathrm{II}}_k]$, $[\tilde{\mathbb{A}}^{\Gamma\mathrm{I}}_k]$ and $[\tilde{\mathbb{A}}^{\Gamma\Gamma}_k]$, defined as

$$[\tilde{\mathbb{A}}^{II}_k] = [P^I_k]^T[\tilde{\mathbf{A}}^I_k][P^I_k], \quad [\tilde{\mathbb{A}}^{I\Gamma}_k] = [P^I_k]^T[\tilde{\mathbf{L}}^I_{A,k}][\mathbf{L}^{\Gamma}_{A,k}]^T[P^{\Gamma}_k], \text{ and } \quad [\tilde{\mathbb{A}}^{\Gamma\Gamma}_k] = [P^{\Gamma}_k]^T[\tilde{\mathbf{A}}^{\Gamma}_k][P^{\Gamma}_k]. \tag{6.22}$$

The assembly of those random matrices yields a random matrix $[\mathbf{A}_{\mathrm{CB2}}]$ that models the statistical fluctuation related to uncertainties on $[A_{\mathrm{CB2}}]$. For instance, for $n_s = 2$, A_{CB2} is given by

$$[\mathbf{A}_{\mathrm{CB2}}] = \begin{pmatrix} [\tilde{\mathbb{A}}_1^{\mathrm{II}}] & [0] & [\tilde{\mathbb{A}}_1^{\mathrm{I}\Gamma}] \\ [0] & [\tilde{\mathbb{A}}_2^{\mathrm{II}}] & [\tilde{\mathbb{A}}_2^{\mathrm{I}\Gamma}] \\ [\tilde{\mathbb{A}}_1^{\Gamma\mathrm{I}}] & [\tilde{\mathbb{A}}_2^{\Gamma\mathrm{I}}] & [\tilde{\mathbb{A}}_1^{\Gamma\Gamma}]+[\tilde{\mathbb{A}}_2^{\Gamma\Gamma}] \end{pmatrix}. \tag{6.23}$$

The levels of the statistical fluctuations of random matrix $[\mathbf{A}_{\mathrm{CB2}}]$ are controlled by two dispersion coefficients $\delta_{A,\mathrm{I},k}$ and $\delta_{A,\Gamma,k}$, which are related to the nonparametric models of $[\tilde{\mathbf{A}}_k^{\mathrm{I}}]$ and $[\tilde{\mathbf{A}}_k^{\Gamma}]$, respectively. Here, Stochastic model $\mathrm{SM}_{\mathrm{CB2}}$ allows different levels of uncertainties to be modeled in each substructure by 6 dispersion parameters, totalizing 12 parameters because $n_s = 2$ substructures. In a general way, the probabilistic model of uncertainties is controlled by $6 \times n_s$ dispersion coefficients, that allow controlling the level of statistical fluctuations of the inner and interface coordinates separately for each random matrices, giving more flexibility than the stochastic model $\mathrm{SM}_{\mathrm{CB1}}$. In this case, the dispersion coefficients for the full structure are $\delta_{M,\mathrm{I},1}$, $\delta_{M,\Gamma,1}$, $\delta_{D,\mathrm{I},1}$, $\delta_{D,\Gamma,1}$, $\delta_{K,\mathrm{I},1}$, $\delta_{K,\Gamma,1}$, $\ldots$, $\delta_{M,\mathrm{I},n_s}$, δ_{M,Γ,n_s}, $\delta_{D,\mathrm{I},n_s}$, δ_{D,Γ,n_s}, $\delta_{K,\mathrm{I},n_s}$, δ_{K,Γ,n_s}.

6.5 Comments concerning the nonparametric probabilistic approach - presence of floating substructures

Some substructures of the systems may not be attached to a fixed frame, that means they present rigid body modes. This is the case, for instance, for the BHA of the drill string showed in figure 2.1. These floating substructures yield a positive semi-definite stiffness matrix $[\tilde{K}_k]$ and then the nonparametric construction presented in the previous sections cannot be applied directly. To circumvent this difficulty, the projection of the stiffness matrix into the rigid body subspace is kept equal to zero almost surely while the projections into the subspace of flexible displacements are randomized. Such construction makes sense since the rigid body subspace is not perturbed by the presence of uncertainties. The construction proposed here corresponds to the ensemble of random matrices

"SE^{+0}" introduced in [128]. Let $[P_{\text{rb},k}]$ be the matrix whose columns are vectors that span the null space of $[\tilde{K}_k]$ and let $[P_{\text{flex},k}]$ be the matrix whose columns are vectors that spans the range space of $[\tilde{K}_k]$. It is assumed that the columns of $[P_{\text{rb},k}]$ and $[P_{\text{flex},k}]$ are normalized. In this way, $[P_{\text{rb},k}]^T [P_{\text{flex},k}] = [I]$. Letting $[P_k] = ([P_{\text{rb},k}][P_{\text{flex},k}])$, $\tilde{K}_k$ is given by

$$[\tilde{K}_k] = [P_k] \begin{pmatrix} [0] & [0] \\ \\ [0] & [C_k] \end{pmatrix} [P_k]^T , \tag{6.24}$$

in which $[C_k]$ is the diagonal matrix of the nonzero eigenvalues of $[\tilde{K}_k]$.

The stochastic models SM_{CB1} and SM_{CB2} are then constructed by replacing the deterministic matrix $[C_k]$ by the random matrix $[\mathbf{C}_k]$, for which the probabilistic model is constructed by using the nonparametric approach presented in section 6.1. Finally, for $[\mathbf{K}_k] = [\tilde{\mathbf{K}}_k]$ (for the stochastic model SM_{CB1}), $[\tilde{\mathbf{K}}_k^{\text{I}}]$ and $[\tilde{\mathbf{K}}_k^{\Gamma}]$ (for Stochastic Model SM_{CB2}), $\mathbf{K}_k$ is written as

$$[\mathbf{K}_k] = [P_k] \begin{pmatrix} [0] & [0] \\ [0] & [\mathbf{C}_k] \end{pmatrix} [P_k]^T . \tag{6.25}$$

6.6 New stochastic model (SM_{CB2}): application and verification

The objective of this section is just to validate and illustrate the proposed methodology using a simple torque model, which allows to perform a comparison among the nonparametric probabilistic models, and to check how robust is this computational model according some inferred fluctuations in order to evaluate the impact of the different sources of uncertainties.

In order to verify the new stochastic model (SM_{CB2}) presented in section 6.4, it is implemented taking into account the uncertainties related to the computational model of the drill string presented in section 2.1, considering an unitary torque is applied to the bottom-end of BHA for all frequency range of analysis. It is noticed that the unitary torque applied to the bit is not a real representation of a bit-rock interaction torque, but it is necessary as a comparison methodology.

The stochastic model SM_{CB2} 6.4 is compared to the stochastic models SM_{full} (see section 6.1) and SM_{CB1} (see section 6.2). Then, the stochastic model SM_{CB2} is analyzed in order to evaluate the impact of the different sources of uncertainties: DP versus BHA,

mass versus damping versus stiffness, and inner versus interface DOFs.

Hypothetic drill string are used for the implementation, considering 1,700 m DP length and 300 m BHA length. As stated before, only two substructures are considered in this analysis: DP and BHA. The mass and stiffness matrices for this substructure are constructed using 100 elements with linear shape functions for each substructure, considering the top-end of the DP clamped. The top-end of the BHA is coupled with the bottom-end of the DP. Therefore, there is only one interface DOF.

For better visualization, the acceleration response is given in logarithmic scale (dB) according to $20log_{10}\ddot{\mathbf{u}}(\omega)$. Three points are observed: $\mathrm{P_{obs,1}}$, which corresponds to the first non-clamped node at the top of the DP, $\mathrm{P_{obs,2}}$, which corresponds to the interface node, and $\mathrm{P_{obs,3}}$, which corresponds to the bottom node of the BHA. The statistical envelope with probability level 0.95 is estimated using 2,500 Monte Carlo simulations (see Appendix C).

Craig-Bampton projection matrices $[\Phi_1^{\mathrm{I}}]$ and $[\Phi_2^{\mathrm{I}}]$ are both constructed using the number of modes above the number obtained by convergence analysis obtained after the convergence analysis (see Appendix C) due to the user's prudence: $m_1 = m_2 = 25$ fixed-interface elastic modes. The reduced damping matrices $[\tilde{D}_1]$ and $[\tilde{D}_2]$ are both constructed using a Rayleigh model [40], i.e., $[\tilde{D}_1] = a_1[\tilde{M}_1] + b_1[\tilde{K}_1]$ and $[\tilde{D}_2] = a_2[\tilde{M}_2] + b_2[\tilde{K}_2]$ where a_1, b_1, a_2 and b_2 are calculated such that the damping ratios are 0.05 and 0.01 at frequencies 1 Hz and 10 Hz for each substructure, respectively. Dispersion parameters (δ's) are set to 0.1, that means 10% of fluctuation range.

6.6.1 Validation of the new stochastic model $\mathrm{SM_{CB2}}$: one comparison

In order to validate the new stochastic model $\mathrm{SM_{CB2}}$, this one is compared to $\mathrm{SM_{full}}$ and $\mathrm{SM_{CB1}}$, using all δ's set equal to 0.1 (user's choice), that means 10% of dispersion: for the full model $\mathrm{SM_{full}}$, $\delta_M = \delta_D = \delta_K = 0.1$; for model $\mathrm{SM_{CB1}}$, $\delta_{M,1} = \delta_{M,2} = \delta_{D,1} = \delta_{D,2} = \delta_{K,1} = \delta_{K,2} = 0.1$; for model $\mathrm{SM_{CB2}}$, $\delta_{M,\mathrm{I},1} = \delta_{M,\Gamma,1} = \delta_{M,\mathrm{I},2} = \delta_{M,\Gamma,2} = \delta_{D,\mathrm{I},1} = \delta_{D,\Gamma,1} = \delta_{D,\mathrm{I},2} = \delta_{D,\Gamma,2} = \delta_{K,\mathrm{I},1} = \delta_{K,\Gamma,1} = \delta_{K,\mathrm{I},2} = \delta_{K,\Gamma,2} = 0.1$. The normalized random matrices $[\mathbf{G}_A]$ are constructed for each case using Gamma distribution, based on the maximum entropy principle [45].

Figures 6.1, 6.2 and 6.3 show the comparison of the statistical envelopes at the three observed points for each stochastic model. It can be observed that the statistical

envelopes get wider as the frequency increases, especially for the response in the top-end of the DP node, as showed in Fig. 6.1. The three figures present similar envelopes for all methodologies. These results indicate that the proposed strategy is consistent, with one advantage of allowing more parameters to control uncertainties.

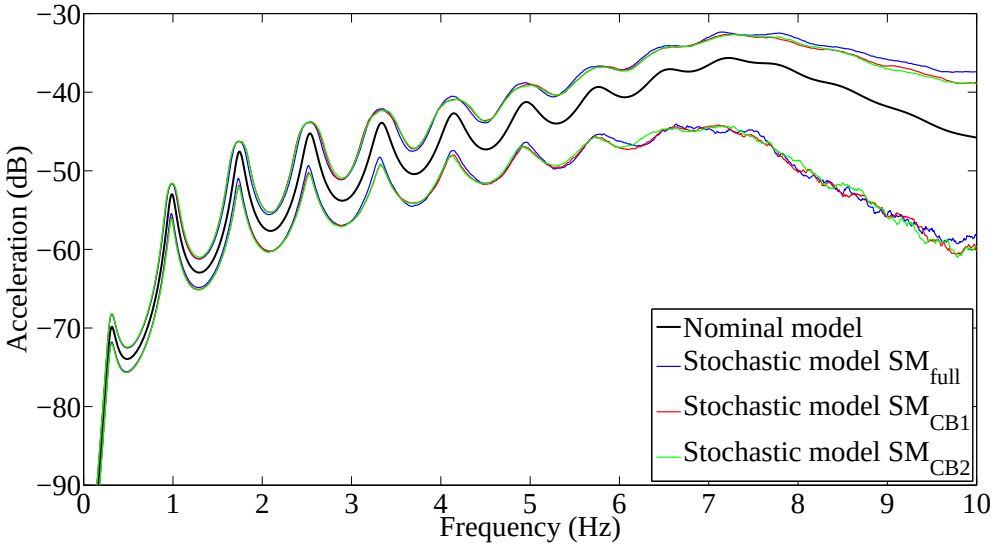

Figure 6.1: Comparison of three stochastic models - frequency response in acceleration for point $P_{obs,1}$.

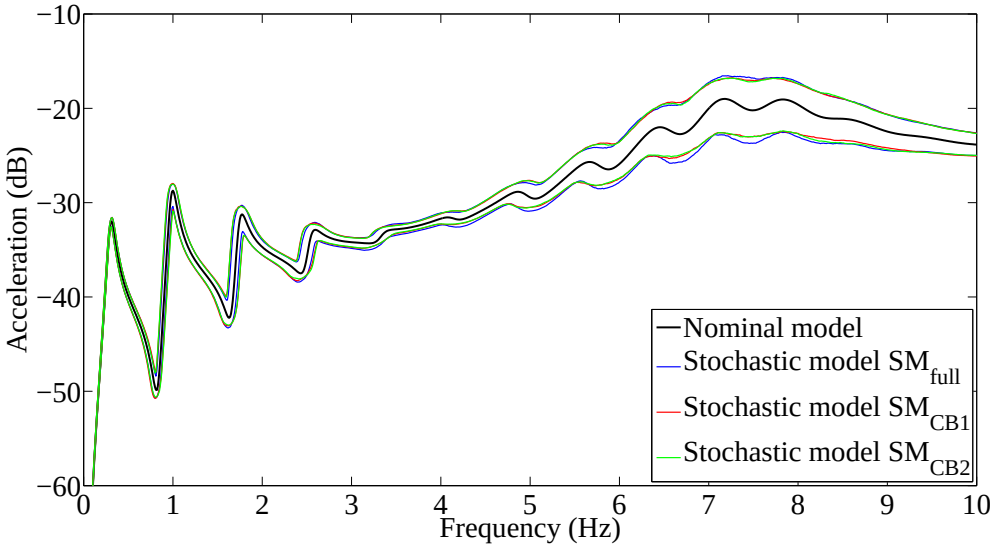

Figure 6.2: Comparison of three stochastic models - frequency response in acceleration for point $P_{obs,2}$.

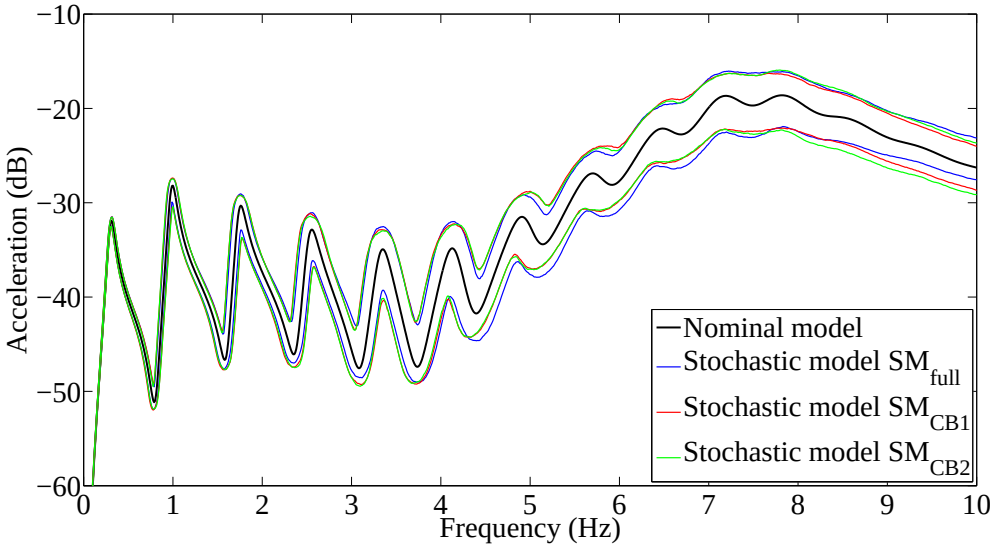

Figure 6.3: Comparison of three stochastic models - frequency response in acceleration for point $P_{obs,3}$.

Next, results of the new stochastic model for different levels of uncertainties will be explored, which allows the control of uncertainties for each operator, each substructure and each inner or interface DOF.

6.6.2 Random response of stochastic model SM_{CB2}

Mass versus damping versus stiffness

i- Case study 1: mass uncertainty, Table 6.1.

	DP-inner	DP-interface	BHA-inner	BHA-interface
Mass	$\delta_{M,\mathrm{I},1} = 0.1$	$\delta_{M,\Gamma,1} = 0.1$	$\delta_{M,\mathrm{I},2} = 0.1$	$\delta_{M,\Gamma,2} = 0.1$
Damping	$\delta_{D,\mathrm{I},1} = 0$	$\delta_{D,\Gamma,1} = 0$	$\delta_{D,\mathrm{I},2} = 0$	$\delta_{D,\Gamma,2} = 0$
Stiffness	$\delta_{K,\mathrm{I},1} = 0$	$\delta_{K,\Gamma,1} = 0$	$\delta_{K,\mathrm{I},2} = 0$	$\delta_{K,\Gamma,2} = 0$

Table 6.1: Case study 1 - values of the dispersion parameters.

ii- Case study 2: damping uncertainty, Table 6.2.
iii- Case study 3: stiffness uncertainty, Table 6.3.

Figures 6.4, 6.5 and 6.6 show the random responses comparing uncertainties in the mass, damping and stiffness matrices. The results are very similar for uncertain mass

	DP-inner	DP-interface	BHA-inner	BHA-interface
Mass	$\delta_{M,\mathrm{I},1} = 0$	$\delta_{M,\Gamma,1} = 0$	$\delta_{M,\mathrm{I},2} = 0$	$\delta_{M,\Gamma,2} = 0$
Damping	$\delta_{D,\mathrm{I},1} = 0.1$	$\delta_{D,\Gamma,1} = 0.1$	$\delta_{D,\mathrm{I},2} = 0.1$	$\delta_{D,\Gamma,2} = 0.1$
Stiffness	$\delta_{K,\mathrm{I},1} = 0$	$\delta_{K,\Gamma,1} = 0$	$\delta_{K,\mathrm{I},2} = 0$	$\delta_{K,\Gamma,2} = 0$

Table 6.2: Case study 2 - values of the dispersion parameters.

	DP-inner	DP-interface	BHA-inner	BHA-interface
Mass	$\delta_{M,\mathrm{I},1} = 0$	$\delta_{M,\Gamma,1} = 0$	$\delta_{M,\mathrm{I},2} = 0$	$\delta_{M,\Gamma,2} = 0$
Damping	$\delta_{D,\mathrm{I},1} = 0$	$\delta_{D,\Gamma,1} = 0$	$\delta_{D,\mathrm{I},2} = 0$	$\delta_{D,\Gamma,2} = 0$
Stiffness	$\delta_{K,\mathrm{I},1} = 0.1$	$\delta_{K,\Gamma,1} = 0.1$	$\delta_{K,\mathrm{I},2} = 0.1$	$\delta_{K,\Gamma,2} = 0.1$

Table 6.3: Case study 3 - values of the dispersion parameters.

and stiffness matrices, except at very low frequencies, where stiffness uncertainties are predominant. Besides, the statistical envelopes increase with the frequency .

On the other hand, these figures show that the sensitivity of the response for an uncertain damping model is very low (very thin statistical envelopes): that means the system is robust to damping model uncertainties, considering the used dispersion parameters.

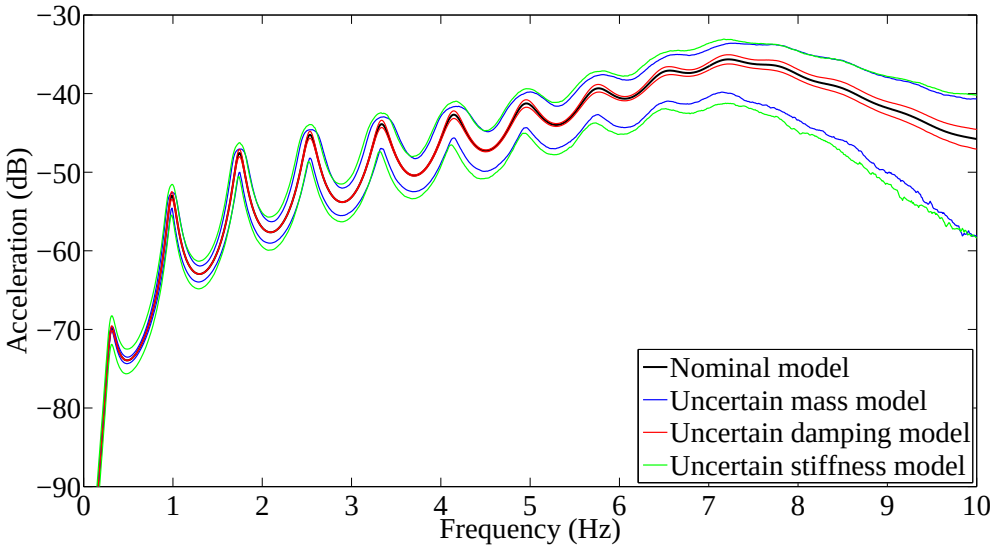

Figure 6.4: Case study 1, 2 and 3 - frequency response in acceleration for point $P_{obs,1}$.

DP versus BHA

i- Case study 4: DP uncertainty, Table 6.4.

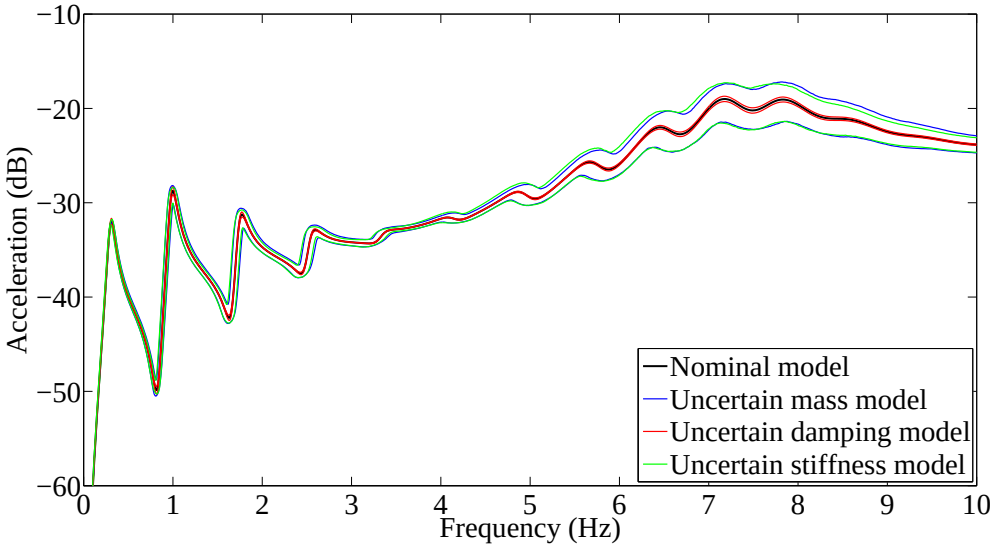

Figure 6.5: Case study 1, 2 and 3 - frequency response in acceleration for point $P_{obs,2}$.

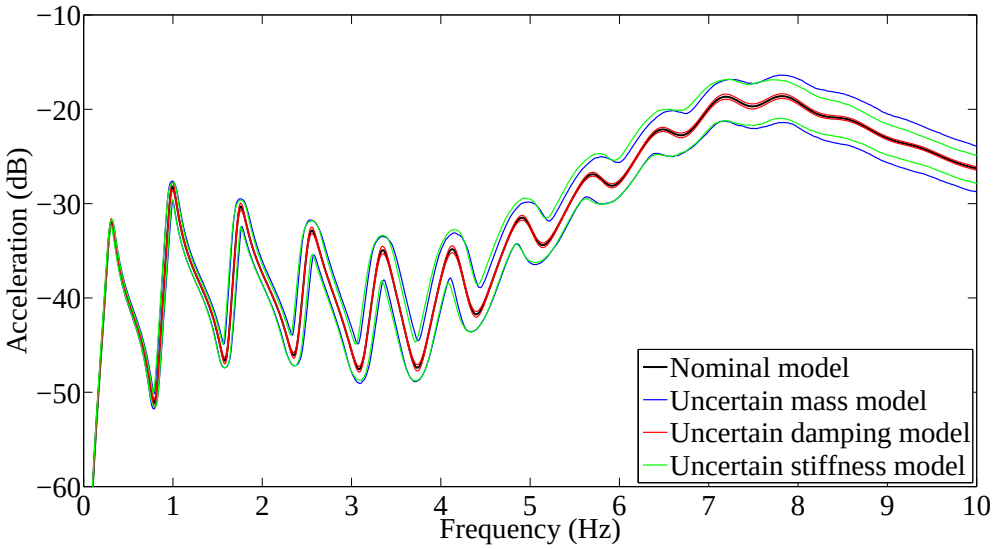

Figure 6.6: Case study 1, 2 and 3 - frequency response in acceleration for point $P_{obs,3}$.

	DP-inner	DP-interface	BHA-inner	BHA-interface
Mass	$\delta_{M,\mathrm{I},1} = 0.1$	$\delta_{M,\Gamma,1} = 0.1$	$\delta_{M,\mathrm{I},2} = 0$	$\delta_{M,\Gamma,2} = 0$
Damping	$\delta_{D,\mathrm{I},1} = 0.1$	$\delta_{D,\Gamma,1} = 0.1$	$\delta_{D,\mathrm{I},2} = 0$	$\delta_{C,\Gamma,2} = 0$
Stiffness	$\delta_{K,\mathrm{I},1} = 0.1$	$\delta_{K,\Gamma,1} = 0.1$	$\delta_{K,\mathrm{I},2} = 0$	$\delta_{K,\Gamma,2} = 0$

Table 6.4: Case study 4 - values of the dispersion parameters.

ii- Case study 5: BHA uncertainty, Table 6.5.

	DP-inner	DP-interface	BHA-inner	BHA-interface
Mass	$\delta_{M,\mathrm{I},1} = 0$	$\delta_{M,\Gamma,1} = 0$	$\delta_{M,\mathrm{I},2} = 0.1$	$\delta_{M,\Gamma,2} = 0.1$
Damping	$\delta_{D,\mathrm{I},1} = 0$	$\delta_{D,\Gamma,1} = 0$	$\delta_{D,\mathrm{I},2} = 0.1$	$\delta_{C,\Gamma,2} = 0.1$
Stiffness	$\delta_{K,\mathrm{I},1} = 0$	$\delta_{K,\Gamma,1} = 0$	$\delta_{K,\mathrm{I},2} = 0.1$	$\delta_{K,\Gamma,2} = 0.1$

Table 6.5: Case study 5 - values of the dispersion parameters.

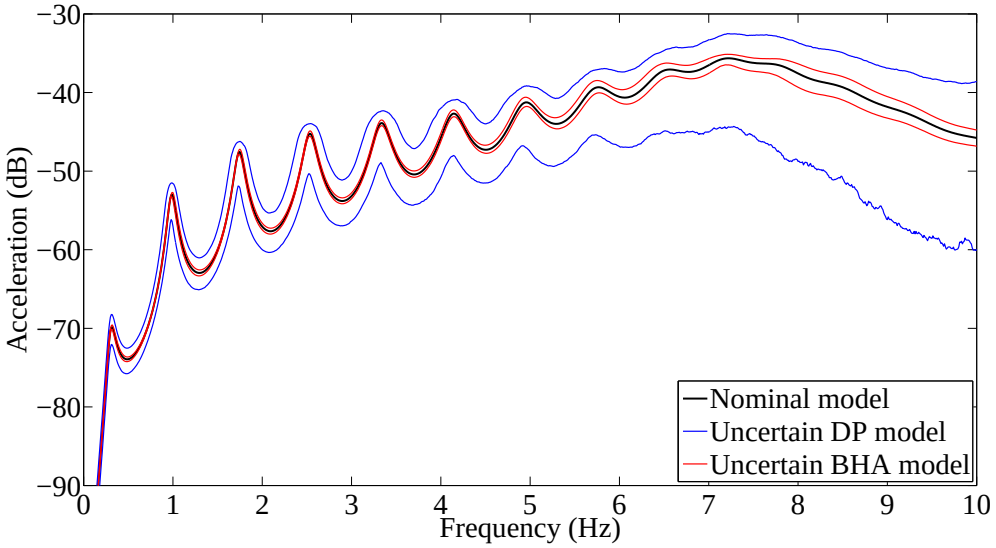

Figure 6.7: Case study 4 and 5 - frequency response in acceleration for point $\mathrm{P}_{\mathrm{obs},1}$.

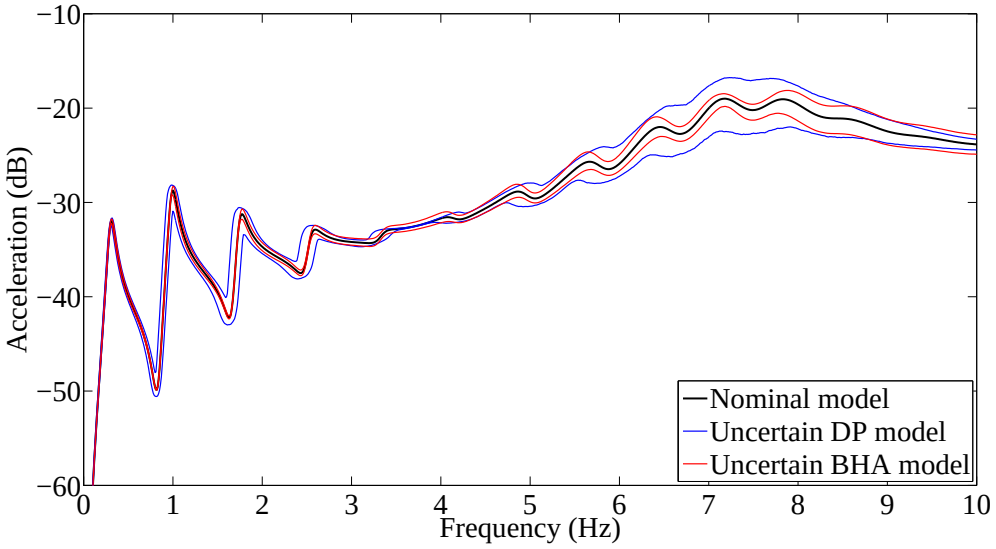

Figure 6.8: Case study 4 and 5 - frequency response in acceleration for point $\mathrm{P}_{\mathrm{obs},2}$.

Figures 6.7, 6.8, and 6.9 show the random responses comparing uncertainties in

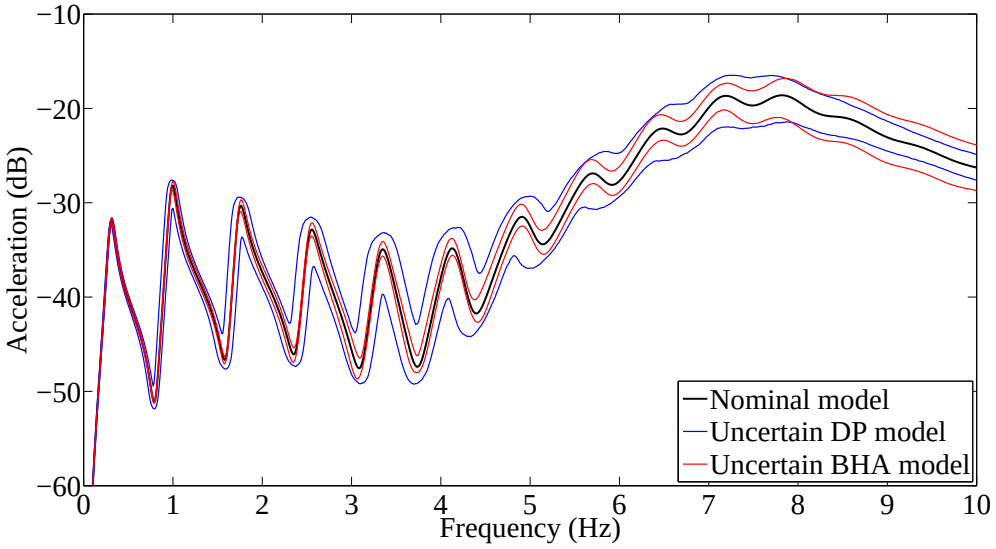

Figure 6.9: Case study 4 and 5 - frequency response in acceleration for point $P_{obs,3}$.

the DP and in the BHA. The statistical envelopes for uncertain DP increase significantly when frequency increases, except around 3.7 Hz, where they become thinner. It can be concluded that the DP uncertainties affect more the response of the system for the frequency range analyzed, due to low stiffness of the DP compared to BHA stiffness.

For uncertain BHA, the envelopes increase more significantly from 5 Hz, but they are much thinner than the response of the system for an uncertain DP. Specially for point $P_{obs,3}$, this behaviour means that the strategy in Eq. (2.5) is not robust for uncertainties present in bit-rock interaction for high frequencies; however, the strategy in Eq. (2.5) is robust for low frequencies that is the operational range. Therefore, a stochastic bit-interaction model is valid, as it done in chapter 4.

Inner DOFs versus interface DOFS

i- Case study 6: Inner DOFs uncertainty, Table 6.6.

	DP-inner	DP-interface	BHA-inner	BHA-interface
Mass	$\delta_{M,\mathrm{I},1} = 0.1$	$\delta_{M,\Gamma,1} = 0$	$\delta_{M,\mathrm{I},2} = 0.1$	$\delta_{M,\Gamma,2} = 0$
Damping	$\delta_{D,\mathrm{I},1} = 0.1$	$\delta_{D,\Gamma,1} = 0$	$\delta_{D,\mathrm{I},2} = 0.1$	$\delta_{C,\Gamma,2} = 0$
Stiffness	$\delta_{K,\mathrm{I},1} = 0.1$	$\delta_{K,\Gamma,1} = 0$	$\delta_{K,\mathrm{I},2} = 0.1$	$\delta_{K,\Gamma,2} = 0$

Table 6.6: Case study 6 - values of the dispersion parameters.

ii- Case study 7: Interface DOFs uncertainty, Table 6.7.

	DP-inner	DP-interface	BHA-inner	BHA-interface
Mass	$\delta_{M,\mathrm{I},1} = 0$	$\delta_{M,\Gamma,1} = 0.1$	$\delta_{M,\mathrm{I},2} = 0$	$\delta_{M,\Gamma,2} = 0.1$
Damping	$\delta_{D,\mathrm{I},1} = 0$	$\delta_{D,\Gamma,1} = 0.1$	$\delta_{D,\mathrm{I},2} = 0$	$\delta_{D,\Gamma,2} = 0.1$
Stiffness	$\delta_{K,\mathrm{I},1} = 0$	$\delta_{K,\Gamma,1} = 0.1$	$\delta_{K,\mathrm{I},2} = 0$	$\delta_{K,\Gamma,2} = 0.1$

Table 6.7: Case study 7 - values of the dispersion parameters.

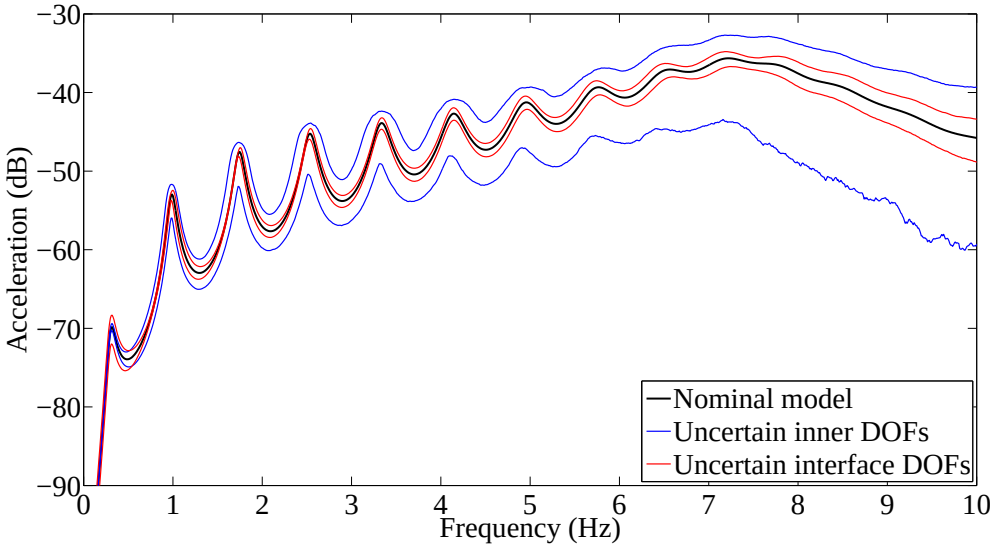

Figure 6.10: Case study 6 and 7 - frequency response in acceleration for point $\mathrm{P}_{\mathrm{obs},1}$.

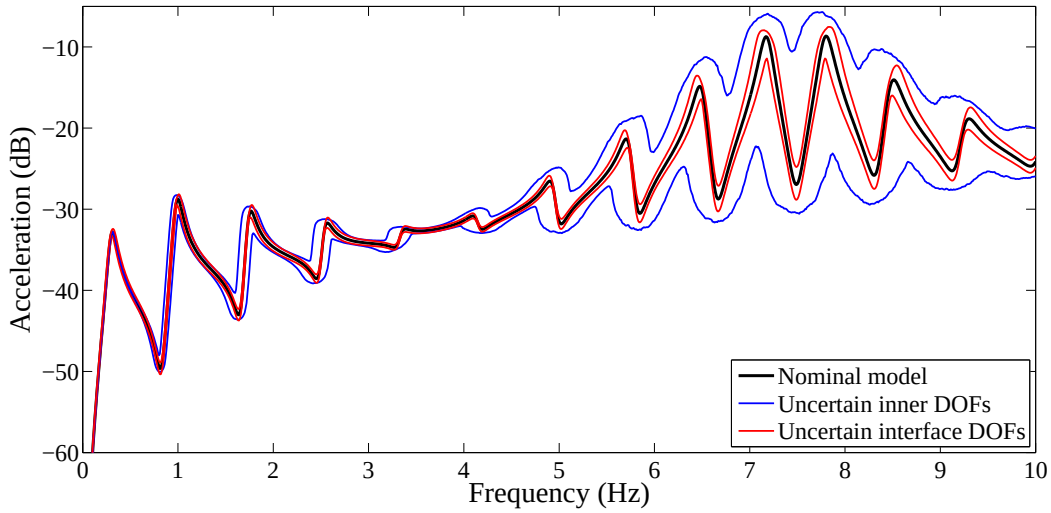

Figure 6.11: Case study 6 and 7 - frequency response in acceleration for point $\mathrm{P}_{\mathrm{obs},2}$.

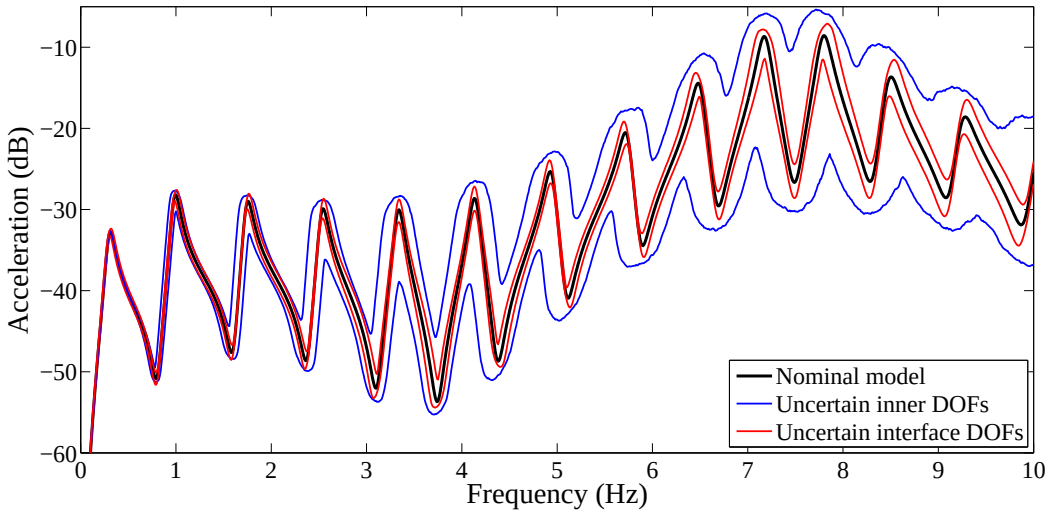

Figure 6.12: Case study 6 and 7 - frequency response in acceleration for point $P_{obs,3}$.

Figures 6.10, 6.11, and 6.12 show the random responses comparing inner and interface uncertainties. Both statistical envelopes increase when frequency increases, except in the region around 3.7Hz for $P_{obs,2}$. However, the statistical envelopes for uncertain interface DOFs are much thinner comparing to the statistical envelopes for uncertain inner DOFs. In the present analysis there is only one DOF in the interface, and the response is robust to uncertainties in this interface DOF, although it has a clear impact in the random response of the system.

This new strategy can allow to control the dispersion level of each inner and interface DOFs of each drill string substructure independently. We have to take into account which substructures and which frequencies the results are robust or not, showing that a bit-interaction stochastic model is valid even for an analysis of global uncertainties in a drill string.

Chapter 7

Conclusions, contributions and future works

This thesis proposes a robust analysis for drill string torsional dynamics, based on modeling and experimental identification under uncertainties. It involves the development of a new deterministic bit-rock interaction model, a new stochastic computational model for bit-rock interaction, an identification strategy, the construction of a simplified test-rig to obtain experimental results, and a new non-parametric approach that allows the assessment of main sources of uncertainties. The methodologies applied here are simple to implement and fitted the field data in all cases, showing good accuracy with low computational cost. This is an important topic for real application.

Only torsional vibrations were analyzed for a torsion bar system, discretized by means of the finite element method. A reduced-order model was constructed to speed up the computations. A new bit-rock interaction model, including a type of hysteresis (non-reversibility), is proposed herein. The verification of the proposed model is based on field data and its validation by experimental results was done. The analysis shows that the system including a bit-rock interaction model with hysteresis effects (1) favors the stability of the system for high nominal surface speeds and low WOB, and (2) induces higher stick-slip oscillations for low nominal surface speeds and high WOB. The reason for that has to do with the hysteretic cycle of the torque on bit versus the bit speed. In addition, the calibration procedure is straightforward, and could be implemented in real-time operations, which is still a challenge.

Furthermore, a new probabilistic model for the bit-rock interaction model is proposed. This model includes a multiplicative stochastic process to take into account fluctuations of the torque on bit during the drilling. The stochastic model was calibrated with field data and validated with experimental data, and it takes into account hysteretic cycles and their stochastic fluctuations. The proposed bit-rock probabilistic model can be

constructed independently from the computational model of the column.

The deterministic and stochastic torsional dynamics of a drill string are analyzed and a reasonable agreement between model predictions and field data is observed. The statistics of the stick and slip duration were also analyzed. Residuals are measured, and both models are representative, but some improvements concerning the parameter identification can refine the fitting procedure.

A considerable impact of the proposed stochastic model on the torsional stability of the system was observed. To such end, the stick-slip severity factor is computed and statistical envelopes are plotted for varying imposed speeds at the top. A robust estimation of the minimum angular speed is estimated using these plots.

A low-cost test-rig was designed to reproduce torsional vibrations of drill strings. The test-rig uses an electrical motor to rotate a slender circular bar with an inertial disk connected to a bit at the bottom. In the lower part, a test-body of concrete is lifted using an electrical jack. The rotation angle and speed are measured at the top (near electrical motor) and at the bit. Besides, the torque on electrical motor and on bit are measured using cantilever load cells. The axial force (WOB) is also measured using load cells. It was obtained 210 samples for 3 bit sizes and an top speed range of 100-220 RPM. The capability of reproducing stick-slip phenomenon is proved by the experimental data presented. The obtained results are in accordance to the field data behavior and they are validated with known models in the literature. The stick-slip cycle was then explained in detail by dividing the independent cycles and by extracting a single cycle, which presented a hysteretic effect for both torque on bit and WOB versus bit speed. It was concluded that uncertainties are clearly present in stick-slip cycles for the same sample and that bit-rock interaction highly depends on drilling conditions.

A new probabilistic model of uncertainties is implemented, in order to efficiently quantify the sensitivity of outputs with respect to these uncertainties. This new strategy is based on the terms of nonparametric probabilistic approach, together with Craig-Bampton substructuring method, which considers the uncertainties at the operator level globally, allowing to control the dispersion level of each inner and interface DOF of each drill string substructure independently. The random vibrations of the torsional drill string were analyzed, where the column is divided in two substructures (DP and BHA). For uncertain BHA, the envelopes increase more significantly from 5 Hz until 7 Hz, but they are much thinner than the response of the system for an uncertain DP, showing that the strategy for drill string torsional model is not robust for uncertainties present in bit-rock interaction for high frequencie, but it is robust for low frequencies (operational

range). Therefore, a bit-interaction stochastic model is valid even for an analysis of global uncertainties in a drill string.

Contributions of this work were published on or submitted to international journals. The first one [93] was published on journal *Archive of Applied Mechanics* (impact factor equal to 1.103), with the title *A probabilistic model of uncertainties in the substructures and interfaces of a dynamical system - application to the torsional vibration of a drill string*. This article is about the application of the new stochastic model, which is shown in this work. The second article [94] is published on *Mechanical System and Signal Processing* (impact factor equal to 4.116), with the title *Hysteretic Bit/Rock Interaction Model to Analyze the Torsional Dynamics of a Drill String*. This article proposes a novel hysteretic (non-reversible) bit-rock interaction model for the torsional dynamics of a drill string, where the non-linear torsional vibration and the stability map of the drill string system are analyzed employing the proposed bit-rock interaction model and also a commonly used reversible model (without hysteresis). A third article [95] has already been published on *Journal of Petroleum Science and Engineering* (impact factor equal to 2.382), with the title *Experimental analysis of stick-slip in drilling dynamics in a laboratory test-rig*, about the new and simple test-rig to analyze drilling dynamics, especially stick-slip oscillations, which might take into account hysteric effects for the bit-rock interaction. Yet another article is submitted to *Journal of Vibration and Control*, about a new stochastic model for the hysteretic behavior of the nonlinear bit-rock interaction, where the fluctuations of the stick-slip oscillations and the hysteretic effect provided by the nonlinear bit-rock interaction are modelled by introducing a stochastic process associated with the variations during the drilling.

The next steps of this work need to be developed: (1) for applying the new stochastic model for bit-rock interaction into the new strategy SM_{CB2}, in order to get a full analysis of torsional dynamics under uncertainties, which demands a deep and careful study; (2) for experimenting with more tests to improve the test-rig skills; (3) validation of the proposed models using numerical simulations; (4) for enabling axial DOF for the test-rig, in order to propose coupled axial-torsional models; and (5) for proposing a new strategy to control the torsional oscillations under uncertainties using hysteresis modeling, simulating a real operation of a drill string.

Bibliography

[1] Abbassian, F., Dunayevsky, V. A., 1998, Application of stability approach to torsional and lateral bit dynamics. SPE Drilling and Completion, vol. 13, no. 2, pp. 99-107.

[2] Adhikari, S., Manohar, C. S., 1999, Dynamic analysis of framed structures with statistical uncertainties. International Journal for Numerical Methods in Engineering, vol 44, pp. 1157-1178.

[3] Aguirre, L. A., 2007, Introdução à identificação de sistemas - Técnicas lineares e não-lineares aplicadas a sistemas reais. 3rd. edition, Editora UFMG, Brazil.

[4] Baker, R. O., Yarranton, H. W., Jensen, J. L., 2015, Practical Reservoir Engineering and Characterization. Gulf Professional Publishing, Oxford.

[5] Batou, A., Soize, C., 2009, Experimental identification of turbulent fluid forces applied to fuel assemblies using an uncertain model and fretting-wear estimation. Mechanical Systems and Signal Processing, vol. 23, no. 7, pp. 2141-2153.

[6] Batou, A., Soize, C., Corus, M., 2011, Experimental identification of an uncertain computational dynamical model representing a family of structures. Computers and Structures, vol. 89, pp. 1440-1448.

[7] Batou, A., 2015, A global/local probabilistic approach for reduced-order modelling adapted to the low- and mid-frequency structural dynamics. Computer Methods in Applied Mechanics and Engineering, vol. 294, pp. 123-140.

[8] Benaroya, H., Han, S. M., 2005, Probability Models in Engineering and Science. Taylor and Francis.

[9] Berlioz, A., Hagopian, J. D., Dufour, R., Draoui, E., 1996, Dynamic behavior of a drill-string: experimental investigation of lateral instabilities. Journal of Vibration and Accoustics, vol. 118, no. 3, pp. 292-298.

[10] Besselink, B., Van De Wouw, N., Nijmeijer, H., 2011, A semi-analytical study of stick-slip oscillations in drilling systems. Journal of Computational and Nonlinear Dynamics, vol. 6, no. 2, art. no. 021006.

[11] Breiman, L., 1973, Statistics With a View Toward Applications. Houghton Mifflin Company.

[12] Butlin, T., Langley, R. S., 2015, An efficient model of drillstring dynamics. Journal of Sound and Vibration, vol. 356, art. no. 12541, pp. 100-123.

[13] Cayres, B., da Fonseca, C., Santos, A., Weber, H. I., 2015, Analysis of dry friction-induced stick-slip in an experimental test rig modeling a drill string. Mechanisms and Machine Science, vol. 21, pp. 195-204.

[14] Chebli, H., Soize, C., 2004, Experimental validation of a nonparametric probabilistic model of nonhomogeneous uncertainties for dynamical systems. The Journal of the Acoustical Society of America, vol. 115, no. 2, pp. 697-705.

[15] Chen, C., Duhamel, D., Soize, C., 2006, Probabilistic approach for model and data uncertainties and its experimental identification in structural dynamics: Case of composite sandwich panels. Journal of Sound and Vibration, vol. 294, no. 1, pp. 64-81.

[16] Chin, W. C., 1994, Wave Propagation in Petroleum Engineering: Modern Applications to Drillstring Vibrations. Gulf Publishing.

[17] Chou, Y., 1975, Statistical Analysis. Holt International, Canada.

[18] Cook, R. D., 1995, Finite Element modelling for Stress Analysis. University of Wisconsin-Madson,John Wiley & Sons.

[19] Cook, R. et al., 2002, Concepts and applications of finite element analysis. John Wiley & Sons, Madison, USA.

[20] Craig, R. R., 2000, A Brief tutorial on substructuring analysis and testing. In: 18th International Modal Analysis Conference, pp. 899-908.

[21] Craig, R. R., Bampton, M., 1968, Coupling of Substructures for Dynamic Analysis. AIAA Journal, vol. 6, no. 7, pp. 1313-1319.

[22] Crandall, S. H., Mark, W. D., 1963, Random Vibration in Mechanical Systems. Academic Press, Inc.

[23] Corradi, M., 2006, A Short Account of the History of Structural Dynamics between the Nineteenth and Twentieth Centuries. Proceedings of the Second International Congress on Construction History, Cambridge University, vol. 1, pp. 837-854.

[24] Depouhon, A., Detournay, E., 2014, Instability regimes and self-excited vibrations in deep drilling systems. Journal of Sound and Vibration, vol. 333, no. 7, pp. 2019-2039.

[25] Divenyi, S., Savi, M. A., Wiercigroch, M., Pavlovskaia, E., 2012, Drill-string vibration analysis using non-smooth dynamics approach. Nonlinear Dynamics, vol. 70, no. 2, pp. 1017-1035.

[26] Duchereau, J., Soize, C., 2006, Transient dynamics in structures with non-homogeneous uncertainties induced by complex joints. Mechanical Systems and Signal Processing, vol. 20, no. 4, pp. 854-867.

[27] Durand, J. F., Soize, C., Gagliardini, L., 2008, Structural-acoustic modelling of automotive vehicles in presence of uncertainties and experimental identification and validation. The Journal of the Acoustical Society of America, vol. 124, no. 3, pp. 1513-1525.

[28] Einstein, A., 1905, On the motion of small particles suspended in liquids at rest required by the molecular-kinetic theory of heat. Annalen der Physik, no. 17, pp. 549-560.

[29] Elishakoff, I., Yongjian, R., 2003, Finite Element Methods for Structures with Large Stochastic Variations. Oxford University Press, USA.

[30] Elsayed, M., 2007, A novel approach to dynamic representation of drill strings in test rigs. Journal of Energy Resources Technology, Transactions of the ASME, vol. 129, no. 4, pp. 281-288.

[31] Fagan, A., 1991, An introduction to the petroleum industry. Department of Mines and Energy, Government of New Found land and Labrador, Canada.

[32] Fernandez, C., Soize, C., Gagliardini, L., 2010, Sound-insulation layer modelling in car computational vibroacoustics in the medium-frequency range. Acta Acustica united with Acustica (AAUWA), vol. 96, no. 3, pp. 437-444.

[33] Germay, C., Van de Wouw, N., Nijmeijer, H., Sepulchre, R., 2009, Nonlinear drill-string dynamics analysis. SIAM Journal on Applied Dynamical Systems, vol. 8, no. 2, pp. 527-553.

[34] Ghasemloonia, A., Rideout, D. G., Butt, S. D., Hajnayeb, A., 2015, Elastodynamic and finite element vibration analysis of a drillstring with a downhole vibration generator tool and a shock sub. Proceedings of the Institution of Mechanical Engineers, Part C: Journal of Mechanical Engineering Science, vol. 229, no. 8, pp. 1361-1384.

[35] Ghanem, R. G., Spanos, P. D., 1991, Stochastic Finite Elements: A Spectral Approach. Dover Publications Inc.

[36] Hakimi, H., Moradi, S., 2010, Drillstring vibration analysis using differential quadrature method. Journal of Petroleum Science and Engineering, vol. 70, no. 3-4, pp. 235-242.

[37] Hong, L., Girsang, I. P., Dhupia, J. S., 2016,Identification and control of stick-slip vibrations using Kalman estimator in oil-well drill strings. Journal of Petroleum Science and Engineering, vol. 140, pp. 119-127.

[38] Hu, Y. -B., Di, Q. -F., Wang, W. -C., Yao, J. -L., Yao, Y. -H., 2010, Influence of rotary table speed on the dynamic characteristics of drillstring in inclined straight hole. Gongcheng Lixue/Engineering Mechanics, vol. 27, no. 5, pp. 184-190.

[39] Hu, Y., Di, Q., Zhu, W., Chen, Z., Wang, W., 2012, Dynamic characteristics analysis of drillstring in the ultra-deep well with spatial curved beam finite element. Journal of Petroleum Science and Engineering, vol. 82-83, pp. 166-173.

[40] Inman, D. J., 2001, Engineering Vibration. International Edition, 2nd. ed., Prentice Hall International Inc., Nova Jersey, EUA.

[41] Irvine, T., 2013, Vibration Data. Available in: < https://vibrationdata.wordpress.com/2013/04/30/craig-bampton-method/>. Accessed to the web page on Jan. 28, 2015, 22:21:13.

[42] Jansen, J. D., 1993, Nonlinear dynamics of oilwell drillstrings. PhD thesis, Technische Universiteit Delft.

[43] Jaynes, E. T., 1957, Information theory and statistical mechanics. The Physical Review, vol. 106, no. 4, pp. 1620-630.

[44] Jaynes, E. T., 1957, Information theory and statistical mechanics II. The Physical Review, vol. 108, pp. 171-190.

[45] Jaynes, E. T., 2003, Probability Theory: The Logic of Science. Cambridge University Press, pp. 727.

[46] JCGM/WG 1, 2008, JCGM 100:2008 - Evaluation of measurement data - Guide to the expression of uncertainty in measurement. Joint Committee for Guides in Metrology.

[47] Kapitaniak, M., Vaziri Hamaneh, V., Chávez, J. P., Nandakumar, K., Wiercigroch, M., 2015, Unveiling complexity of drill-string vibrations: Experiments and

modelling. International Journal of Mechanical Sciences, vol. 101-102, art. no. 3042, pp. 324-337.

[48] Kapitaniak, M., Vaziri, V., Wiercigroch, M., 2018, Helical buckling of drill-strings. MATEC Web of Conferences 148, no. 16007.

[49] Karkoub, M., Zribi, M., Elchaar, L., Lamont, L., 2010, Robust $\hat{\mathrm{I}}\frac{1}{4}$-synthesis controllers for suppressing stick-slip induced vibrations in oil well drill strings. Multibody System Dynamics, vol. 23, pp. 191-207.

[50] Khulief, Y. A., Al-Naser, H., 2005, Finite element dynamic analysis of drillstrings. Finite Elements in Analysis and Design, vol. 41, pp. 1270-1288.

[51] Khulief, Y. A., Al-Sulaiman, F. A., Bashmal, S., 2007, Vibration analysis of drill-strings with self-excited stick-slip oscillations. Journal of Sound and Vibration, vol. 299, n. 3, pp. 540-558.

[52] Khulief, Y. A., Al-Sulaiman, F. A., 2009, Laboratory investigation of drillstring vibrations. Journal of Mechanical Engineering Science, vol. 233 (Part C), pp. 2249-2262.

[53] Kleiber, M., Tran, D. H., Hien, T. D., 1993, The Stochastic Finite Element Method. John Wiley & Sons, New York, USA.

[54] Klerk, D., Rixen, D. J. e Voormeeren, S. N., 2008, General Framework for Dynamic Substructuring: History, Review, and Classification of Techniques. AIAA Journal, vol. 46, no. 5, pp. 1169-1180.

[55] Ko, P. L., Brockley, C. A., 1970, The Measurement of Friction and Friction-Induced Vibration. Journal of Lubrication Tech, vol. 92, no. 4, pp. 543-549.

[56] Kree, P., Soize, C., 1986, Mathematics of Random Phenomena: Random Vibrations of Mechanical Structures (Mathematics and Its Applications). Springer, New York, USA, 1986.

[57] Kreuzer, E., Steidl, M., 2012, Controlling torsional vibrations of drill strings via decomposition of traveling waves. Archive of Applied Mechanics, vol. 82, no. 4, pp. 515-531.

[58] Kurrer, K. E., Ramm, E., 2012, The History of the Theory of Structures: From Arch Analysis to Computational Mechanics. John Wiley & Sons, pp.848.

[59] Kyllingstad, A., Halsey, G.W., 1988, Study of slip/stick motion of the bit. SPE drilling engineering, vol. 3, n. 4, pp. 369-373.

[60] Legault, J., Langley, R.S., Woodhouse, J., 2012, Physical consequences of a non-parametric uncertainty model in structural dynamics. Journal of Sound and Vibration, vol. 331, no. 25, pp. 5469-5487.

[61] Leine, R. I., Van Campen, D. H., van den Steen, L., 1998, Stick-slip vibrations induced by alternate friction models. Nonlinear Dynamics, vol. 16, pp. 41-54.

[62] Leine, R. I., Van Campen, D. H., Keultjes, W. J. G., 2002, Stick-slip Whirl Interaction in Drillstring Dynamics. Journal of Vibration and Acoustics, vol. 124, pp. 209-220.

[63] Liao, C., Vlajic, N., Karki, H., Balachandran, B., 2012, Parametric studies on drill-string motions. International Journal of Mechanical Sciences, vol. 54, pp. 260-268.

[64] Lin, Y. K., 1967, Probabilistic Theory of structural Dynamics. McGraw-Hill, Inc.

[65] Liu, X., Vlajic, N., Long, X., Meng, G., Balachandran, B., 2013, Nonlinear motions of a flexible rotor with a drill bit: Stick-slip and delay effects. Nonlinear Dynamics, vol. 72, no. 1-2, pp. 61-77.

[66] Liu, X., Vlajic, N., Long, X., Meng, G., Balachandran, B., 2014, State-dependent delay influenced drill-string oscillations and stability analysis. Journal of Vibration and Acoustics, Transactions of the ASME, vol. 136, no. 5, art. no. 051013.

[67] Liu, Y., Chávez, J. P., Sa, R., Walker, S., 2017, Numerical and experimental studies of stick-slip oscillations in drill-strings. Nonlinear Dynamics, vol. 90, pp. 2959-2978.

[68] Lopez, R. H., Ritto, T. G., Sampaio, R., Cursi, E. S., 2010, Optimization of a flexible rotor-bearing system considering uncertainties. Proceedings of 11th Pan-American Congress of Applied Mechanics - PACAM XI, Foz do IguaÃ§u, PR, Brazil.

[69] Lopez, R. H., Ritto, T. G., Sampaio, R., Cursi, E. S., 2014, Optimization of a stochastic dynamical system. Journal of the Brazilian Society of Mechanical Sciences and Engineering, vol. 36, pp. 257-264.

[70] Lutes, L. D., Sarkani, S., 1997, Stochastic Analysis of Structural and Mechanical Vibrations. Prentice-Hall, Inc., Upper Saddle River, New Jersey, USA.

[71] Maia, N. et al., 1997, Theoretical and experimental modal analysis. John Wiley & Sons, Somerset, EN.

[72] Mehta, M. L., 1991, Random Matrices. Revised and Enlarged Second Edition. Academic Press.

[73] Melakhessou, H., Berlioz, A., Ferraris, G., 2003, A Nonlinear Well-Drillstring Interaction Model. ASME J. Vib. Acoust., vol. 125, no. 1, pp. 46-52, DOI:10.1115/1.1523071.

[74] Mihajlovic, N., Van De Wouw, N., Hendriks, M. P. M., Nijmeijer, H., 2006, Friction-induced limit cycling in flexible rotor systems: An experimental drill-string set-up. Nonlinear Dynamics, vol. 46, no. 3, pp. 273-291.

[75] Meko, D. M., 2015, Applied Time Series Analysis. GEOS 585A, $Notes_6$, Spring Inc.

[76] Mignolet, M., Soize, C., Avalos, J., 2013, Nonparametric stochastic modelling of structures with uncertain boundary conditions/coupling between substructures. AIAA Journal, vol. 51, no. 6, pp. 1296-1308.

[77] Morand, H. P. J, Ohayon, R., 1979, Substructure variational analysis for the vibrations of coupled fluid-structure systems. International Journal for Numerical Methods in Engineering, vol. 14, no. 5, pp. 741-755.

[78] Murthy, R. et al., 2012, Uncertainty-based experimental validation of nonlinear reduced order models. Journal of Sound and Vibration, vol. 331, no. 5, pp. 1097-1114.

[79] Nandakumar, K., Wiercigrochn, M., 2013, Stability analysis of a state dependent delayed,coupled two DOF model of drill-string vibration. Journal of Sound and Vibration, vol. 332, pp. 2575-2592.

[80] Navarro-López, E. M., Licéaga-Castro, E., 2009, Non-desired transitions and sliding-mode control of a multi-DOF mechanical system with stick-slip oscillations. Chaos, Solitons and Fractals, vol. 41, no. 4, pp. 2035-2044.

[81] Pang, S. -Q., Zhu, X. -Z., Chen, L., 2011, Finite element analysis of dynamics characteristics for the BHA system in vertical well. Shiyou Huagong Gaodeng Xuexiao Xuebao/Journal of Petrochemical Universities, vol. 24, no. 4, pp. 55-59.

[82] Park, K. C., 2005, Curso ASEN 5022-Dynamics of Aerospace Structures. Universidade de Colorado Boulder, cap. 21, pp. 1-15.

[83] Paslay, P. R., Jan, Y. M., Kingman, J. E. E., MacPherson, J. D., 1992, Detection of lateral ressonances while drilling with surface longitudinal and torsional sensors. 67th SPE Annual Conferencem Washington.

[84] Patil, P. A., Teodoriu, C., 2013, A comparative review of modelling and controlling torsional vibrations and experimentation using laboratory setups. Journal of Petroleum Science and Engineering, vol. 112, pp. 227-238.

[85] Pavone, D. R., Desplans, J. P., Application of high sampling rate downhole measurements for analysis and cure of stick-slip in drilling. Proceedings - SPE Annual Technical Conference and Exhibition Delta, pp. 335-345.

[86] Petroleum History Institute website, 2018, Oil History - The Drill String - Cable Tools. Available on: <http://petroleumhistory.org/OilHistory/pages/String/string.html>. Accessed to the web page on Jul. 12, 2017, 14:53:21.

[87] Piiroinen, P. T., Kuznetsov, Y. A., 2008, An event-driven method to simulate Filippov systems with accurate computing of sliding motions. ACM Transactions on Mathematical Software, vol. 34, no. 3, art. no. 13.

[88] Piovan, M. T., Sampaio, R., 2015, Parametric and nonparametric probabilistic approaches in the mechanics of thin-walled composite curved beams. Thin-Walled Structures, vol. 90, pp. 95-106.

[89] Pei, Y. -C., Sun, Y. -H., Wang, J. -X., 2013, Dynamics of rotating conveying mud drill string subjected to torque and longitudinal thrust. Meccanica, vol. 48, no. 9, pp. 2189-2201.

[90] Piovan, M. T., Sampaio, R., 2009, Continuous models for drill-strings of the oil industry: Analysis of approaches and discretization schemes [Modelos continuos de sondas de perforación para la industria petrolera: Análisis de enfoques y su discretización]. Revista Internacional de Metodos Numericos para Calculo y Diseno en Ingenieria, vol. 25, no. 3, pp. 259-277.

[91] Priestley, M.B., 1981, Spectral Analysis and Time Series. Academic Press, New York.

[92] Raymond, D. W., Elsayed, M. A., Polsky, Y., Kuszmaul, S. S., 2008, Laboratory simulation of drill bit dynamics using a model-based servohydraulic controller. Journal of Energy Resources Technology, Transactions of the ASME, vol. 130, no. 4, pp. 0431031-04310312.

[93] Real, F. F., Fontanela, F., Ritto, T. G., Batou, A., Desceliers, C., 2017, A probabilistic model of uncertainties in the substructures and interfaces of a dynamical system - application to the torsional vibration of a drill-string. Archive of Applied Mechanics, vol. 87, pp. 685-698, DOI 10.1007/s00419-016-1217-6.

[94] Real, F. F., Batou, A., Ritto, T. G., Desceliers, C., Aguiar, R. R., 2018, Hysteretic Bit/Rock Interaction Model to Analyze the Torsional Dynamics of a Drill String. Mechanical System and Signal Processing, vol. 111, pp. 222-233.

[95] Real, F. F., Lobo, D. M., Ritto, T. G., Pinto, F. A. N. C., 2018, Experimental analysis of stick-slip in drilling dynamics in a laboratory test-rig. Journal of Petroleum Science and Engineering, vol. 170, pp. 755-762.

[96] Ren, F. S., Yao, Z. G., 2013, Study on nonlinear dynamics and bifurcations in rotating compressive-drill string. Gongcheng Lixue/Engineering Mechanics, vol. 30, no. 10, pp. 251-256.

[97] Ren, F., Wang, B., Chen, S., Yao, Z., Bai, B., 2016, Nonlinear Model and Qualitative Analysis for Coupled Axial/Torsional Vibrations of Drill String. Shock and Vibration, 2016, art. no. 1646814.

[98] Richard, T., Detournay, E., 2004, Self-excited stick-slip vibrations of drill bits. Comptes Rendus de Mecanique, vol. 332, pp. 619-626.

[99] Richard, T., Germay, C., Detournay, E., 2007, A simplified model to explore the root cause of stick-slip vibrations in drilling systems with drag bits. Journal of Sound and Vibration, vol. 305, pp. 432-456.

[100] Blog Prof. Ritto. Available on: <http://thiagoritto.blogspot.com/p/research.html>.

[101] Ritto, T. G., Sampaio, R., Cataldo, E., 2008, Timoshenko Beam with Uncertainty on the Boundary Conditions. Journal of the Brazilian Society of Mechanical Science and Engineering, vol. XXX, no. 4, pp. 295-303.

[102] Ritto, T. G., Soize, C., Sampaio, R., 2009, Nonlinear dynamics of a drill-string with uncertain model of the bit-rock interaction. International Journal of NonLinear Mechanics, vol. 44, no. 8, pp. 865-876.

[103] Ritto, T. G., Soize, C., Sampaio, R., 2010, Robust optimization of the rate of penetration of a drill-string using a stochastic nonlinear dynamical model. Computational Mechanics, vol. 45, no. 5, pp. 415-427.

[104] Ritto, T. G., Soize, C., Sampaio, R., 2010, Probabilistic model identification of the bit rock-interaction-model uncertainties in nonlinear dynamics of a drill-string. Mechanics Research Communications, vol. 37, pp. 584-589.

[105] Ritto, T. G., 2010, Numerical analysis of the nonlinear dynamics of a drill-string with uncertainty modelling. D.Sc. thesis, Mechanical Engineering Department, Scientific Research Center of Pontifical Catholic University of Rio de Janeiro (PUC-Rio).

[106] Ritto, T. G., Sampaio, R., 2012, Stochastic drill-string dynamics with uncertainty on the imposed speed and on the bit-rock interaction parameters. International Journal for Uncertainty Quantification, vol. 2, no. 2, pp. 111-124.

[107] Ritto, T.G., Escalante, M.R., Sampaio, R., Rosales, M.B., 2013, Drill-string horizontal dynamics with uncertainty on the frictional force. Journal of Sound and Vibration, vol. 332, no. 1, pp. 145-153.

[108] Ritto, T. G., Sampaio, R., 2013, Measuring the efficiency of vertical drill-strings: A vibration perspective. Mechanics Research Communications, vol. 52, pp. 32-39.

[109] Ritto, T. G., 2014, Choice of Measurement Locations of Nonlinear Structures Using Proper Orthogonal Modes and Effective Independence Distribution Vector. Shock and Vibration, vol. 2014, Article ID 697497, 6 pp.

[110] Ritto, T. G., Soize, C., Rochinha, F. A., Sampaio, R., 2014, Dynamic stability of a pipe conveying fluid with an uncertain computational model. Journal of Fluids and Structures, vol. 49, pp. 412-426.

[111] Ritto, T. G., 2015, Bayesian approach to identify the bit-rock interaction parameters of a drill-string dynamical model. Journal of the Brazilian Society of Mechanical Sciences and Engineering, vol. 37, no. 4, pp. 1173-1182.

[112] Ritto, T. G., Aguiar, R. R., Baieb, S. H., 2017, Validation of a drill string dynamical model and torsional stability. Meccanica, article accepted in 2017, January.

[113] Rubinstein, R.Y., 2007, Simulation and the Monte Carlo Method. Series in Probability and Statistics. John Wiley and Sons, New Jersey, USA, 2nd edition.

[114] Sampaio, R., Piovan, M. T., Lozano, G. V., 2007, Coupled axial/torsional vibrations of drilling-strings by mean of nonlinear model. Mechanics Research Comunications, vol. 34, no. 5-6, pp. 497-502.

[115] Serfling, R. J., 1980, Approximation Theorems of Mathematical Statistics. John Wiley & Sons, Maryland, USA, pp. 371.

[116] Schlumberger Oilfield Glossary, 2017, The Oilfield Glossary: Where the Oil Field Meets the Dictionary. Available on: <http://www.glossary.oilfield.slb.com/>. Accessed to the web page on Jan. 18, 2017, 10:55:34.

[117] Schuller, G. I., 1997, A state-of-the-art report on computational stochastic mechanics. Probabilistic Engineering Mechanics, vol. 12, no. 4, pp. 197-321.

[118] Schueller, G. I., 2006, Developments in stochastic structural mechanics. Archive of Applied Mechanics, vol.75, no. 10-12, pp. 755-773.

[119] Schueller, G. I., 2007, On the treatment of uncertainties in structural mechanics and analysis. Computers and Structures, vol. 85, no. 5-6, pp. 235-243.

[120] Schuster, A., 1898, On the investigation of hidden periodicities with application to a supposed 26 day period of meteorological phenomena. Terrestrial Magnetism, vol. 3, no. 1, pp. 13-41.

[121] Shannon, C. E., 1948, A mathematical theory of communication. Bell System Technical Journal, vol. 27, pp. 379-423 and 623-659.

[122] Shen, Y., Zhang, Z., Zhao, J., Chen, W., Hamzah, M., Hammer, R., and Downton, G., Schlumberger, 2017, The Origin and Mechanism of Severe Stick-Slip. SPE Annual Technical Conference and Exhibition.

[123] Shinozuka, M., Deodatis, G., 1988, Response variability of stochastic Finite element systems. Journal of Engineering Mechanics, vol. 114, no. 3, pp.499-519.

[124] Soize, C., 2000, A nonparametric model of random uncertainties for reduced matrix models in structural dynamics. Probabilistic Engineering Mechanics, vol. 15, no. 3, pp. 277-294.

[125] Soize, C., 2001, Maximum entropy approach for modelling random uncertainties in transient elastodynamics. Journal of the Acoustical Society of America, vol. 109, no. 5, pp. 1979-1996.

[126] Soize, C., Chebli, H., 2003, Random uncertainties model in dynamic substructuring using a nonparametric probabilistic model. Journal of Engineering Mechanics, vol. 129, no. 24, pp. 449-457.

[127] Soize, C., 2005, A comprehensive overview of a non-parametric probabilistic approach of model uncertainties for predictive models in structural dynamics. Journal of Sound and Vibration, vol. 288, no. 3, pp. 623-652.

[128] Soize, C., 2005, Random matrix theory for modelling uncertainties in computational mechanics. Computer Methods in Applied Mechanics and Engineering, vol 194, no. 12-16, pp. 1333-1366.

[129] Soize, C., Capiez-Lernout, E., Durand, J. F., Fernandez, C., Gagliardini, L., 2008, Probabilistic model identification of uncertainties in computational models for dynamical systems and experimental validation. Computer Methods in Applied Mechanics and Engineering, vol. 198, no. 1, pp. 150-163.

[130] Soize, C., 2009, Nonparametric probabilistic approach of uncertainties for elliptic boundary value problem. International Journal for Numerical Methods in Engineering, vol. 80, no. 2, pp. 673-688.

[131] Soize, C., 2010, Generalized probabilistic approach of uncertainties in computational dynamics using random matrices and polynomial chaos decompositions. International Journal for Numerical Methods in Engineering, vol. 81, no. 8, pp. 939-970.

[132] Soize, C., 2012,Stochastic Models of Uncertainties in Computational Mechanics (Lecture Notes in Mechanics). Amer Society of Civil Engineers, Reston, USA, pp. 125.

[133] Spanos, P. D., Chevallier, A. M., Politis, N. P., 2002, Nonlinear stochastic drillstring vibrations. Journal of Vibration and Acoustics, Transactions of the ASME, vol. 124, no. 4, pp. 512-518.

[134] Spanos, P. D., Chevalier, A. M., Politis, N. P., Payne, M. L., 2003, Oil and gas well drilling: A vibrations perspective. The Shock and Vibration Digest, vol. 35, no. 2, pp.85-103.

[135] Spanos, P. D., Politis, N. P., Esteva, M., Payne, M. L., 2009, Drillstring vibrations. Advanced Drilling and Well Technology (Society of Petroleum Engineers), pp. 117-156.

[136] Terrand-Jeanne, A., Martins, V. S., 2016, modellingś approaches for Stick-Slip phenomena in drilling. IFAC-Papers On Line, vol. 49, no. 8, pp. 118-123.

[137] Tikhonov, V. S., Safronov, A. I., 2011, Analysis of postbuckling drillstring vibrations in rotary drilling of extended-reach wells. Journal of Energy Resources Technology, Transactions of the ASME, vol. 133, no. 4, art. no. 043102.

[138] Tucker, R. W., Wang, C., 1997, The excitation and control of torsional slip-stick in the presence of axial vibrations.Available on: <http://citeseerx.ist.psu.edu/viewdoc/summary?doi=10.1.1.24.4347>. Accessed to the web page on Jan. 18, 2017, 10:24:55.

[139] Tucker, R. W., Wang, C., 1999, On the effective control of torsional vibrations in drilling systems. Journal of Sound and Vibration, vol. 224, no. 1, pp. 101-122.

[140] Tucker, R. W., Wang, C., 1999, An integrated model for drill-string dynamics. Journal of Sound and Vibration, vol. 224, no. 1, pp. 123-165.

[141] Tucker, R. W., Wang, C., 2003, Torsional vibration control and Cosserat dynamics of a drill-rig assembly. Meccanica, vol. 38, no. 1, pp. 143-159.

[142] Vance, J., Zeidan, F., Murphy, B., 2010, Machinery vibration and rotordynamics. John Wiley & Sons, New Jersey, USA.

[143] Vanmarcke, E., Grigoriu, M., 1983, Stochastic Finite element analysis of simple beams. Journal of Engineering Mechanics, vol. 109, no. 5, pp. 1203-1214.

[144] Viguié, R., Kerschen, G., Golinval, J. -C., McFarland, D. M., Bergman, L. A., Vakakis, A. F., van de Wouw, N., 2009, Using passive nonlinear targeted energy transfer to stabilize drill-string systems. Mechanical Systems and Signal Processing, vol. 23, no. 1, pp. 148-169.

[145] Vincent, T. L., Novara, C., 2013, Mixed parametric/non-parametric identification of systems with discontinuous nonlinearities. Automatica, vol. 49, pp. 3661-3669.

[146] Vlajic, N., Liao, C. -M., Karki, H., Balachandran, B., 2014, Stick-slip motions of a rotor-stator system. Journal of Vibration and Acoustics, Transactions of the ASME, vol. 136, no. 2, art. no. 021005.

[147] Wang, X., Chen, P., Ma, T., Liu, Y., 2017, Modeling and experimental investigations on the drag reduction performance of an axial oscillation tool. Journal of Natural Gas Science and Engineering, vol. 39, pp. 118-132.

[148] Weikai, L., Mingxing, S., Ziyi, X., Xuehong, Z., 2014, Gap element method of longitudinal vibration of drill string. Journal of Chemical and Pharmaceutical Research, vol. 6, no. 7, pp. 1523-1530.

[149] Westermann, H., Gorelik, I., Rudat, J., Moritz, C., Neubauer, M., Wallaschek, J., Höhn, O., 2015, A new test rig for experimental studies of drillstring vibrations. SPE Drilling and Completion, vol. 30, no. 2, pp. 119-128.

[150] Wiercigroch, M., Nandakumar, K., Peia, L., Kapitaniak, M., Vaziri Hamaneh, V., Ch/'avez, J. P., 2017, State dependent delayed drill-string vibration: Theory, experiments and new model. Procedia IUTAM Symposium on Nonlinear and Delayed Dynamics of Mechatronic Systems, vol. 22, pp. 39-50.

[151] Wirsching, P. H., Paez, T. L., Ortiz, K., 2006, Random Vibrations: Theory and Practice. Dover Publications, Inc., New York, USA.

[152] Wojewoda, J., Stefański, A., Wiercigroch, M., Kapitaniak, T., 2008, Hysteretic effects of dry friction: modelling and experimental studies. Philos Trans R. Soc. A A, vol. 366, pp. 747-765, DOI: 10.1098/rsta.2007.2125.

[153] Woodhouse, J., Putelat, T., McKay, A., 2015, Are there reliable constitutive laws for dynamic friction?. Philos Trans A Math Phys Eng Sci., vol. 373, no. 2051, DOI: 10.1098/rsta.2014.0401.

[154] Wu, C. F. J., Hamada, M. S., 2009, Experiments: Planning, Analysis, and Optimization. 2nd Edition, John Wiley & Sons, Inc., 760 pp.

[155] Wu, X., Karuppiah, V., Nagaraj, M., Partin, U. T., Machado, M., Franco, M., Duvvuru, H. K., 2012, Identifying the Root Cause of Drilling Vibration and Stick-Slip Enables Fit-for-Purpose, IADC/SPE Drilling Conference and Exhibition, no. 151347.

Appendix A

Modified Euler Scheme

Modified Euler Scheme is a first-order numerical integration method for solving ordinary differential equations (ODEs), which requires low computational cost. This methodology substitutes angular acceleration $\ddot{\mathbf{u}}$ per angular velocity $\dot{\mathbf{u}}$, by the simple approximations:

$$\ddot{\mathbf{u}}_i \approx \frac{\dot{\mathbf{u}}_{(i+1)} - \dot{\mathbf{u}}_i}{\Delta t}, \tag{A.1}$$

$$\dot{\mathbf{u}}_i \approx \frac{\mathbf{u}_i - \mathbf{u}_{(i-1)}}{\Delta t}. \tag{A.2}$$

For convenience, let rewrite the equations above and, specially for Eq. (A.1), let rewrite in the step back,

$$\dot{\mathbf{u}}_i \approx \ddot{\mathbf{u}}_{(i-1)}\,\Delta t + \dot{\mathbf{u}}_{(i-1)}, \tag{A.3}$$

$$\mathbf{u}_i \approx \dot{\mathbf{u}}_i\,\Delta t + \mathbf{u}_{(i-1)}. \tag{A.4}$$

Let the Eq. (2.5) or (2.7), Eq. (A.3) and Eq. (A.4). After some manipulations, it is possible to get the follow system formed by Eq. (A.5) and Eq. (A.6)

$$\dot{\mathbf{u}}_i \approx \dot{\mathbf{u}}_{(i-1)} + \Delta t[\widetilde{M}]^{-1}(\widetilde{\mathbf{T}}(\dot{\mathbf{u}}, \ddot{\mathbf{u}}) - \widetilde{D}]\,\dot{\mathbf{u}}_{(i-1)} - [\widetilde{K}]\,\mathbf{u}_{(i-1)}), \tag{A.5}$$

$$\mathbf{u}_i \approx \dot{\mathbf{u}}_i\,\Delta t + \mathbf{u}_{(i-1)}. \tag{A.6}$$

It is important to mention that this system is stable if

$$\Delta t < \frac{\pi}{5\,\omega_{n_{max}}}, \tag{A.7}$$

where $\omega_{n_{max}}$ is the maximum value for the natural frequency of the structure.

Appendix B

Algorithm

The Algorithm 2 details the steps of drilling simulation methodology.

Algorithm 2: Drilling simulation algorithm.

INITIALIZATION:
Input initial values (geometrical, physical and mechanical characteristics);
Load the field or experimental data;
Implement the FEM strategy:
  Input the number of elements;
  Construct the full matrices;
  Get the reduced-order matrices;
Determine the torque on bit and its standard-deviation from deterministic models;
Identify the parameters related to the torque on bit and its standard-deviation using the field or experimental data;
Estimate the PSD by Periodogram Method;
Generate the simulated track (Gauss distribution);
Initiate the drill string simulation;
LOOP: for $k = 1, \ldots, (n_t)$ **do**
  Prediction of angular velocity and displacement (reduced-order);
    $\dot{\mathbf{q}} = \dot{\mathbf{q}}_{i-1} + (\Delta t[\widetilde{M}]^{-1}).*([\widetilde{T}] - ([\widetilde{D}].*\dot{\mathbf{q}}) - ([\widetilde{K}].*\mathbf{q}_{i-1}))$;
    $\mathbf{q} = \mathbf{q}_{i-1} + \Delta t * \dot{\mathbf{q}}$;
  Actualization (reduced-order);
    $\dot{\mathbf{q}}_{i-1} = \dot{\mathbf{q}}$;
    $\mathbf{q}_{i-1} = \mathbf{q}$
  Angular velocity and displacement on bit;
    $\dot{\theta} = \Phi * \dot{\mathbf{q}}$;
    $\theta = \Phi * \mathbf{q}$;
  Calculate the torque on bit according to the selected model;
  Calculate the stochastic torque on bit (including simulated track);
  Actualization of torque (reduced-order);

Appendix C

Convergence analysis

For each Monte Carlo loop, an independent realization of the stochastic bit-rock interaction model is generated and a realization of the stochastic angular velocity is calculated.

Convergence for stick-slip severity factor is determined on the stationary regime. The convergence with respect to the number of samplings n_s is analyzed by introducing the convergence function

$$Conv_1(n_s) = \sqrt{\frac{1}{n_s}\sum_{i=1}^{n_s}\int_B SS_i(\dot{\theta}_{top\ drive})^2 d\dot{\theta}_{top\ drive}}, \tag{C.1}$$

where $SS_i(\dot{\theta}_{top\ drive})$ corresponds to the ith calculated realization of the stick-slip severity factor. Equation (C.1) is plotted in Figure C.1.It can see in this figure that a good convergence is achieved using 500 realizations.

Convergence analysis is also demanded for number of simulations and number of normal modes for the whole structure and for each substructure (DP and BHA) separately, according to the Tab. 3.1 data. The mean square convergence method is applied through the equation:

$$Conv_2(n_s, N) = \sqrt{\frac{1}{n_s}\sum_{i=1}^{n_s}\int_B \|a, (\omega_i, \theta_i)\|^2 d\omega} \tag{C.2}$$

where θ_i represents one generated simulation i, ω_i is the frequency, n_s is the number of simulations, and N is the number of normal modes. The Fig. C.2 shows the convergence analysis for number of iterations acoording to the Eq. (C.2), and the Figs.C.3 and C.4 show the convergence analysis for BHA and DP normal modes, respectively,

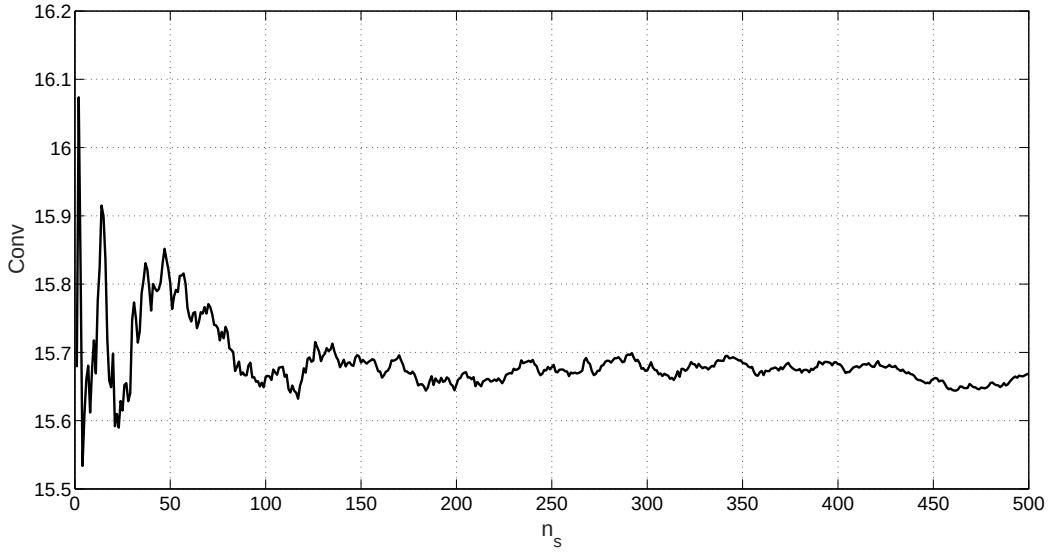

Figure C.1: Convergence function $n_s \mapsto Conv(n_s$.

according to the Eq. (C.2).

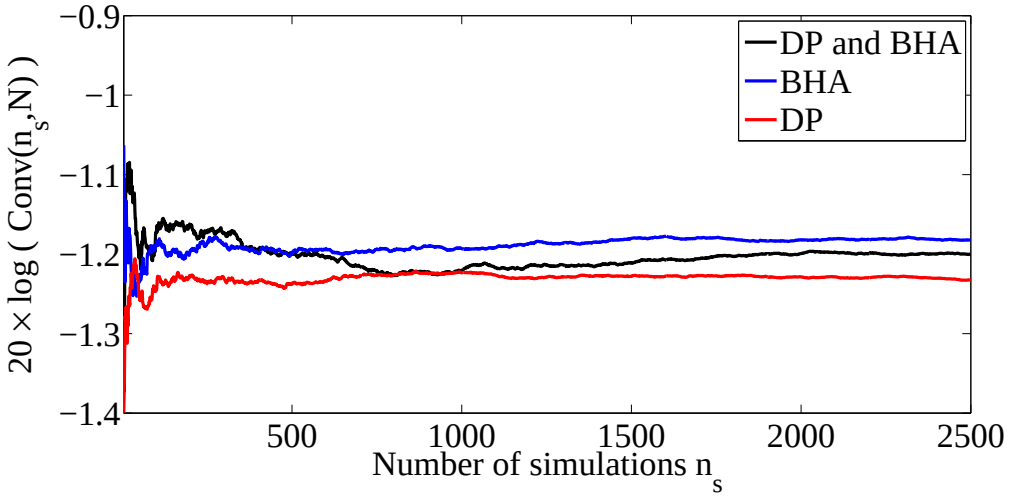

Figure C.2: Convergence analysis for number of iterations.

It is noticed the Fig. C.2 shows the convergence in $n_s = 2,500$ simulations safely, and Figs. C.3 and C.4 ensure the convergence after 7 modes for DP and BHA, that is why it was used here 20 modes for both. Uncertainty level δ is considered in these figures in three scenarios:

1. first one considers uncertainties for both, DP and BHA, at level δ equal to 0.1 for stiffness, damping and mass matrices;

2. second one considers uncertainties only for BHA, at level δ equal to 0.1 for stiffness, damping and mass matrices;

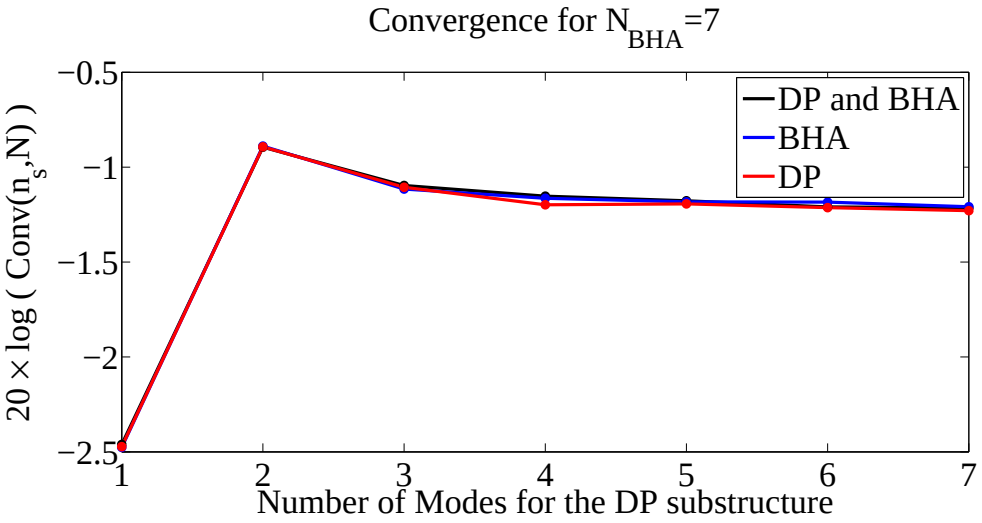

Figure C.3: Convergence analysis for DP normal modes.

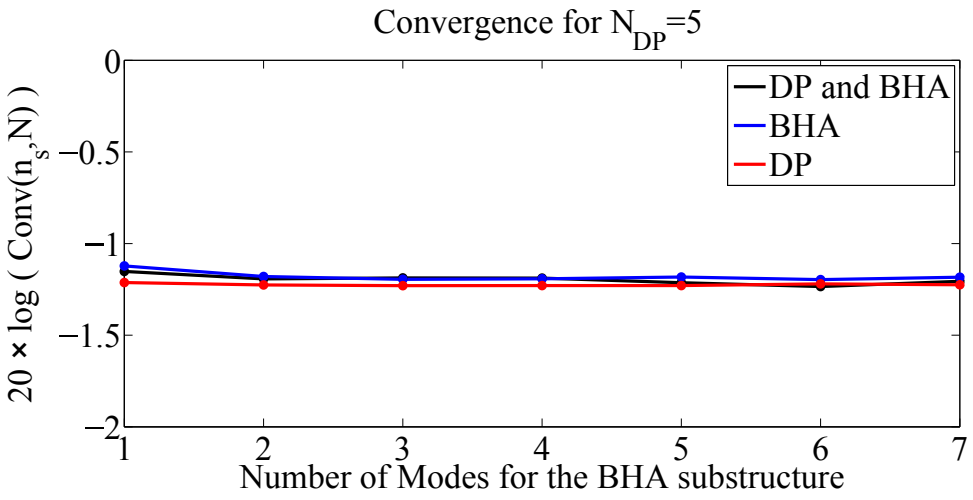

Figure C.4: Convergence analysis for BHA normal modes.

3. third one considers uncertainties only for DP, at level δ equal to 0.1 for stiffness, damping and mass matrices.